SKB

TECHNICAL REPORT 86-26

Model Shear Tests of Canisters with Smectite Clay Envelopes in Deposition Holes

Lennart Börgesson
Swedish Geological Co, Lund

December 1986

SVENSK KÄRNBRÄNSLEHANTERING AB
SWEDISH NUCLEAR FUEL AND WASTE MANAGEMENT CO

BOX 5864 S-102 48 STOCKHOLM
TEL 08-665 28 00 TELEX 13108-SKB

MODEL SHEAR TESTS OF CANISTERS WITH SMECTITE CLAY ENVELOPES IN DEPOSITION HOLES

Lennart Börgesson
Swedish Geological Co, Lund

December 1986

A list of other reports published in this series during 1986 is attached at the end of this report. Information on KBS technical reports from 1977-1978 (TR 121), 1979 (TR 79-28), 1980 (TR 80-26), 1981 (TR 81-17), 1982 (TR 82-28), 1983 (TR 83-77), 1984 (TR 85-01) and 1985 (TR 85-20) is available through SKB.

SWEDISH GEOLOGICAL CO
Lennart Börgesson/JS

Date: 1986-12-31
ID-no: IRAP 86522

MODEL SHEAR TESTS OF CANISTERS WITH SMECTITE CLAY ENVELOPES IN DEPOSITION HOLES

Lennart Börgesson
Swedish Geological Co, Lund

December 1986

Key words: Radioactive waste, bentonite, shear test, model test, deposition hole, stresses, strains

CONTENTS

SUMMARY

The consequences of rock displacement across a deposition hole has been investigated by some model tests. The model was scaled 1:10 to a real deposition hole. It was filled with a canister made of solid copper surrounded by highly compacted water saturated MX-80 bentonite. Before shear the swelling pressure was measured by six transducers in order to follow the water uptake process. During shear, pressure, strain, force and deformation were measured in altogether 18 points. The shearing was made at different rates in the various tests.

An extensive sampling after shear was made through which the density, water content, degree of saturation, homogenization and the effect of shear on the bentonite and canister could be studied. The results from the shear tests were compared to different calculations. The relevance of the calculations and the need for improved mathematical models could then be studied.

One important conclusion from these tests was that the rate dependence is about 10 % increased shear resistance per decade increased rate of shear. This resulted also in a very clear increase in strain in the canister with increased rate. The results also showed that the saturated bentonite has excellent stress distributing properties and that there is no risk of destroying the canister if the rock displacement is smaller than the thickness of the bentonite cover. The high density of the clay (ρ_m = 2.05 t/m^3) makes the bentonite produce such a high swelling pressure (~8 MPa) that the material will be very stiff. In the case of a large shear deformation corresponding to ~50 % of the bentonite thickness the result will be a rather large deformation of the canister. A lower density would be preferable if it can be accepted with respect to other required isolating properties.

The results also showed that three-dimensional FEM calculation using non-linear material properties is necessary to simulate the shear process. The rate dependence may be taken into account by adapting the properties to the actual rate of shear but might in a later stage be included in the model by giving the material viscous properties.

PREFACE

This project was financed by SKB and carried through thanks to the involvement of many people.

The shear apparatus was built by Bertil Nilsson at the workshop in the Technical University of Lund. The data collection was made with the assistance of Olof Forslund, Swedish Geological Co, Malå (Tests 1 and 2), and Rune Persson, Kockums Verkstäder AB, Malmö (Test 3).

Ola Karnland and Harald Hökmark, Swedish Geological Co made most of the arrangements for the tests as well as the sampling after the tests.

The manuscipt was typed by Jeanette Stenelo and the figures drawn by Birgitta Hellström.

Roland Pusch, Swedish Geological Co, and Anders Bergström, SKB, read the manuscript and gave valuable comments.

Lund December 1986

Lennart Börgesson

1 INTRODUCTION

According to the Swedish KBS concept the high level radioactive waste is going to be disposed in a copper canister surrounded by a clay envelope with a thickness of 37 cm. The canisters will be placed in 7.5 m deep holes with a diameter of 1.5 m bored from the bottom of long tunnels in crystalline rock at a depth of at least 500 m. The roles of the clay is multiple. One is to serve as a soft buffer between the canister and the hard rock and another is to form a homogeneous medium with a very low hydraulic conductivity. According to this concept the clay preferably consists of highly compacted bentonite with a density at saturation of 2.0-2.1 t/m^3. The geometry of a deposition hole is shown in Fig 1:1. The rock displacement scenario is shown in Fig 1:2.

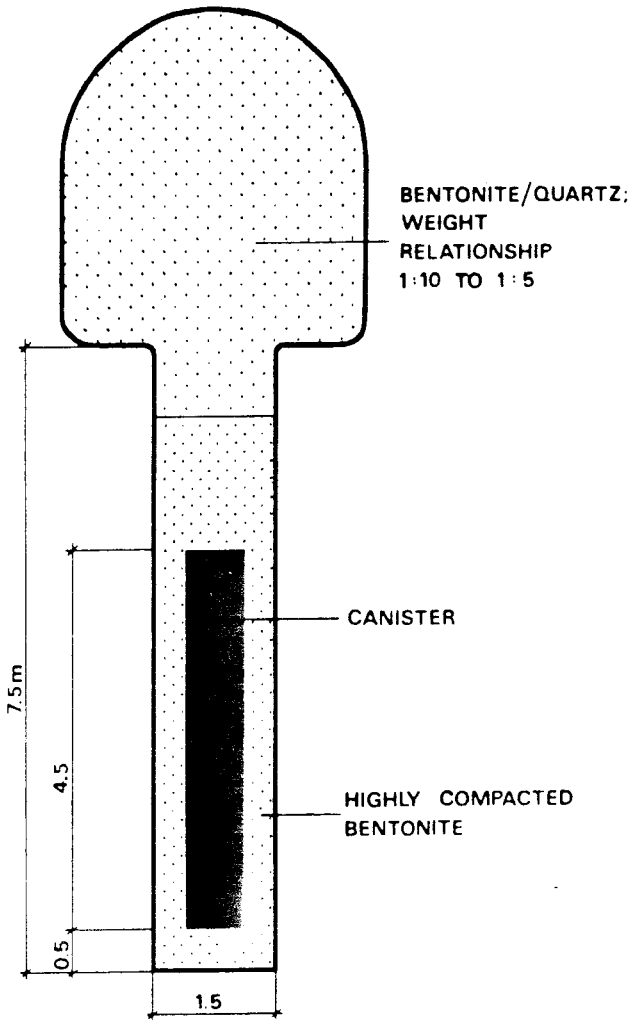

Fig 1:1. The Swedish KBS concept for disposal of radioactive waste

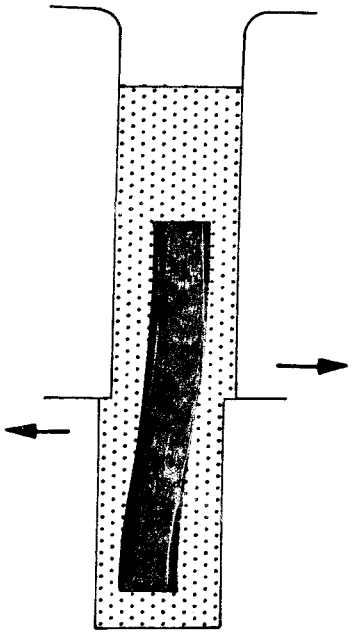

Fig 1:2. Rock displacements generating strains and stresses in the canister

Small or large rock movements, caused by tectonical activities, thermal stresses or rock excavations, will induce strain and stresses in the copper canister. It is favorable for the canister if the surrounding clay has a low shear strength and a plastic behaviour at small strains. It is also favorable if the shear stresses from a horizontal rock shear plane is well distributed along the vertical canister surface. A high shear strength and brittle behaviour of the clay would allow for only very small rock shear displacements before canister failure takes place.

Fig 1:3 shows some different possible stress-strain relationships of a buffer material. Curves a and b represent the most unfavourable behaviour with a high shear strength and for curve b, brittle failure. Curve c has a low shear strength and an ideal elasto-plastic behaviour with an elastic modulus which is initially high and exhibiting perfectly plastic behaviour after a small strain. Curve d represents the most favorable stress-strain curve with an instant, plastic, strain-hardening behaviour.

The actual stress-strain behaviour of compacted smectite clays appears to be intermediate to curves c and d. Fig 1:4 shows a typical result from a triaxial test. The clay is a saturated Ca-bentonite with a density of 2.06 t/m^3 and an applied cell pressure of 8.22 kPa.

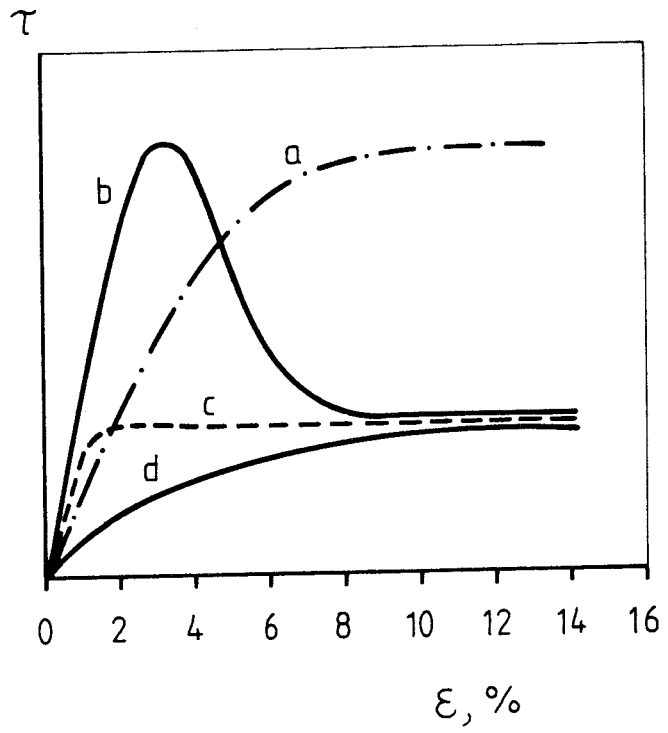

Fig 1:3. Possible stress-strain relations of a buffer material

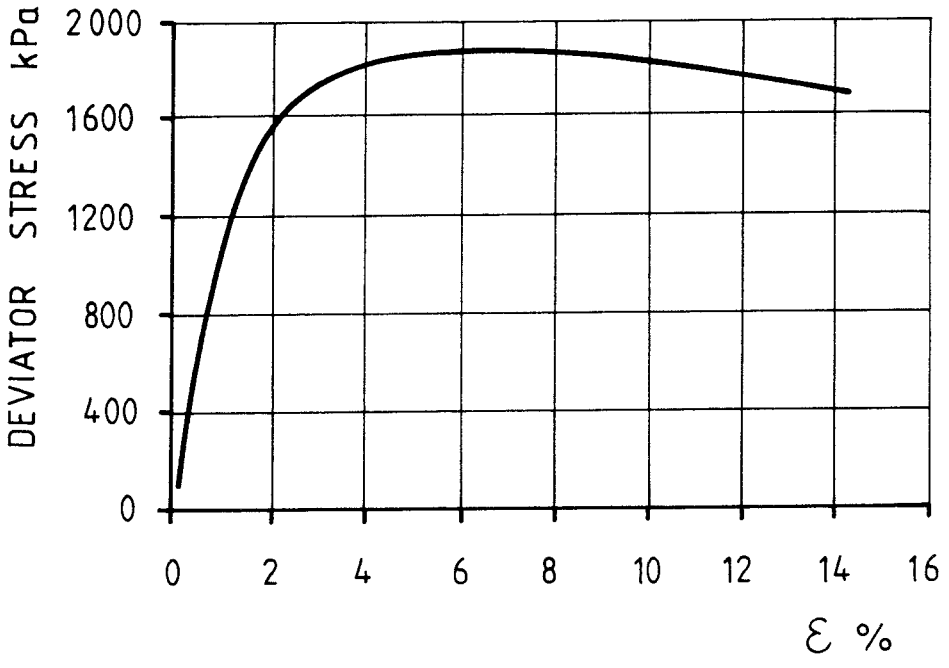

Fig 1:4. Typical stress-strain relations of a buffer material (Ca-bentonite with ρ_m = 2.06 t/m^3)

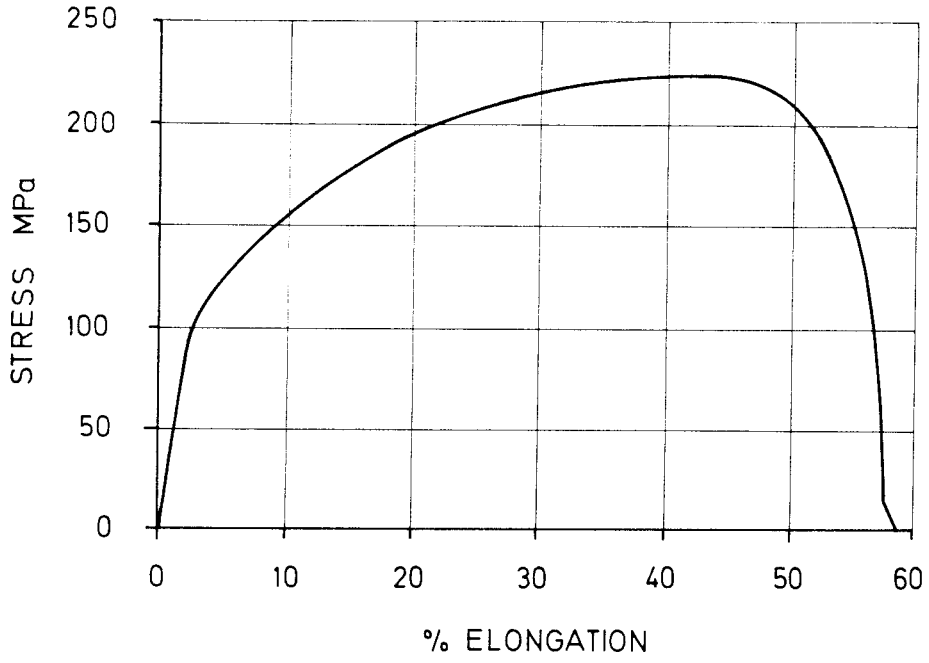

Fig 1:5. Stress-strain relation of copper

The properties of the copper is naturally also of vital importance. Fig 1:5 shows the stress-strain relation. Failure is not reached until after a strain of 40-50 %.

The effect on the canister of a rock shear is of course also dependent on the geometry of the deposition hole. A thick clay layer between the canister and the rock surface redistributes the stresses over a larger part of the canister than a thin layer.

It is very difficult to estimate the effect of a rock shear on the clay/canister system. Reliable calculations can only be made using the finite element method or similar techniques. So far, three different FEM calculations have been made with different degrees of complexibility, see Chapter 2.

It is not possible to evaluate the calculations and to really understand the effect of a rock shear without comparing them with results from real tests. In order to have such an understanding, 4 model shear tests have been conducted in this project using different shear rates. The model has been scaled 1:10 to a real deposition hole. It was filled with MX-80 sodium bentonite having a density at saturation of ρ_m = 2.05 t/m^3 and a canister consisting of oxygen free pure copper. The model is described in Chapter 3 and the results are accounted for in Chapter 4.

2 THEORETICAL CALCULATIONS

2.1 General

In addition to a simple pilot study of the shear process and a calculation of the water uptake process, three FEM or BEM calculations have been made. They comprised one linear elastic three-dimensional FEM, one non-linear two-dimensional FEM, and one three-dimensional BEM calculation. The calculations were made using different material properties and geometries are therefore not completely comparable. In the last calculation the boundary element method (BEM) was used to simulate the clay as a viscous material.

The model of the deposition hole was scaled 1:10 to the real KBS concept, which gave a canister diameter of 8 cm, a canister length of 45 cm and a diameter of the deposition hole of 16 cm.

2.2 Estimation of required shear force

Failure in the copper occurs after 40-50 % deformation at a stress of σ_f = 250 MPa as demonstrated by Fig 1:5. The shear strength will thus be τ_f = 125 MPa. Failure in the bentonite occurs at τ_f = 0.95 MPa after 7 % deformation if the stress-strain relation in Fig 1:4 is used. A simple strength calculation of the model shear test in which both materials are supposed to fail at the shear plane will give the upper limit of the required force.

$$F = \tau_{copper} \cdot A_{copper} + \tau_{bent} \cdot A_{bent} = 625 \text{ kN} + 14 \text{ kN} = 639 \text{ kN}$$

The other extreme assumption is the case that no shear stress at all will be generated in the copper which means that the canister will only tilt. These two cases (a and b) together with more realistic shear influences are shown in Fig 2:1. In case c the canister is supposed to be fixed at both ends without tilting and sheared over a certain zone with the length l_s and a shear strain γ. Case d is similar to c with the exception that some tilting has occurred which will reduce the shear strain in the canister by a factor D. Case c or d will probably occur in the real tests but without sharp breaking points (case e).

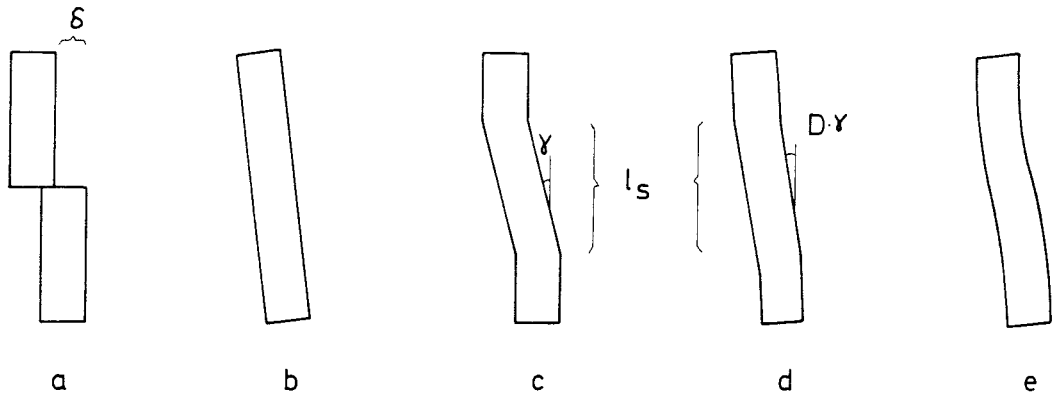

Fig 2:1. Possible canister deformations due to rock displacements in a deposition hole

An estimation of the required force from assumptions according to figures c and d can be made by using Eq. (2:1)

$$\gamma = \frac{\delta}{l_s} \quad \text{were } \gamma, \delta \text{ and } l_s \text{ are defined in Fig 2:1} \qquad (2:1)$$

If the shear deformation γ is 3 cm and the sheared length of the canister l_s is supposed to be equal to the diameter of the deposition hole, which means a stress distribution of 1:1, the shear strain according to case c will be

$$\gamma = 0.1875$$

A rough translation from strain (ε) to shear strain (γ) from the stress/strain curve of the copper (Fig 1:5) can be performed if the copper is considered to be incompressible (ν=0.5), which leads to Eq. (2:2).

$$\gamma = (1 + \nu)\varepsilon = 1.5 \cdot \varepsilon \qquad (2:2)$$

According to Fig 1:5 ε=0.125 corresponds to σ=160 MPa and $\tau = \frac{\sigma}{2}$ =80 MPa. This leads to a required force of

$$F = 414 \text{ kN}$$

If case d is considered and D is taken as 50 % we find that half the shear deformation has caused tilting and half has caused shear strain. Thus, the applied strain will be ε=0.063, resulting in τ = 63 MPa which leads to a required force of

F = 329 kN

The most probable case, e, will certainly mean a further reduction in required force since some of the shear strain will instead appear as bending.

2.3 Calculation of the water uptake process

The process of water uptake can in the case of compacted bentonite and unlimited water supply be simulated as a diffusion process:

$$\frac{dw}{dt} = D_w \left(\frac{d^2w}{dx^2} + \frac{d^2w}{dy^2} + \frac{d^2w}{dz^2} \right) \qquad (2:3)$$

where

w = water ratio
t = time
D_w = coefficient of water diffusion

Laboratory tests have shown that the constant $D_w = 0.3 \cdot 10^{-9}$ m/s^2.

A finite element calculation was made to predict the time to achieve complete saturation of the clay in the model deposition hole. A two-dimensional FEM model was used for this purpose. The boundary conditions were those of unlimited water supply from the filters and from the center symmetry line. Fig 2:2 shows the element mesh and the boundary conditions. A hole was drilled in the top and bottom bentonite pieces in order to accelerate the water uptake process and this hole was simulated in the calculations as a water supply boundary along the symmetry line.

The bentonite had an original water content of 9 % and a final saturated water content of 23 %. The result of the calculation was complete saturation after less than 60 days. After 20 days the aver-

age water content will be w=19 %. The swelling pressure at the final density reached at saturation ρ_m=2.05 t/m^3 will be between 7 and 10 MPa, according to earlier measurements, and the measured swelling pressure after equlibrium should therefore be in this interval. After 20 days the pressure should be 70-80 % of the maximum value. Fig 2:3 shows the expected water content distribution after 20 days according to the calculations.

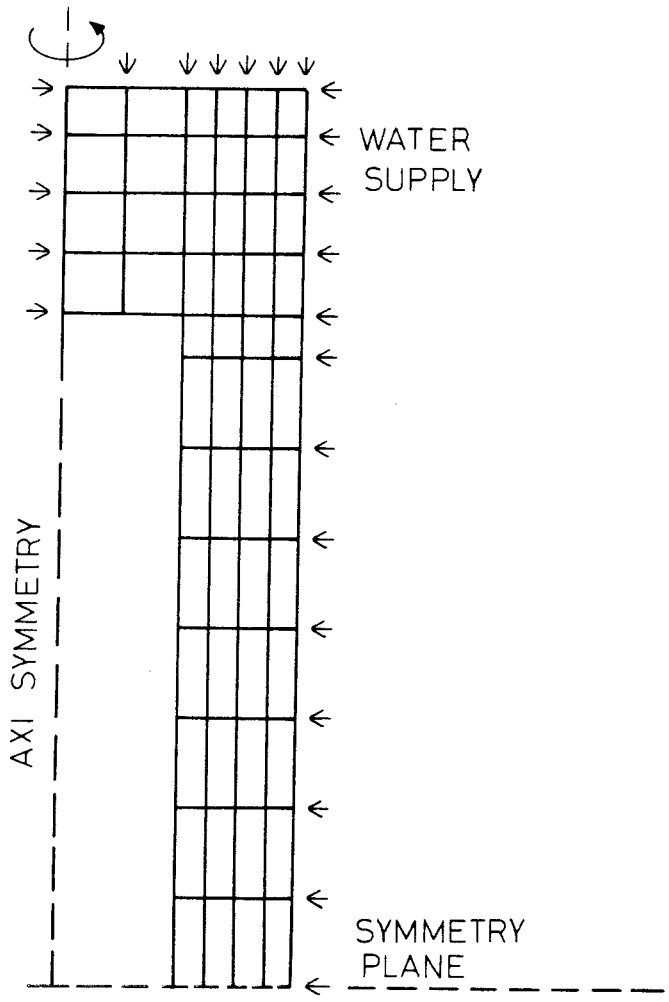

Fig 2:2. Element mesh and boundary conditions in the water uptake calculation

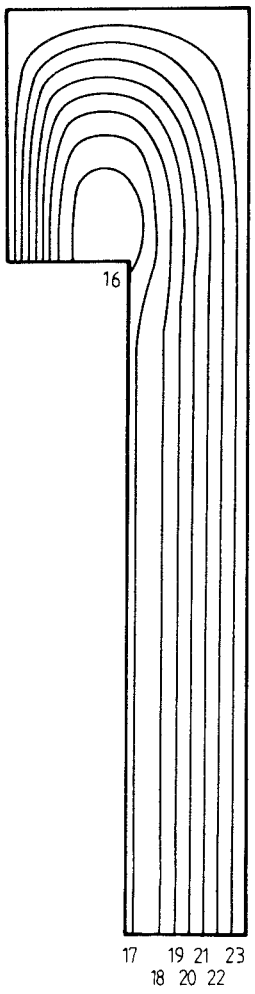

Fig 2:3. Calculated water content distribution in the bentonite after 20 days. The figures refer to %.

2.4 Linear elastic three dimensional FEM calculation

The three different FEM calculations which were made a few years ago in order to estimate the strains and stresses in the clay/canister system are described in Chapters 2.3-2.5. In the first calculation a linear elastic material model and a three-dimensional geometry were applied. The element mesh is shown in Fig 2:4. The radius of the canister was set at 0.35 m, the radius of the deposition hole at 0.70 m and the height of the canister at 4.7 m, thus simulating a full scale KBS 3 deposition hole. Shearing took place nonsymmetrically in the upper part of the canister but the deviation from symmetrical condition did not affect the results very much. A shear deformation of 0.01 m was simulated by letting the upper part of the boundary move horizontally. The deformation corresponds to only 2.4 % of the bentonite thickness. The elastic input data shown in Table 1 were used in the calculation.

Table 1. Elastic parameters

	E MPa	ν
Copper	$1.33 \cdot 10^5$	0.35
Bentonite	$6.0 \cdot 10^3$	0.45

The calculation was made by Fred Nilsson, IFM Akustikbyrån AB. It showed that the highest stresses in the canister were in the z direction, that is along the canister. The calculation also showed high stress concentrations at the surface of the canister, the highest stress being σ_z = 390 MPa. Fig 2:5 shows the stresses σ_z 4 cm from the surface.

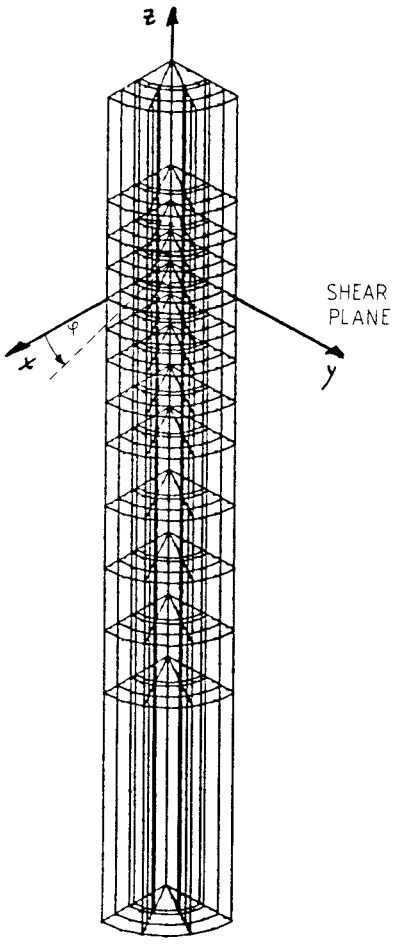

Fig 2:4. Element mesh in the linear elastic three-dimensional FEM calculation

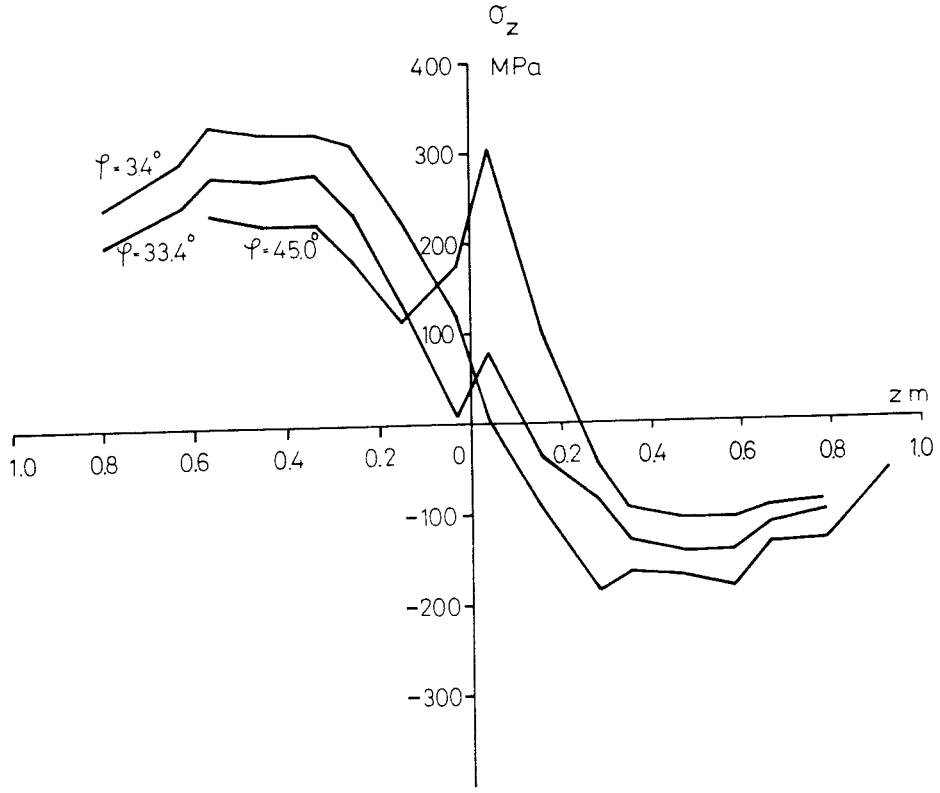

Fig 2:5. Calculated stresses in the axial direction of the canister 4 cm from the surface. φ is the angle to the shear direction (x-axis in Fig 2:4)

2.5 Non-linear two-dimensional FEM calculation

This calculation (made by K. Axelsson) was aimed at investigating the influence of the non-linear behaviour of copper and bentonite and at comparing two-dimensional calculations with three-dimensional ones. A two-dimensional plane, sandwich-like model of the deposition hole was made using a canister thickness of 0.7 m and a bentonite thickness of 0.95 m. The non-linear behavior was simulated by a simple bi-linear stress-strain curve. The applied shear deformation was 0.01, m corresponding to only 1.1 % of the bentonite thickness.

Four calculations were made, one of them assuming elastic properties using the stress-strain properties shown in Table II. The maximum stress obtained in the two-dimensional calculation was only one third of the corresponding value from the three-dimensional calculation showed in Chapter 2.4. However, the relative thickness of the clay barrier was almost three times greater, thus making the comparison difficult.

Two non-linear calculations were made using the material properties shown in Table II.

Table II. Elastic and plastic parameters

		E MPa	ν	τ_p MPa	E_p MPa
Copper	alt 1	$1.33 \cdot 10^5$	0.35	50	$2.8 \cdot 10^3$
	alt 2	$1.22 \cdot 10^5$	0.35	30	$8.5 \cdot 10^3$
Bent	alt 1	$2.0 \cdot 10^3$	0.45	8.0	20.0
	alt 2	$2.0 \cdot 10^2$	0.45	8.0	20.0

The stress-strain relation is thus a bi-linear curve with the elastic modulus E up to the point where the shear stress τ_p is reached at which point plastic behavior begins characterized by the plastic modulus (hardening modulus) E_p. Subsequent laboratory tests have shown that the shear strength is strongly overestimated in these calculations and corresponds to $\rho_m \sim 2.25$ t/m^3.

In the calculation where the stiff bentonite ($E = 2.0 \cdot 10^3$ MPa) was used, the copper began to plasticize in certain zones and the maximum stresses reached were between 50 and 70 MPa. In the calculation with the soft bentonite ($E=2.0 \cdot 10^2$ MPa) no plasticizing occurred in the copper and the maximum stresses were 20 MPa.

Since the elastic modulus was lower in the non-linear than in the linear calculation, an additional linear calculation using $E=2.0 \cdot 10^3$ MPa was made for comparison of the two techniques. This calculation resulted in a maximum stress in the canister of 80-90 MPa, which is 30-60 % higher than in the non-linear calculation.

The final conclusion from these calculations was that reliable results can only be reached with a non-linear three-dimensional calculation.

2.6 Viscous three-dimensional BEM calculation

Bentonite may be considered as a viscous material. The rate dependence of such a viscosity is very high which means that the simple Newtonian viscosity

$$\mu = \frac{d\tau}{d\dot{\gamma}} = \frac{\tau}{\dot{\gamma}}$$

is not a very good model of the behaviour. Since the difference in strain rate is different parts of the clay/canister system is relatively small the error due to an overestimation of the rate dependence in a Newtonian viscosity calculation is probably not very important as compared with the error caused by the incorrect stress-strain model which is considerable at small strains.

The behaviour of an idealized viscous material is shown in Fig 2:6 and 2:7. Fig 2:6 shows that the strain rate is directly proportional to the shear resistance. Fig 2:7 shows the stress-strain relation of a viscous material. The material is initially behaving as a perfectly plastic material with constant shear resistance which will only change with altered strain rates. The model applies well after a strain of 4-6 %, i.e. close to failure but does not apply at all at small strains.

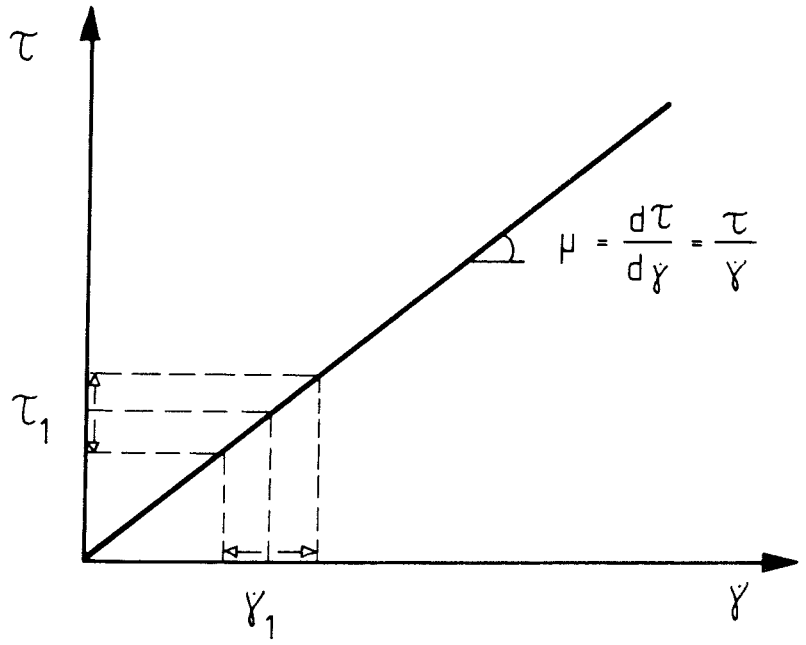

Fig 2:6. Behaviour of a Newtonian viscous material. The shear resistance τ is proportional to the strain rate

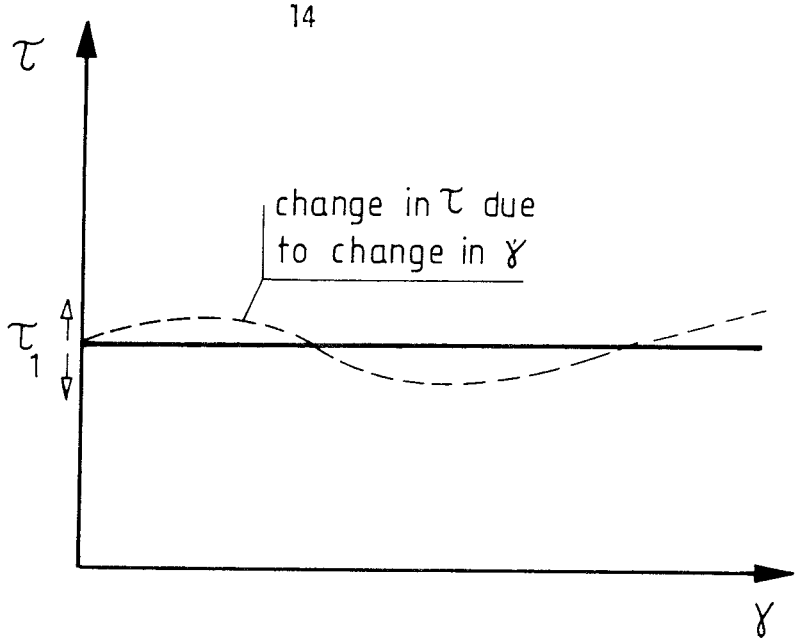

Fig 2:7. Schematic stress-strain behaviour of a Newtonian viscous material. The shear resistance is constant with strain (perfectly plastic)

A viscous material model has been tested in a boundary element calculation made by CMC (Computational Mechanics Consultants). The boundary element method has the advantage of using a simple element structure but the disadvantage of only having the possibility to use one material property.

The calculation had to be divided into two parts. Firstly the stresses in the bentonite were calculated and then the stresses from that calculation were used as input data to calculate the stresses in the canister. In the first calculation the following properties were used:

Bentonite	μ = 20-150 MPas
Copper	μ = 20.000 - 150.000 MPas

This calculation was made by considering the clay to be a purely viscous substance only gave the stresses in the clay. The stresses in the canister were given from the second calculation in which the stresses in the clay on the canister were used as input data. The second calculation was made by applying ordinary elastic properties to the canister. These properties where taken as

E = 30.000 MPa

ν = 0.35

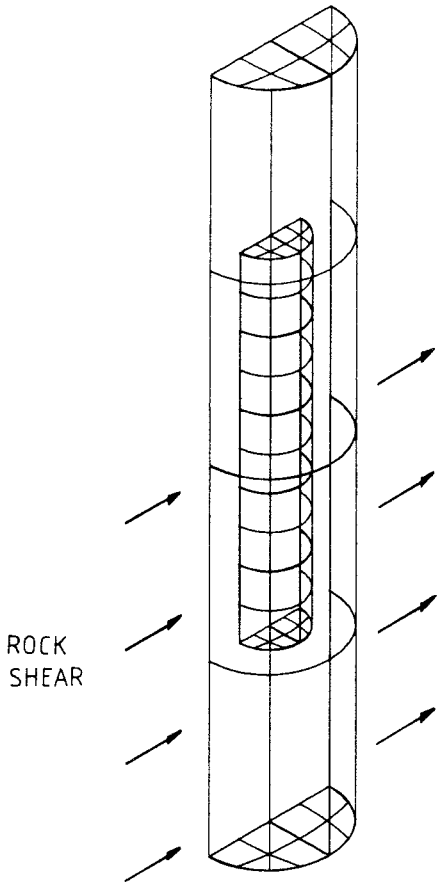

Fig 2:8. Element mesh of the clay-canister system in the viscous calculation

The model of the clay is shown in Fig 2:8. It consisted of 32 boundary elements describing the canister clay interface and the rock surface. The symmetry made it possible to only simulate half the model.

The properties of a viscous material shown in Figs 2:6 and 2:7 with a constant rate of strain leads to strain-independent stresses which means that the calculations can be made in one step. It also means that it is very simple to see the influence of the viscosity and the rate of deformation since the stresses will be proportional to the viscosity and the rate of deformation. The calculations were made using a rate of deformation of 0.01 m/sec.

The results are illustrated in Figs 2:9-2:12. The stresses in the bentonite shown in Fig 2:9 and 2:10 are related to the viscosity μ = 60 MPas while the stresses σ_z in the canister shown in Fig 2:11 and 2:12 are related to the viscosity μ = 20 MPas. The stresses are

linearly proportional to the viscosity and can thus be multiplied by 3 to be comparable to the stresses in the bentonite.

Fig 2:9 shows the results of the stresses in the bentonite along a line from the bottom to the top of the canister. The maximum stress in the bentonite close to the canister is according to the figure σ_x = 43 MPa.

The stresses σ_x in the bentonite along the rock-bentonite interface are shown in Fig 2:10 as a contour plot. The contour line 1 corresponds to -27.9 MPa while line 10 corresponds to +27.9 MPa and the intermediate lines have equidistant pressures. The maximum stress close to the rock is thus σ_x=28 MPa.

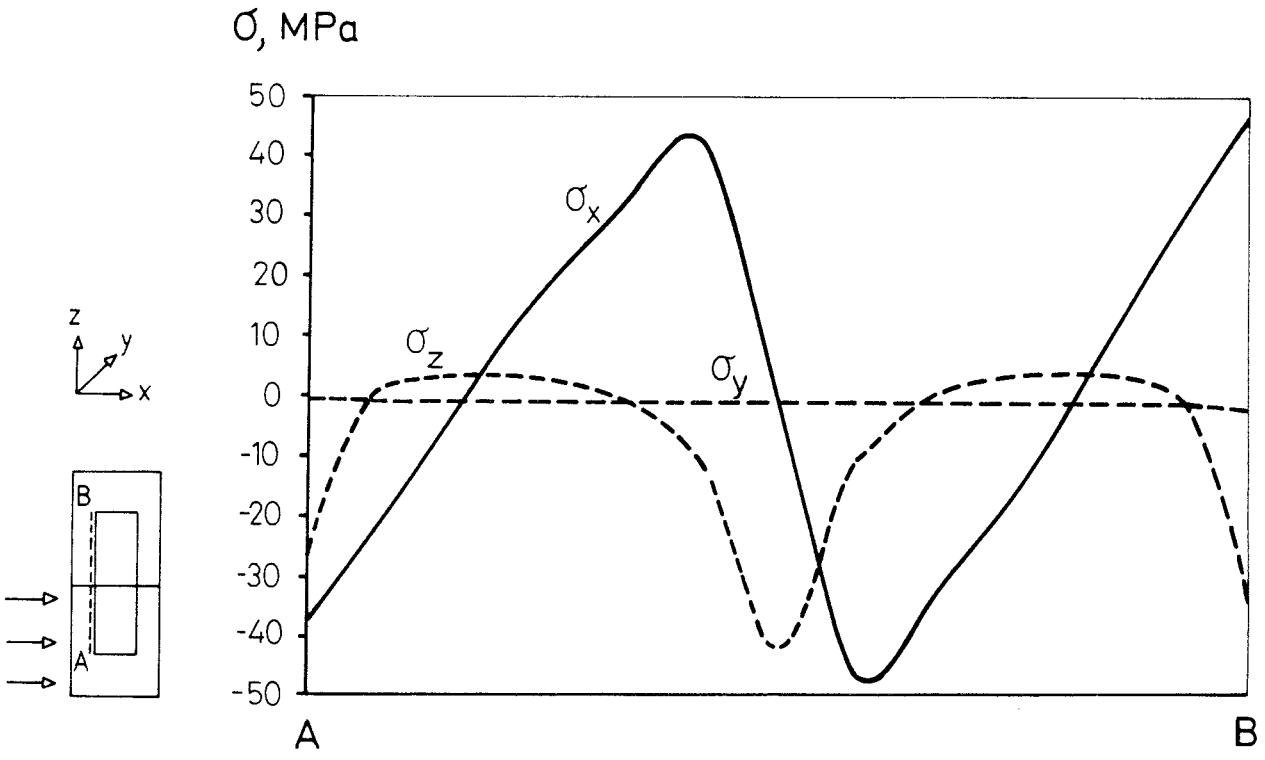

Fig 2:9. Calculated stresses in the bentonite along line A-B. Compression is termed positive

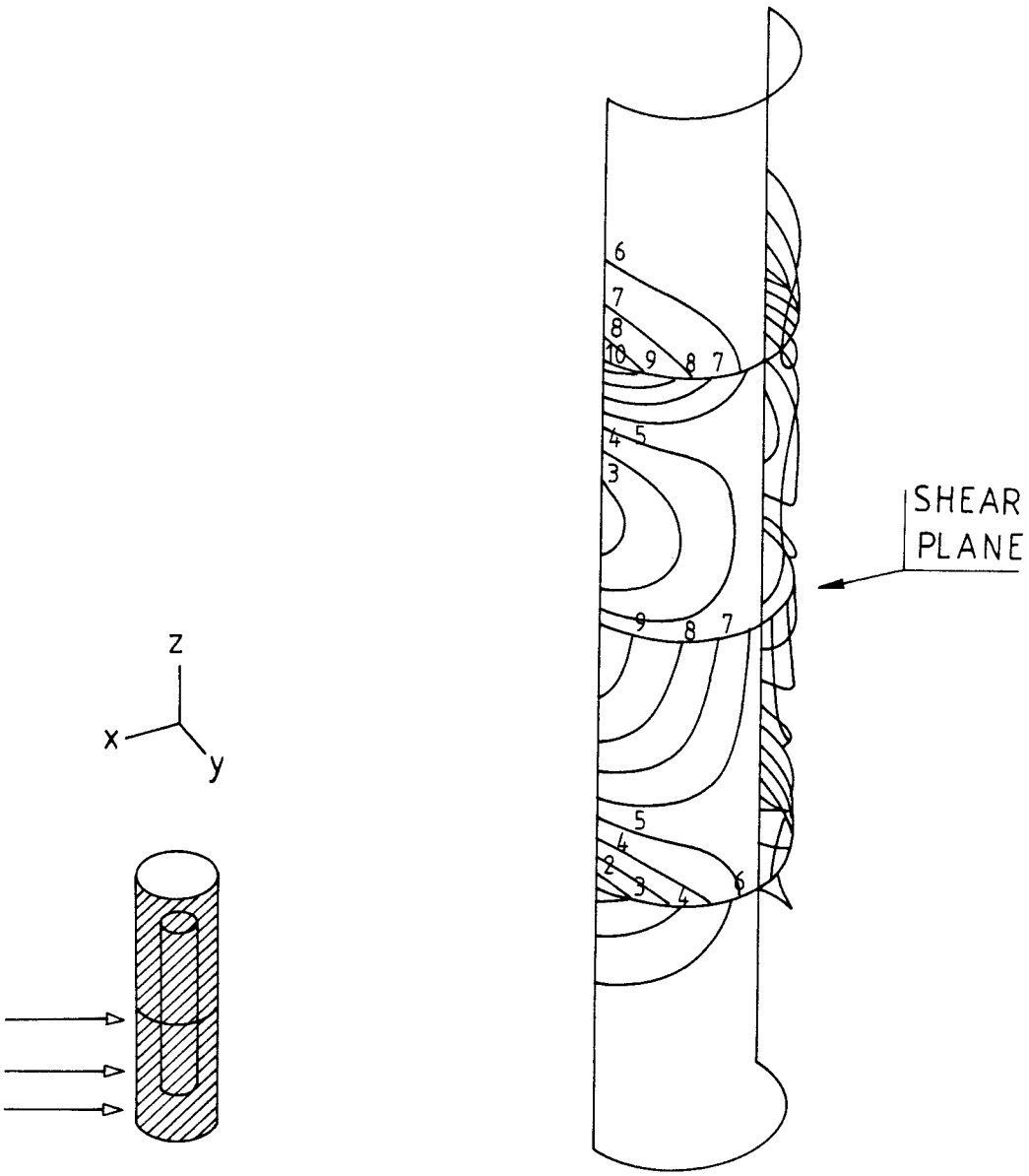

Fig 2:10. Calculated σ_x stresses in the bentonite along the rock surface. The figure shows isolines with line 1 corresponding to -27.9 MPa, line 10 corresponding to +27.9 MPa and 2.79 MPa between each line. Compression is termed positive

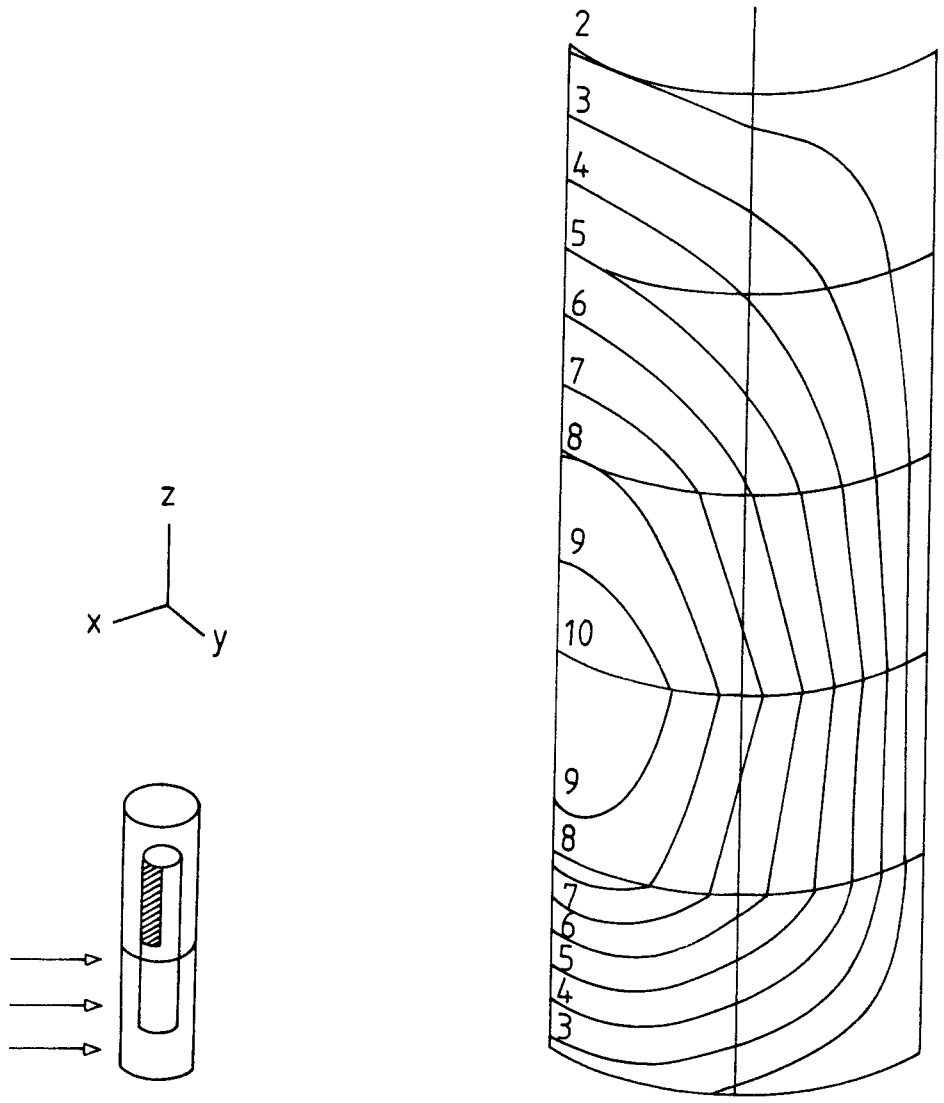

Fig 2:11. Equidistant isolines of the calculated axial stresses σ_z in the canister surface. Isoline 10 corresponds to 122 MPa and isoline 1 to 2 MPa. Compression is termed negative

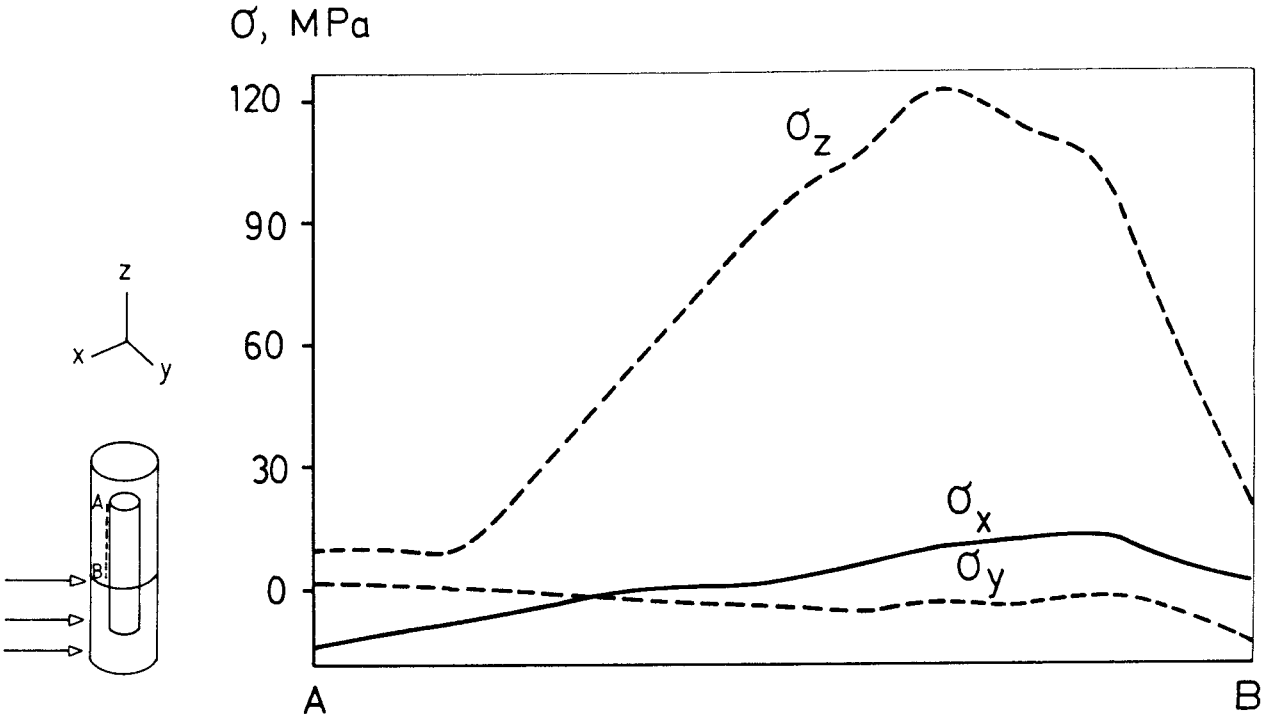

Fig 2:12. Stresses along line A-B in the canister surface. Compression is termed negative

The highest stresses in the canister are, as noted in the previous calculations, the axial stress σ_z. Fig 2:11 shows a contour plot of σ_z in the surface of the canister while Fig 2:12 is a diagram of the stresses along the axial line A-B in the canister. The maximum stress in the canister is according to this calculation σ_z = 120 MPa.

2.7 Comments on the calculations

The general appearance of the stress distributions from the elastic 3D calculation made by IFM agree quite well with those from the viscous 3D calculation made by CMC in spite of the difference in material model and scale. This is logical since the calculation methods are similar and the scale does not effect the general stress appearance. The similarity in calculation methods can be seen when comparing the constitutive equations of the two methods which are identical in the case of incompressible material with 3 μ replacing E, and displacement rates and strain rates replacing displacements and strains.

3 DESCRIPTION OF THE SHEAR APPARATUS

3.1 Design

The apparatus, in which the shearing of the deposition hole was simulated, must be very stiff in order not to be subjected to unwanted deformations.

The deposition hole was scaled about 1:10, the diameter of the hole being 16 cm and the length 60 cm. The copper canister was simulated by rods of solid HPOF copper with a length of 45 cm and a diameter of 8 cm. The permeable rock was simulated by a cylindrical bronze filter with a thickness of 2 cm. This filter was made from small bronze pellets to give a maximum pore size of 12 µm. Such a filter is permeable enough to guarantee unlimited water supply for the bentonite without letting bentonite penetrate into the filter. It is also stiff enough to resist the swelling pressure and the local stress-concentrations during shear. Filters were also mounted to cover the top and bottom of the deposition hole.

The cylindrical filter was surrounded by a cylinder made of acid proof stainless steel 2333. In order to guarantee a perfect fitting, the inner diameter of the steel cylinder was made 0.2 mm smaller than the outer diameter of the filter. The filter was then mounted into the steel cylinder by expanding the steel cylinder through heating. The cylinders were made in two 30 cm long parts in order to locate the shear plane at the center of the canister, and to orient it perpendicularly to its axis. The cylinders were rigidly mounted to form one unit in a steel frame during the water-saturation phase while one of them was free to move during the shearing phase.

The test arrangement is shown in Fig 3:1. The frame consists of four main pieces connected with screws. A fifth piece was used to transfer the shearing force to one of the cylinders.

The mounted apparatus with the frame and the cylinders was kept in a vertical standing position with the fixed cylinder below the moveable during the mounting and water saturating procedures. At shearing the apparatus was turned to a horizontal position as shown in Fig 3:1.

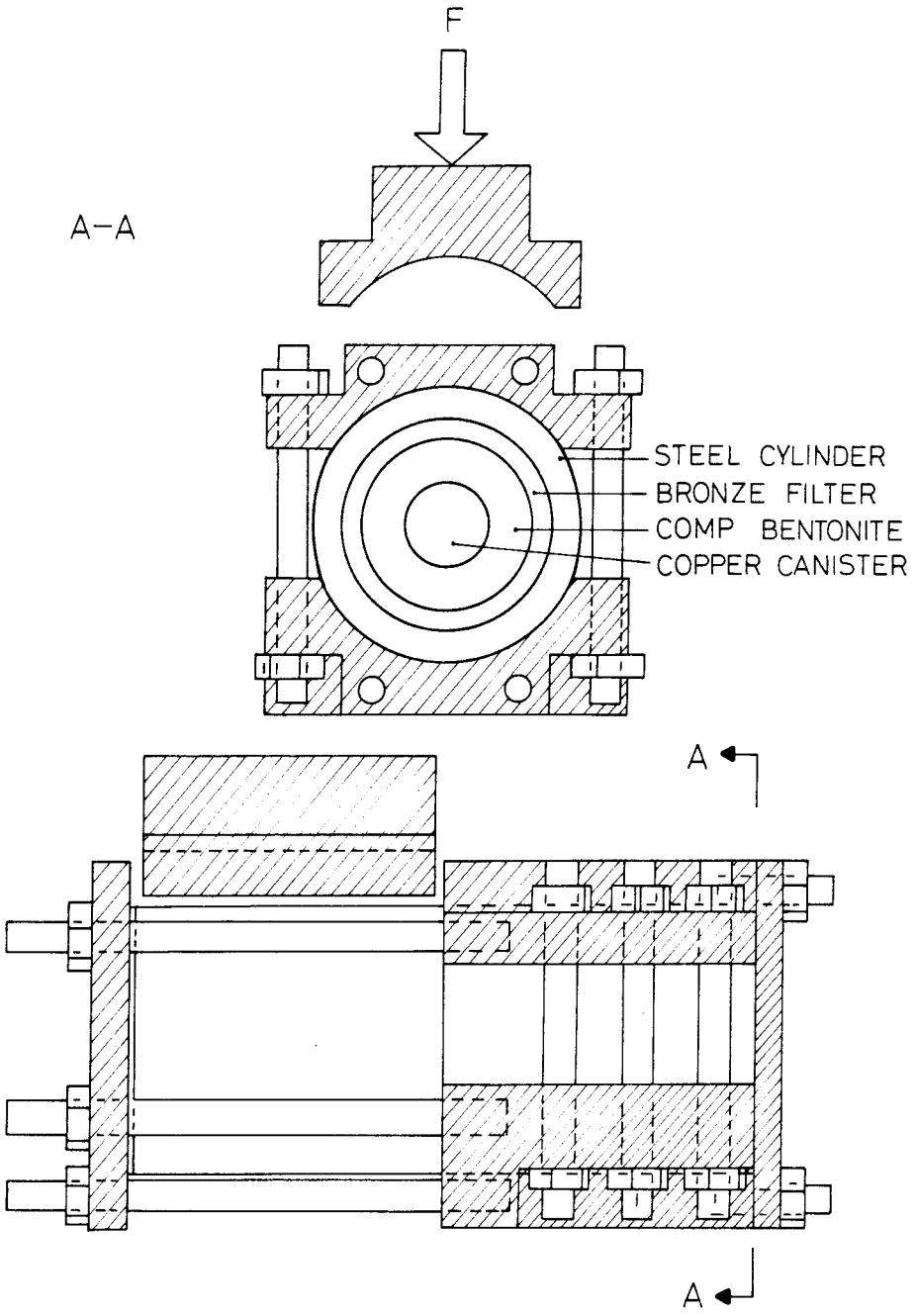

Fig 3:1. Apparatus in which the filled deposition hole was simulated and sheared. The cross-hatched area is the steel frame

The contact between the cylinder halves was prepared in a special way, the requirement being that it had to be water-tight to prevent leakage, and very smooth to prevent friction and still able to transfer water from one filter to the other. The problem was solved by covering each end face with a ringformed plate. The plate had an o-ring seal against leakage, holes and channels for water transportation from the lower filter to the upper, and a smooth lubricated surface (Fig 3:2). At the top of the simulated deposition hole the filter was covered by a lubricated plate which allowed friction-free

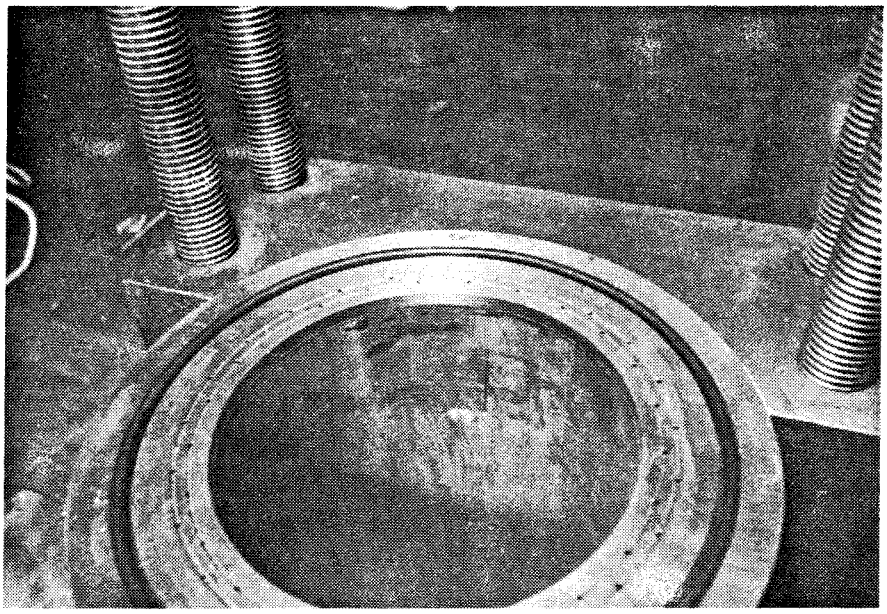

Fig 3:2. The shear plane of the fixed cylinder

displacement of the cylinder. Water was let in by two connections in the bottom and two in the top.

3.2 Instrumentation

Altogether 18 sensors were installed in order to measure stresses and strains during saturation and shear: four force transducers to measure the required force during shear, three strain transducers to measure the shear deformation, six pressure transducers to measure the pressure at the clay/canister interface and at the clay/rock interface, and five strain gauges to measure canister-strain. Fig 3:3 shows the location and coding of the sensors. The four force transducers were later reduced to three. Two of the strain transducers were used to measure the shearing of the modelled rock while the third was used to measure the movement of the end of the canister relative to the rock. This was made by use of a copper tube that was fixed at the canister and passed through the filter and the steel cylinder.

The copper tube was also used to let cables through from the strain gauges in the canister to the data logger. Another copper tube was used to let the cables from the three pressure transducers in the canister pass from the other end of the canister through the cylinder walls.

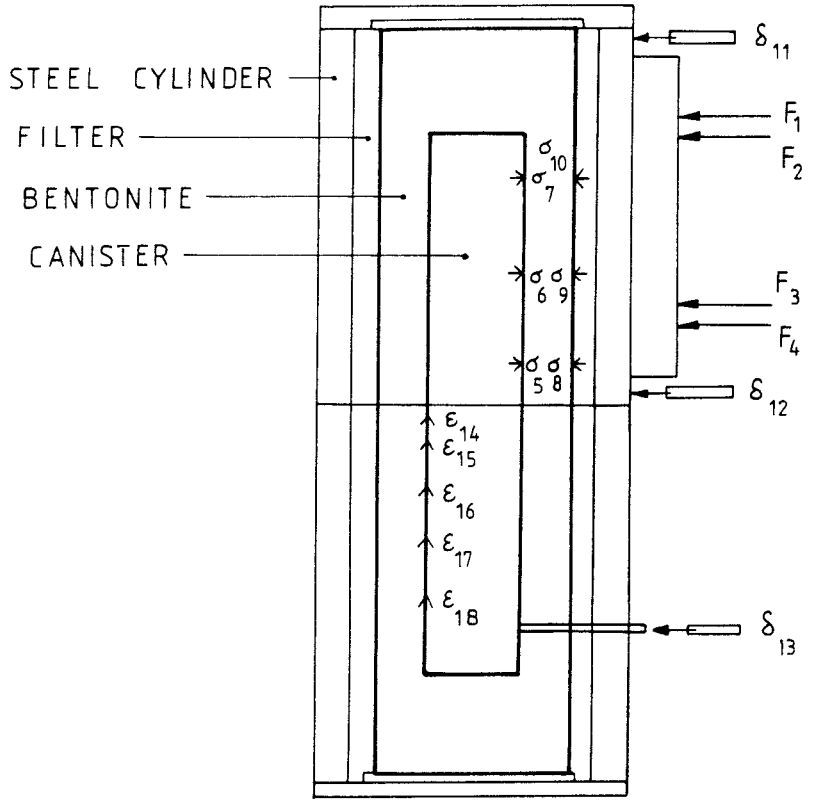

Fig 3:3. Location and coding of the installed transducers and gauges
F_1-F_4 force transducers
σ_5-σ_{10} pressure transducers
δ_{11}-δ_{13} strain transducers
ε_{14}-ε_{18} strain gauges

The pressure transducers, which have a diameter of 4.5 mm, are very strong and have a capacity to measure pressures as high as 70 MPa. They were mounted in the canister and the cables were placed in bored holes through the canister and through the copper tube in order not to be in contact with the bentonite or water. The three mounted transducers are shown in Fig 3:4.

The other three pressure transducers were mounted in the filter opposite to those in the canister in order to measure the stress from the bentonite to the simulated rock. These transducers are a little larger than the others and have a diameter of 6 mm. The transducers were mounted from outside the cylinder as shown in Fig 3:5.

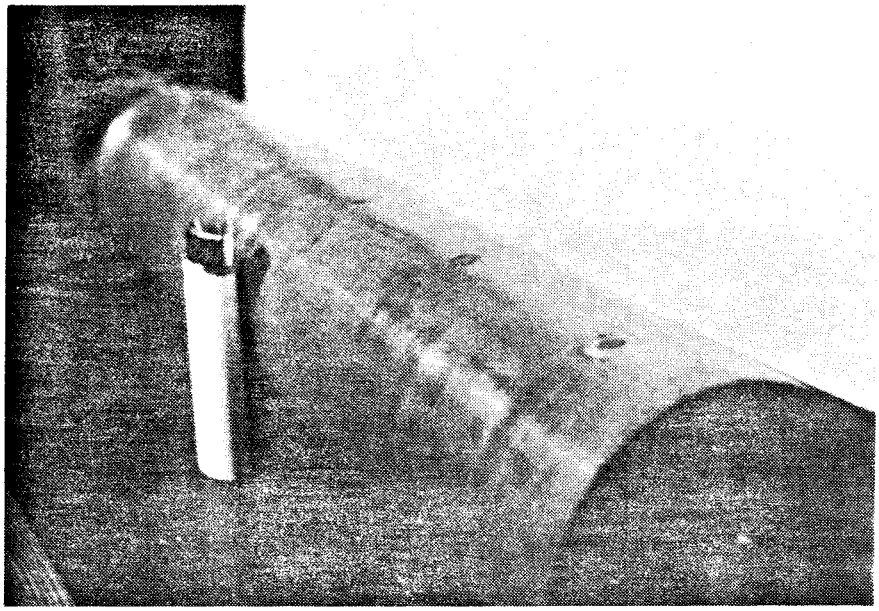

Fig 3:4. The three pressure transducers mounted in the canister

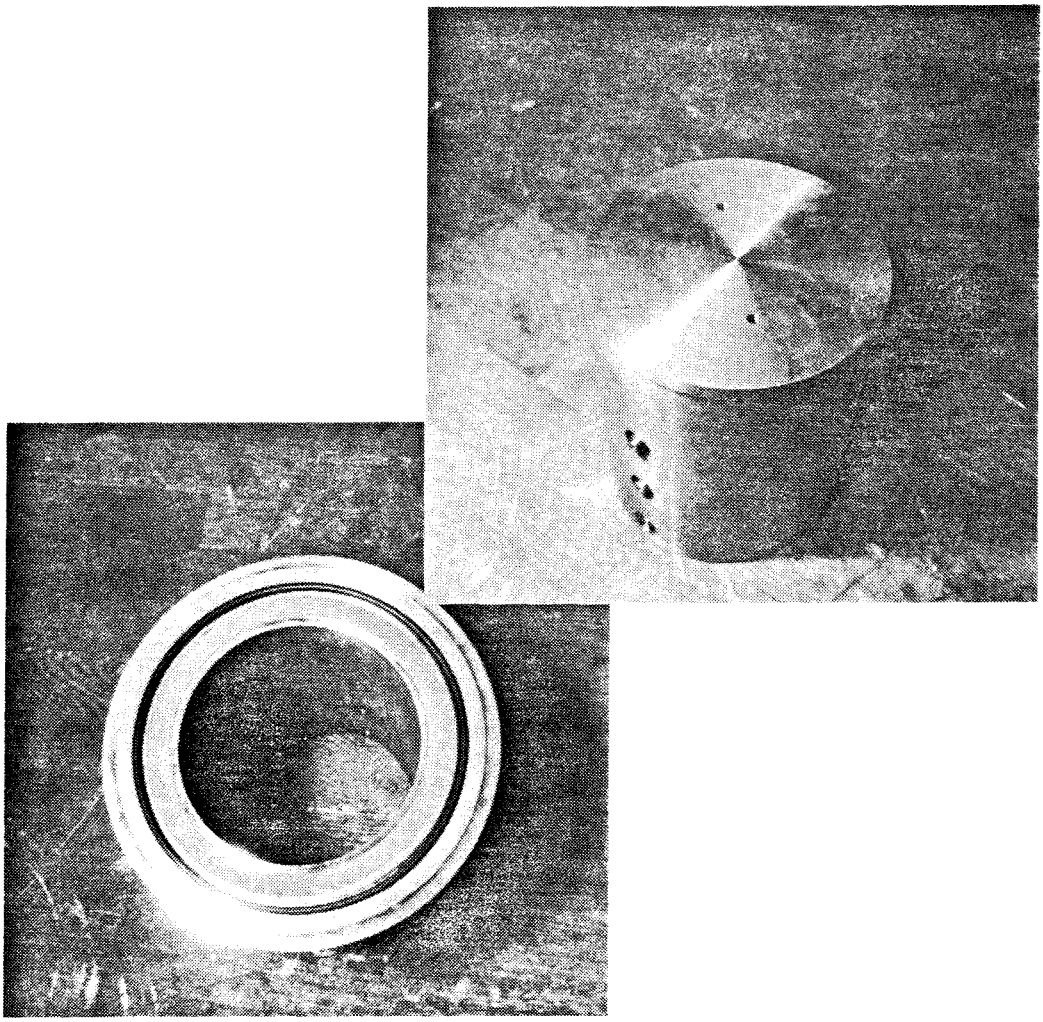

Fig 3:5. Three pressure transducers were mounted in the movable cylinder

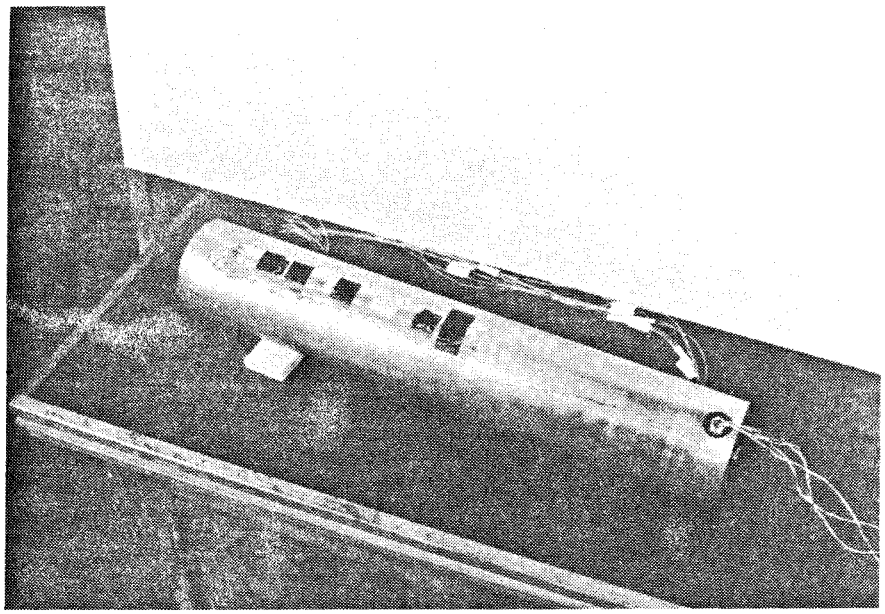

Fig 3:6. Five strain gauges were mounted on each canister. Both the cables from the strain gauges (to the left) and the cables from the pressure transducers (to the right) can be seen in the picture

The strain gauges were glued to the canister in the axial direction in order to measure the strain and the stresses along the surface of the canister. The gauges are of a type that can resist large deformations (10 %). They were mounted at the canister surface in a anti-symmetric pattern with respect to the pressure transducers in order to get the strain to correspond to the stresses measured by the pressure transducers. The strain gauges and cables were covered by silica coting to protect them from water and pressure from the bentonite. The canister with the mounted strain gauges is shown in Fig 3:6.

3.3 Data collection

The signals from the transducers and gauges were collected in two different ways. In the first three tests, the pilot test, the slow test and the quick test, the data was recorded by printers.

In the "super-quick" test the collection was made by a computer and the data recorded by tape. The curves of primary interest, i.e. the measured stresses, strains and forces versus deformation, were computer-plotted.

The data collection in the first three tests was made by aid of Olof Forslund from the SGAB laboratory in Malå. At the "super-quick" test it was made with the aid of Rune Persson from the laboratory of Kockums Verkstäder AB in Malmö.

3.4 Procedure of preparation and mounting

The canister was made from a piece of copper which was turned in a lathe and cut to the correct dimensions. Then the cable paths were drilled and the pressure transducers and strain gauges mounted in the canister. Parallel to this the bentonite was prepared. Blocks were taken from MX-80 samples that were originally intended for the Buffer Mass Test in Stripa. It had a density of ρ=2.14 t/m^3 and a water content of w=9 %. These blocks were sawed to fit into the shear apparatus and given the size and weight suited for a final density of ρ=2.05 t/m^3 in the water saturated and expanded state. The bentonite originally consisted of 6 pieces, one below, one above and 4 surrounding the canister. Central holes were made in the bentonite pieces below and above the canister in order to fasten the saturation phase. The 4 surrounding bentonite pieces are shown in Fig 3:7 together with the canister and the simulated deposition hole just before mounting. The rest of the mounting procedure is shown in Fig 3:8 were also the copper tubes leading the cables from the strain gauges and the pressure transducers can be seen.

Finally, the end pieces were mounted and the water-bearing tubes connected. A slight overpressure was applied to the bottom in order to have a flow of water upwards through the filter during the whole saturation procedure which would prevent big air-bubbles from delaying the saturation. Distilled water was used to saturate the bentonite.

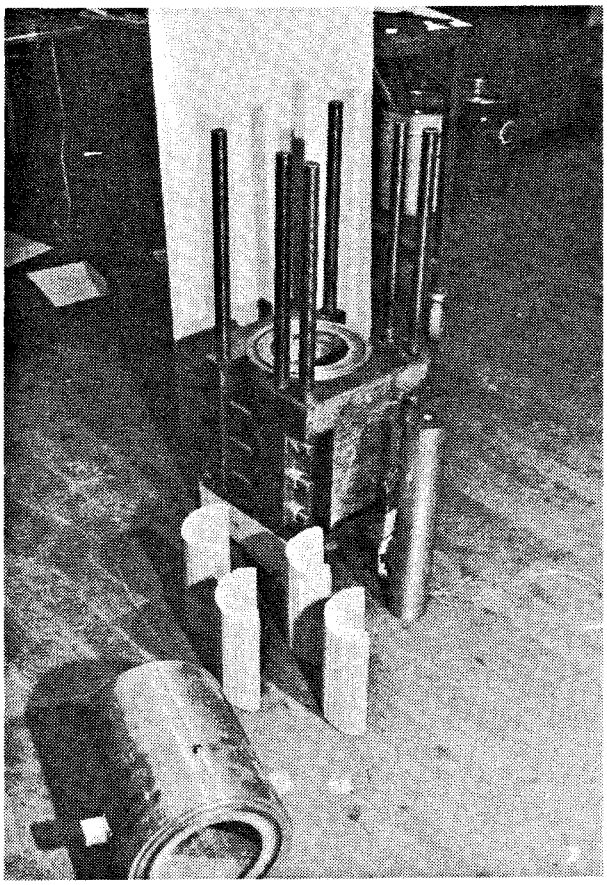

Fig 3:7. The shear apparatus, four of the bentonite blocks and the canister just before mounting

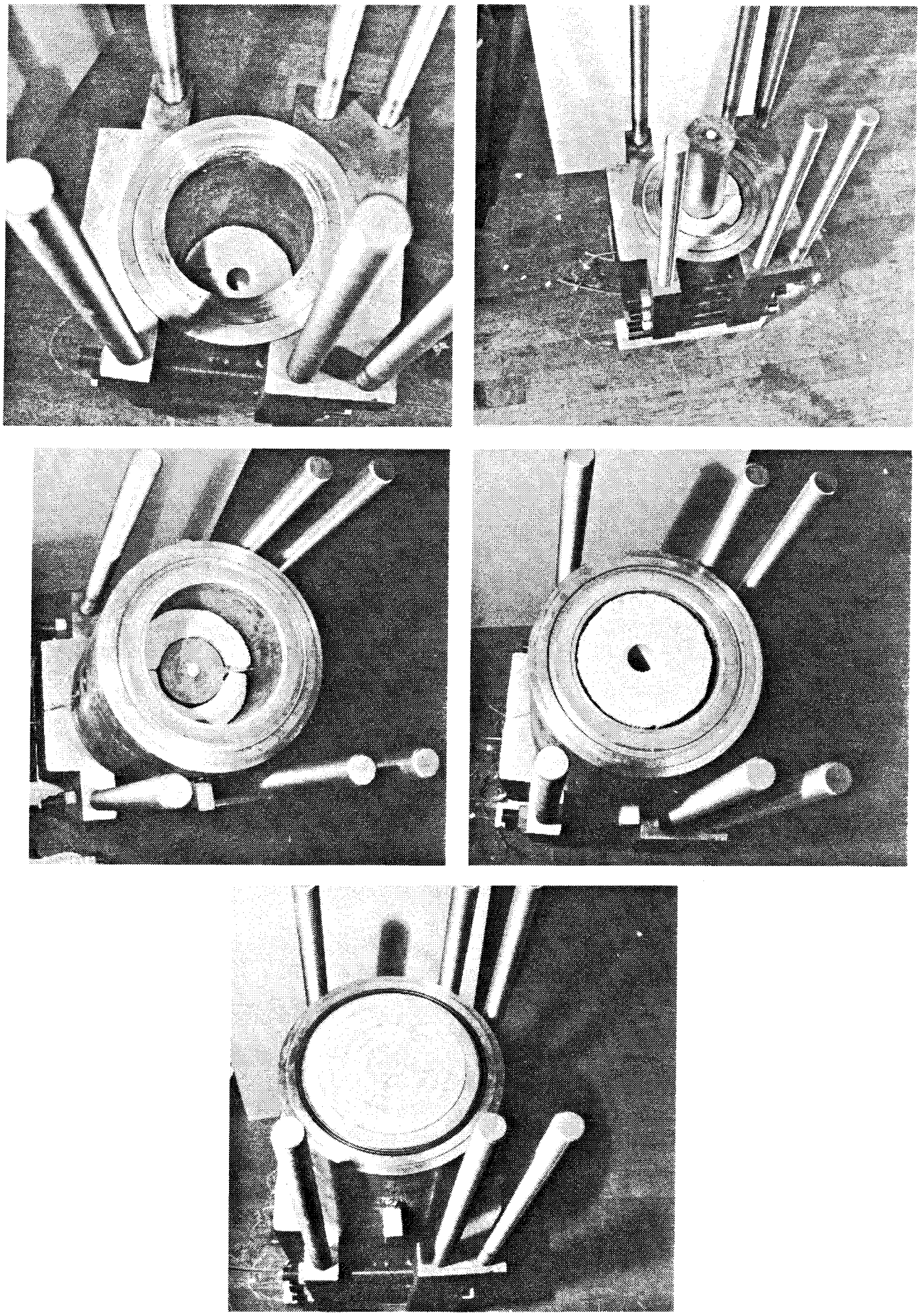

Fig 3:8. Pictures from the mounting of the bentonite blocks and the canister

4 RESULTS

4.1 General

Altogether four tests have been made, one pilot test with nonsaturated sand-bentonite mixture as buffer material and three ordinary tests with saturated compacted bentonite.

The ordinary tests were made at different rates of shear in order to evaluate the rate dependence. The difference in rate between the slowest and the fastest test was 5000 times. The duration of the first slow test was 15 minutes, the second test 15 seconds and the last super quick test about 0.1 second.

4.2 Pilot test

The pilot test was conducted mainly to check the function of the apparatus, the transducers and the data collection system but also to see the effect of a very soft buffer material. At this test all force and strain transducers were used but only one strain gauge. No pressure transducers were used.

A soil mixture consisting of 10 % bentonite and 90 % sand was compacted in an air dry state to a density of ρ=1.8 t/m^3 in the simulated deposition hole. A tube made of iron was used as canister. The simulated rock was sheared 3 cm for about one minute. The position of the canister after shearing was carefully measured and is shown in Fig 4:1. The canister was not deformed or otherwise affected. Since no bending and only tilting of the canister occurred it was clear that the soil material was very soft in relation to the canister and that case b in Fig 2:1 applied. The movement of the end of the canister (δ_1 in Fig 4:1) was registered by the copper tube penetrating the walls. This movement is shown in Fig 4:2 as a function of the shear deformation. The total maximum force was 100 kN which can also be concluded from Fig 4:2. No strain was registered by the strain gauge. At the excavation it could be seen that some compression of the sand-bentonite mixture had occurred close to the shear surface on the compression side while a small gap was noticed on the opposite side.

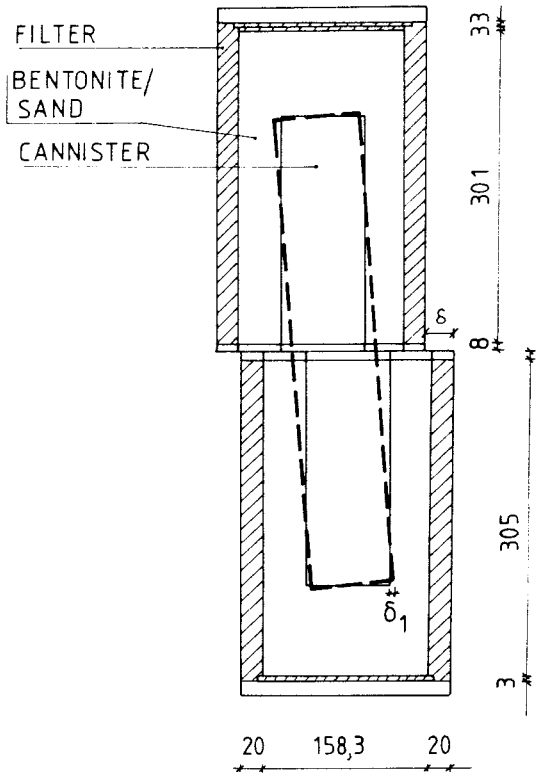

Fig 4:1. The position of the canister after shear (pilot test)

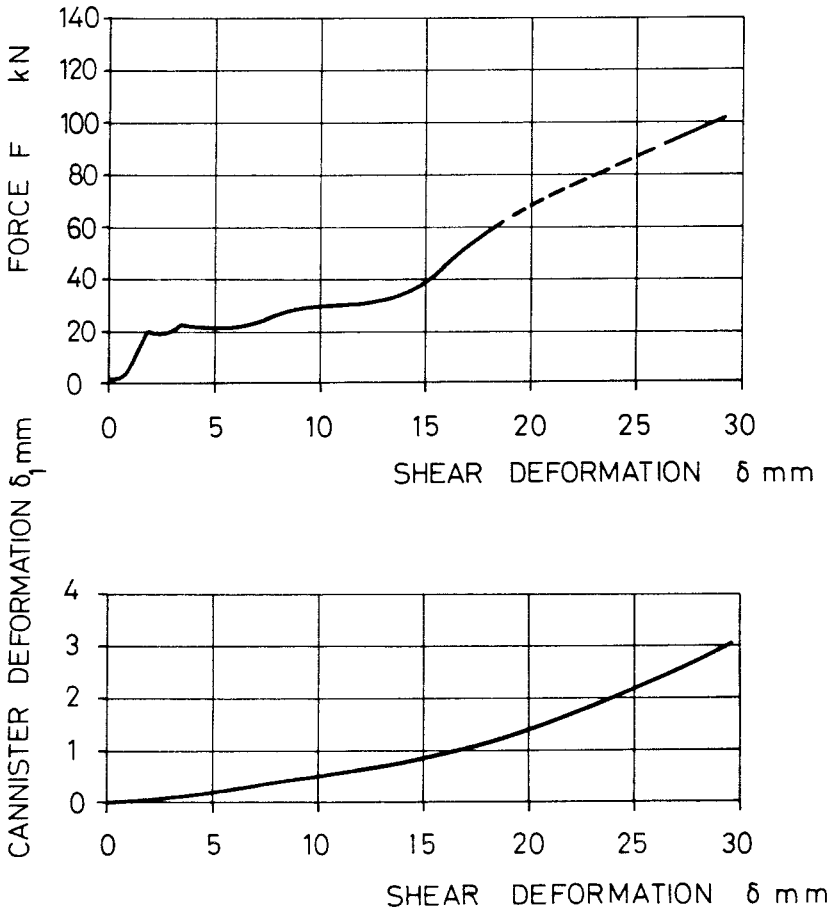

Fig 4:2. The total force F and the movement of the end of the canister as functions of the shear deformation

The conclusion from the pilot test was that the apparatus and the measuring systems worked very well. It was also concluded that the nonsaturated sand-bentonite mixture was very soft and thus well suited as a buffer material as regards the mechanical properties.

4.3 Slow test (Test 1)

This was the first real test using saturated compacted bentonite. The instrumentation was the one shown in Fig 3:3 with one exception, namely that pressure transducer No 10 was not working properly and therefore mounted.

The cylinder was filled with 18.3 kg of highly compacted bentonite with a density of ρ=2.14 t/m^3 and a water content of 9 %. Since the empty inner space of the cylinder was 10.03 dm^3 the density of the water saturated expanded bentonite would be ρ=2.05 t/m^3.

4.3.1 Saturation phase

The saturation was made by keeping the surrounding filters saturated with distilled water. The calculations had shown that the saturation process would take about two months. To make sure that the bentonite was saturated at the shear test one extra month was added and the time between the water connection and the shear test was altogether three months. During the water saturation process the swelling pressure was continuously measured by use of the pressure transducers. The amount of water taken up by the bentonite was also measured.

The total pore volume of the filters is 1.8-2.3 dm^3 (theoretically 2.3 dm^3 but measured at the pilot test 1.8 dm^3). The compacted bentonite, which had an original density of ρ=2.14 t/m^3 and a water ratio of w=9 %, filled up 8.55 dm^3 of the total inner volume of 10.03 dm^3. The air-filled pore space of the bentonite was 0.82 dm^3. The total volume of these three air-filled volumes was thus 4.1-4.6 dm^3. After two months 4.4 dm^3 water had been taken up, while no water was taken up in the last month.

The development of the pressure as measured by the five transducers is shown in Fig 4:3. As can be seen the pressure from four of the

five transducers were stabilized after 40 days. After 60 days there were only slight changes and they were probably due to internal swelling and compression processes. The final pressure was between 8.5 MPa and 10.5 MPa. The variation may reflect an inhomogeneity of the bentonite but may also be caused by a change in reference values of the transducers. The output voltage at zero stress seems to have been changed during mounting and at high stresses, and this is probably due to the fact that the transducers had to be mounted in a somewhat improper way in order not to risk any bentonite penetration between the transducers and the filter. The average swelling pressure σ_s=9.4 MPa is in very good agreement with the laboratory measured value at the density ρ_m=2.05 t/m3.

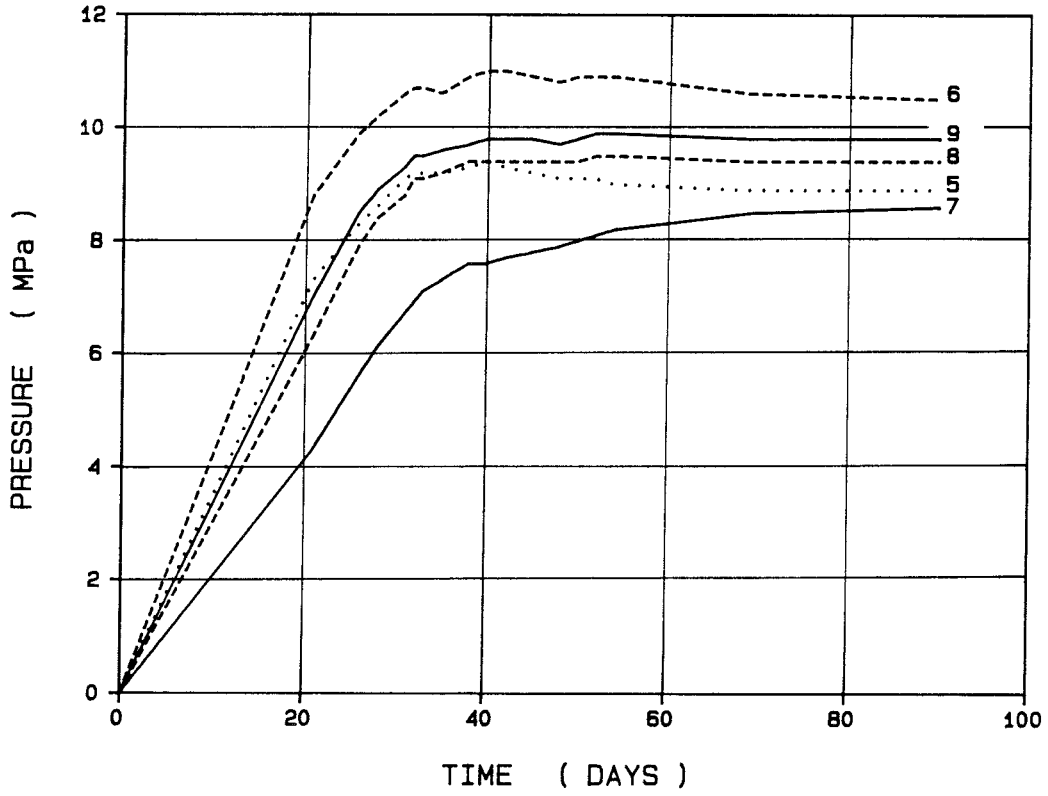

Fig 4:3. Swelling pressures measured during the water uptake process of the first slow test (see Fig 3:3)

4.3.2 Shearing phase

The shearing took place after 90 days in one of the big compression machines at the Technical University of Lund. The rate of shear was 1.9 mm/min and the whole shear deformation 30 mm took 16 min. Data from the transducers were collected and recorded directly by printers which gave the output signals as functions of time. These values were recalculated by aid of calibration curves to the measured values of stress, strain, deformation and force and then plotted.

Figs 4:4-4:7 show the recalculated values as functions of the shear deformation. The shear deformation measured by Transducers 11 and 12 differed. The end of the sheared cylinder had a deformation which was 6 mm more than that of the central part. The measured values given in Figs 4:4-4:7 are plotted as functions of the deformation in the shear plane (transducer 12) since this is the most interesting strain.

The measured pressure change varied from negative values recorded during the larger part of the test by the outer transducer (7) in the canister, to the value 13 MPa, which was the maximum pressure measured by Transducer 9 in the filter.

The strains measured by the strain-gauges show that the copper started to deform after 6-7 mm shear. This effect could not be observed in the other two tests. It is uncertain if this is due to a initial tipping of the canister or if it is caused by any deficiencies of the strain gauges. The maximum strain registered was 1.4 % by the two Gauges 16 and 17. The gauges close to the shear plane (14 and 15) failed after 7-9 mm shear while the outer gauge (18) was very little effected. All the strains had the form of shortening.

As expected the force was concentrated to the two transducers close to the shear plane. The total maximum force was 160 kN. the non-linear behaviour of the copper and bentonite is clearly seen in the force - deformation curve where 70 % of the total force is registered after only 10 % of the total deformation. Fig 4:8 shows two photos of the equipment.

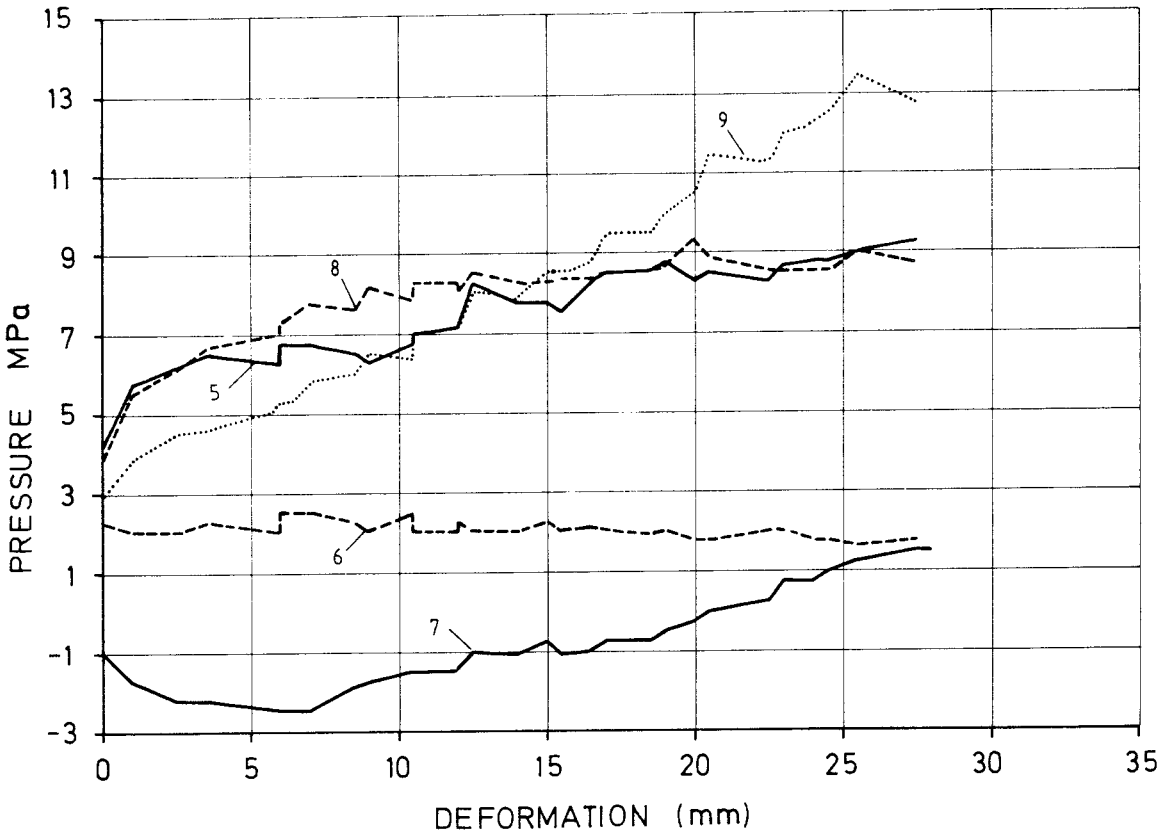

Fig 4:4. The pressure increase from the bentonite on the canister and the filter as function of the shear deformation in Test 1 (see Fig 3:3)

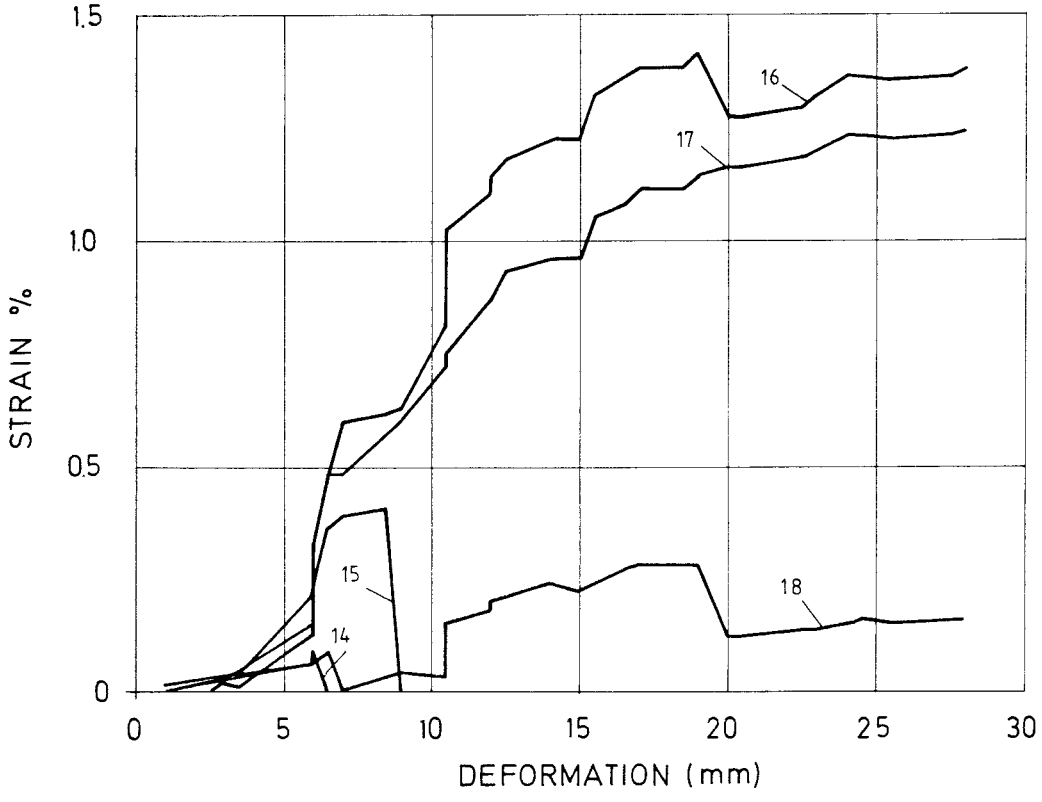

Fig 4:5. The strain of the canister surface measured by the strain gauges as function of the shear deformation in Test 1 (see Fig 3:3)

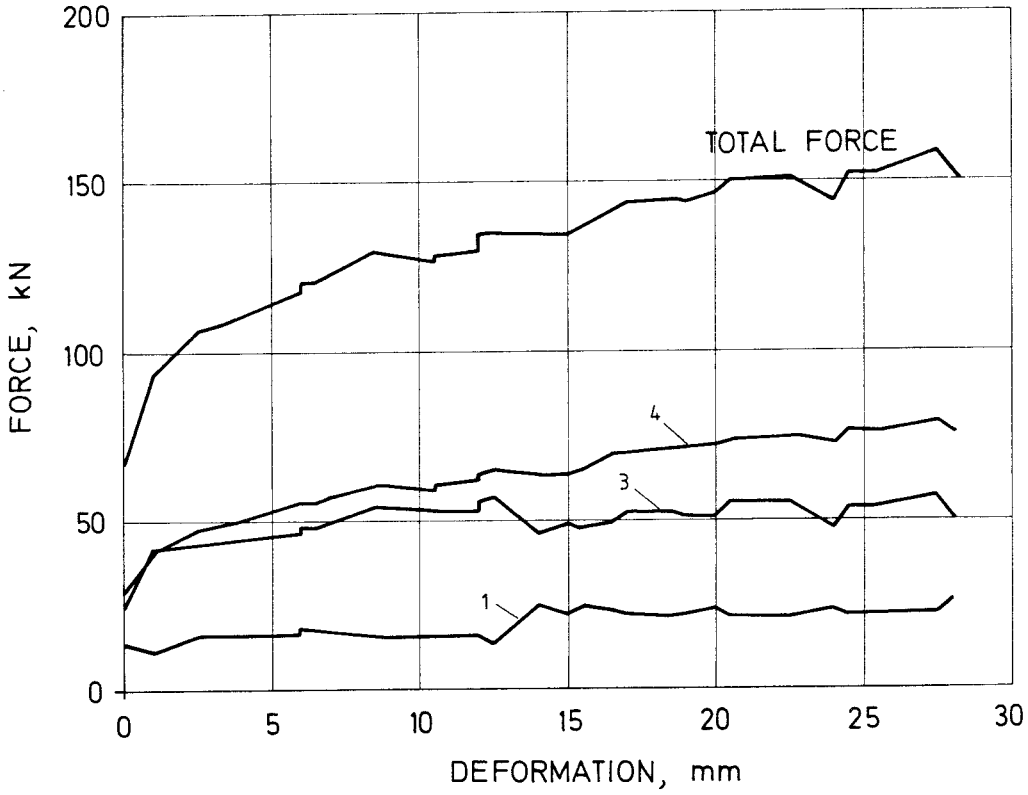

Fig 4:6. The force measured by the force transducers as function of the shear deformation in Test 1 (see Fig 3:3)

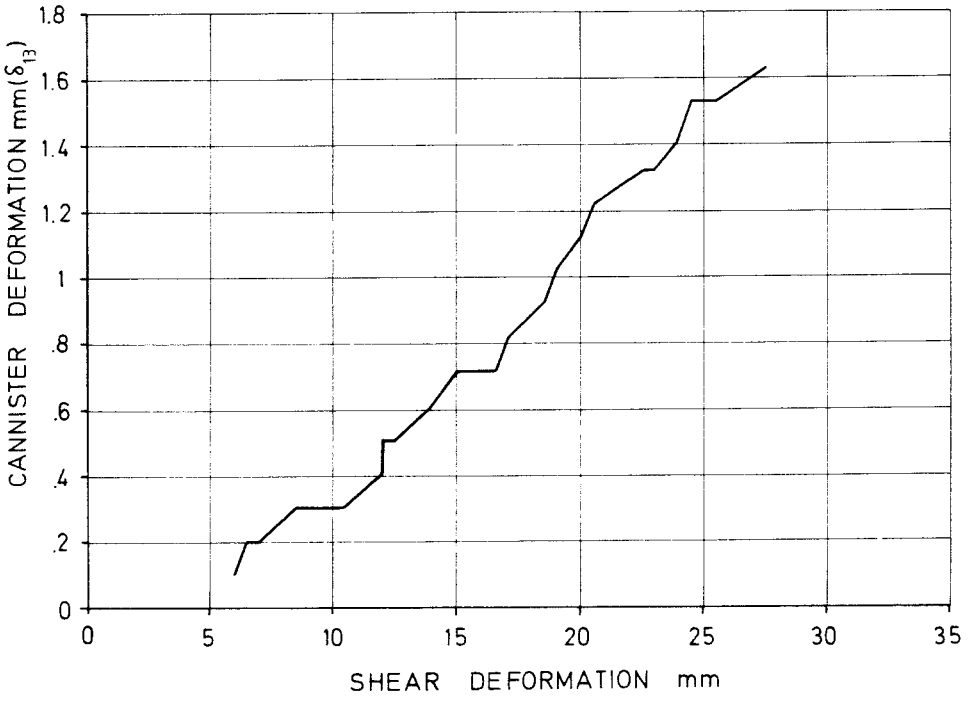

Fig 4:7. Movement of the end of the canister as function of the shear deformation in Test 1 (see Fig 3:3)

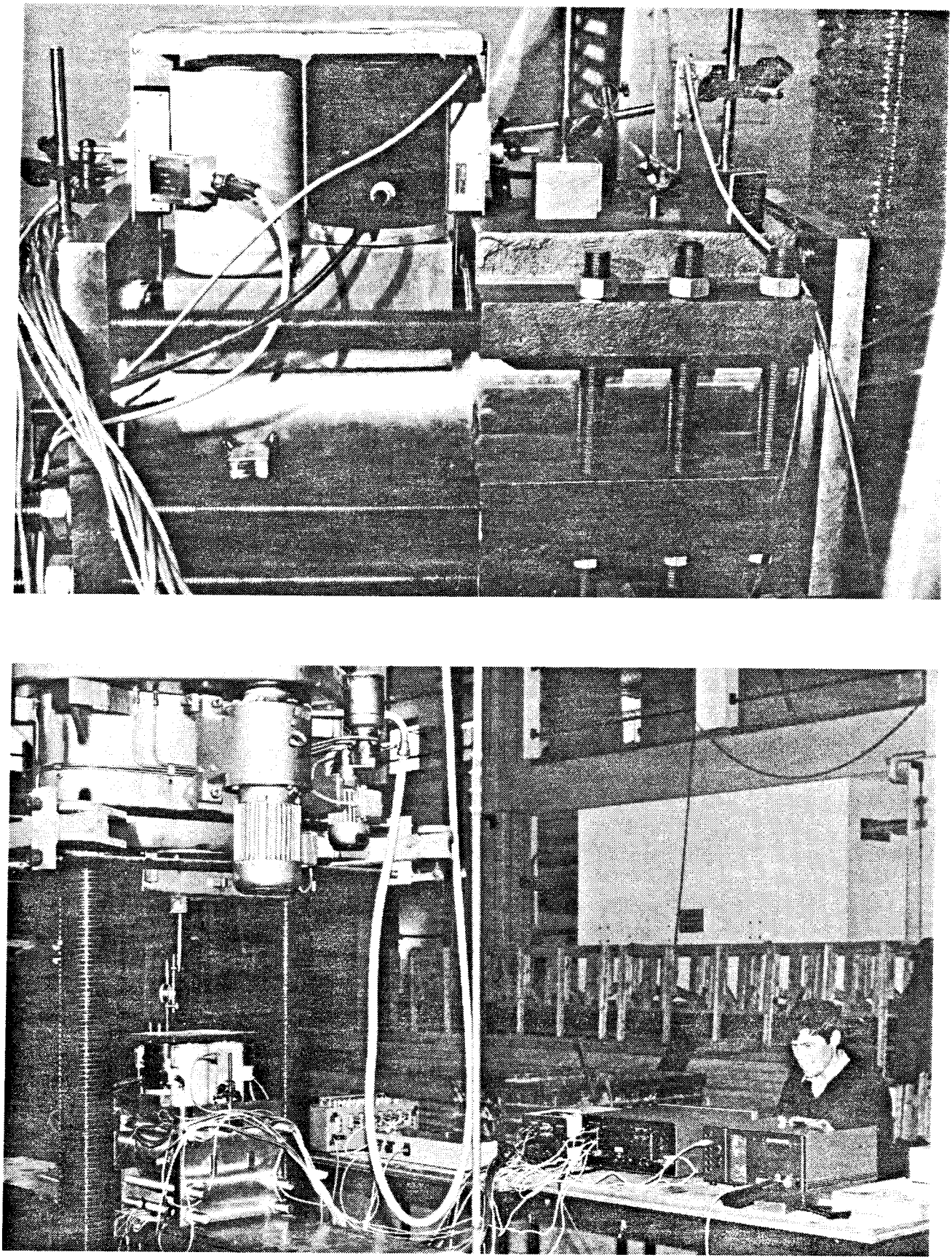

Fig 4:8. The upper picture shows the apparatus just after shear. The deformation of the left cylinder can be seen. The lower picture shows the press and the data collection system

After the end of the test the equipment was taken apart and the bentonite carefully excavated. The water content and density were measured at every fifth centimeter axial distance according to a certain scheme. The results are shown in Table III. Fig 4:9 shows the codes of the data in Table III. The samples were taken at a distance of about two cm from the filter.

The water content values shown are quite evenly distributed but an increase with depth can be noted.

The radial distribution of the water content between the canister and the filter was also determined by sampling radially at the different levels. As can be seen from the results in Fig 4:10 there is an increase in water ratio close to the filter.

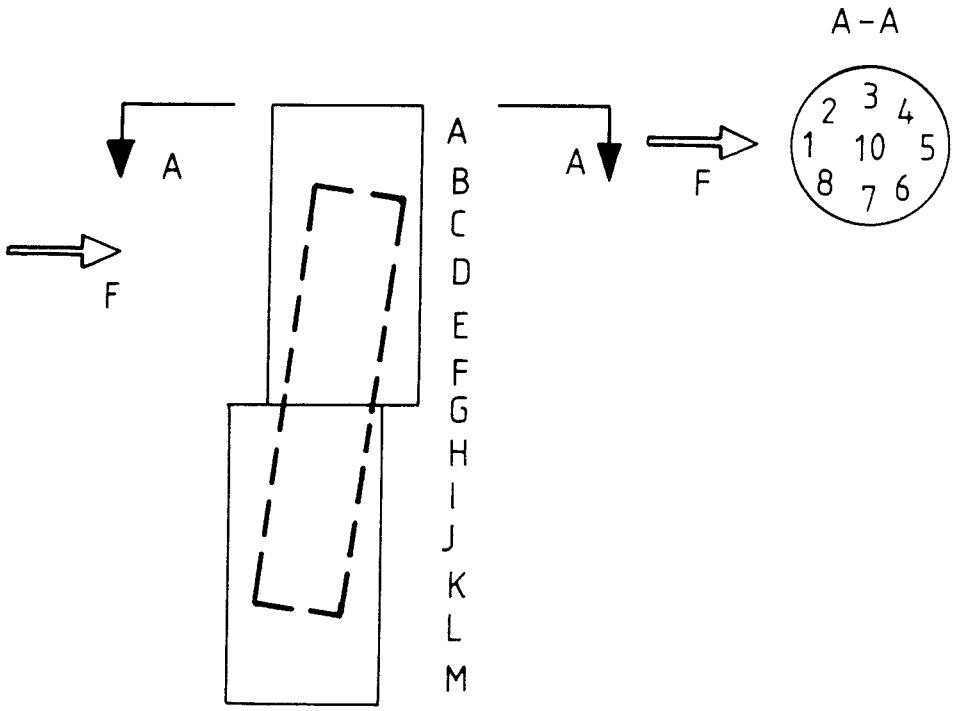

Fig 4:9. Coding of the water content and density determinations

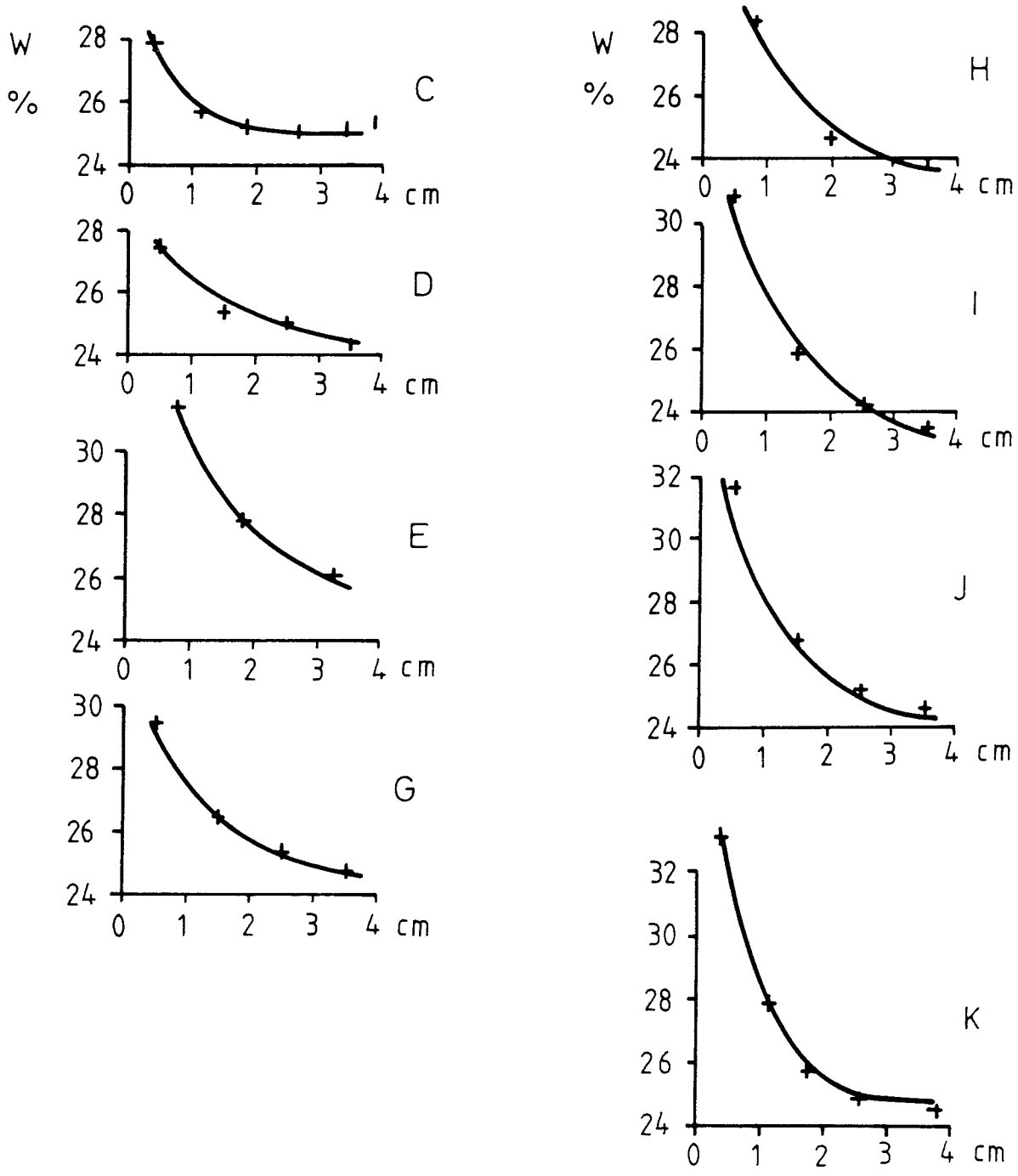

Fig 4:10. Radial water content distribution as function of the distance from the filter in Test 1. The left axis correspond to the filter

The high water content in the lower part was caused by the long time between start and finish of the excavation. The excavation took several days in this test and the bentonite could thus take up water from the filter and swell when the confinement was removed. The excavation of the subsequent two tests was planned to take place in one day to avoid such a swelling.

The radial distribution of the water contents shows a very clear increase in water content near the filter. The homogenization is obviously not completed. This process is further dealt with in Chapter 6.

Table III. Water content (%) and density (t/m^3) in Test 1. See Fig 4:9

Lev/ pos	1	2	3	4	5	6	7	8	G	ρ*	Dist from shear plane cm
A	25.4		24.7		25.0		24.8*		28.4	2.02	30
B	24.3		23.1*		24.0		24.1		25.8	2.02	25
C	24.5*		24.4		25.1		24.1			2.02	20
D	24.0*	23.6	24.2	25.1		24.0	24.0	24.5		2.02	15
E	24.4	24.0	25.3	25.1		25.2	25.4	*		2.01	10
F	25.3	25.3	25.9	25.5		25.7	25.5	26.1*		1.99	5
G	25.3	24.8	24.4	25.4		25.8	25.8	26.3*		1.98	0
H	25.5	25.1	25.5	24.5	25.3	24.7	24.5	24.8*		1.98	-5
I		25.4	24.8	25.1	26.3*	26.3	24.9	28.4		1.97	-10
J		25.2	25.0	25.0	25.9*	26.3	25.9	26.2*		1.99	-15
K	27.8	26.7	26.3	26.6*	27.6	27.3	27.2	26.6		1.96	-20
L	-	-	-	-	-	-	-	-	-	-	
M	27.4	27.5*	27.8	28.0	27.7	28.4	28.1*	26.9	31.6	1.95	-30

The density was determined by cutting cylindrical pieces of bentonite and then measure the height and diameter. The average density was ρ=1.99 t/m^3 and the corresponding water ratio w=25.4 %. Using the density of the soil particle ρ_s=2.70 t/m^3 and the density of water ρ_w

= 1.00 t/m³ the average degree of saturation was ρ_w =98 %. The corresponding density at saturation would be ρ_m = 2.00 t/m³. The difference in density before and after the test can be explained by swelling due to water uptake during excavation and by elastic swelling which occurs when the high stresses are released.

During the excavation, the position of the canister in the simulated deposition hole after shear was measured. After excavation the shape of the deformed canister was also measured. Figs 4:11 and 4:12 show the position of the canister and the deformed canister. The deformed shape is multiplied by 10. As expected, the canister was deformed symmetrically in relation to the shear plane. 25 % of the canister length from the top and bottom had been almost undeformed while the whole deformation had taken place in the remaining central 50 %. However, as can be seen in Fig 4:11 the canister had been somewhat rotated during shear which is confirmed by the displacement of the upper part compared to the lower part which is only 14 mm or 50 % of the total shear deformation. The deformed canister is shown in one of the photos in Fig 4:13. The shape and position of the canister after completion of about 50 % of the excavation is shown in the other photo.

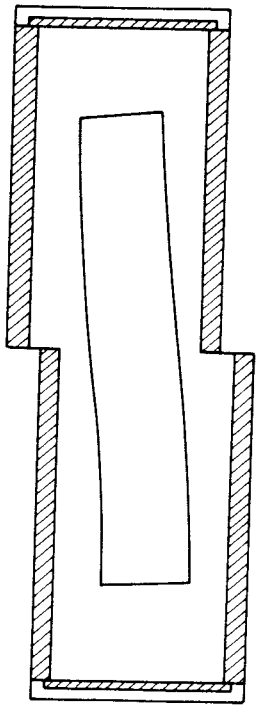

Fig 4:11. Position of the canister after Test 1

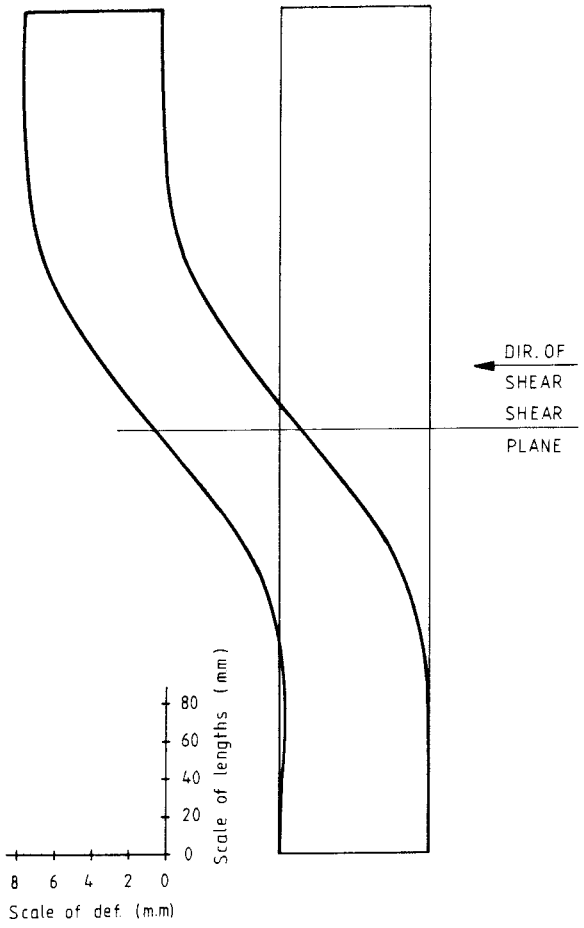

Fig 4:12. The deformed canister after Test 1

4.4 Quick test (test 2)

The instrumentation in Test 2 was the same as shown earlier in Fig 3:3 with the exception that the four force transducers were reduced to three and that strain transducer 13 was not used. Pressure transducer 10 was repaired and mounted in this test.

4.4.1 Saturation phase

The filters were cleaned by ultrasonic treatment in water. The cylinder was filled by 18.2 kg highly compacted MX-80 bentonite in the same way as in test 1. The average water ratio was w=8.4 % which would give a final density at saturation of ρ_m=2.05 t/m^3.

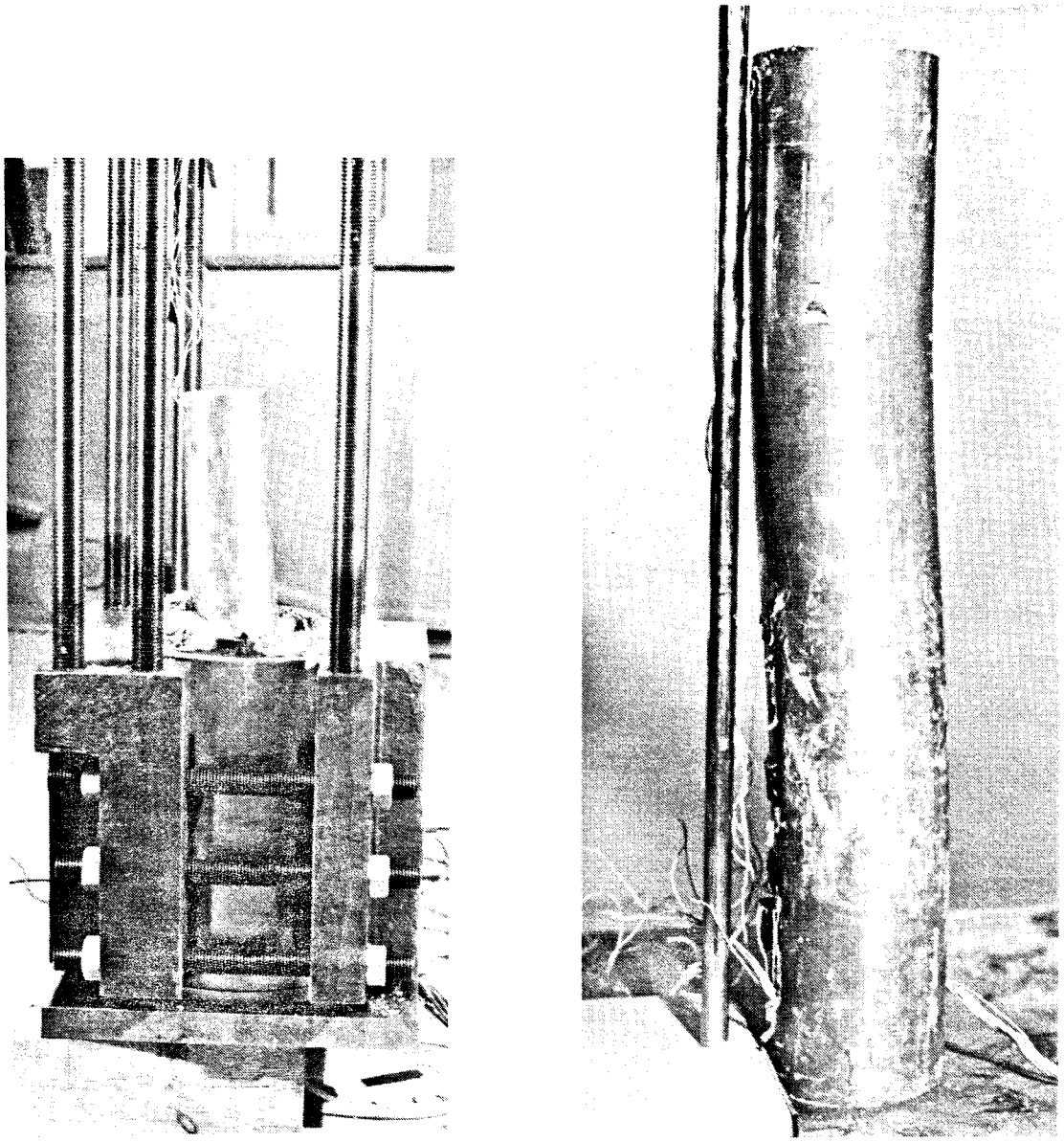

Fig 4:13. The canister during excavation (left photo). The tilting of the canister can clearly be seen. The right photo shows the deformed canister

The saturation was achieved as in Test 1 by letting water flow through the filters. This process was allowed to continue for four months which means twice as long time as necessary according to the theoretical calculations.

The development of the measured swelling pressures is shown in Fig 4:14. Only very small changes were recorded after two months. The scattering is quite large for reasons not known but the average swelling pressure σ_s=8.9 MPa is close to that of Test 1 (9.4 MPa).

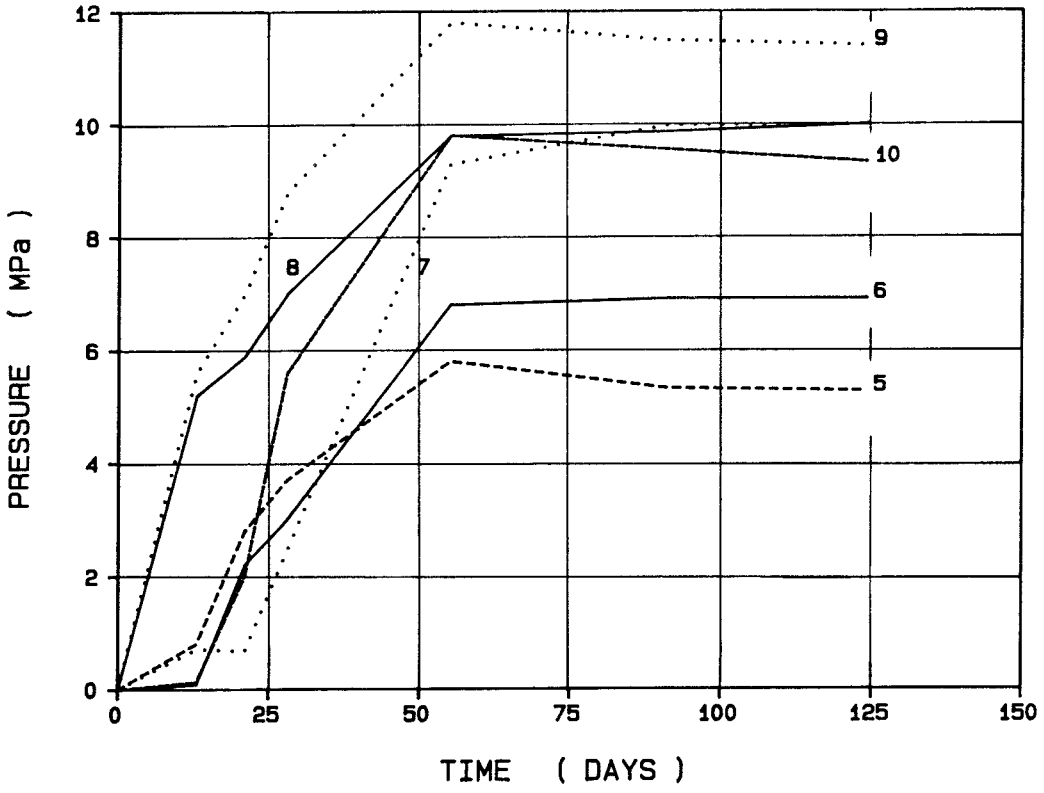

Fig 4:14. Swelling pressure measured during the water uptake process in Test 2 (see Fig 3:13)

4.4.2 Shearing phase

Shearing took place after 4 months in the same way as at test 1, which means that one of the big compression machines at the Technical University of Lund was used. The rate of shear was 1.9 mm/sec and the whole shearing 30 mm took 16 sec, which is 60 times faster than in Test 1. The speed was higher than normally handled by the press and required some reconstruction. Data collection and plotting were made as in test 1.

Figs 4:15-4:17 show the results from the shearing. The development of the force is similar to that of test 1 thus indicating a concentration at transducer 3 and 4 and a non-linear force-deformation curve. A decrease in pressure of the bentonite near the end of the canister occured due to rotation of the canister as illustrated by Fig 4:16. Transducers 7 and 10 show a decrease in pressure of 5 MPa while the other transducers show increasing pressures varying from 7 MPa to as high as 22 MPa.

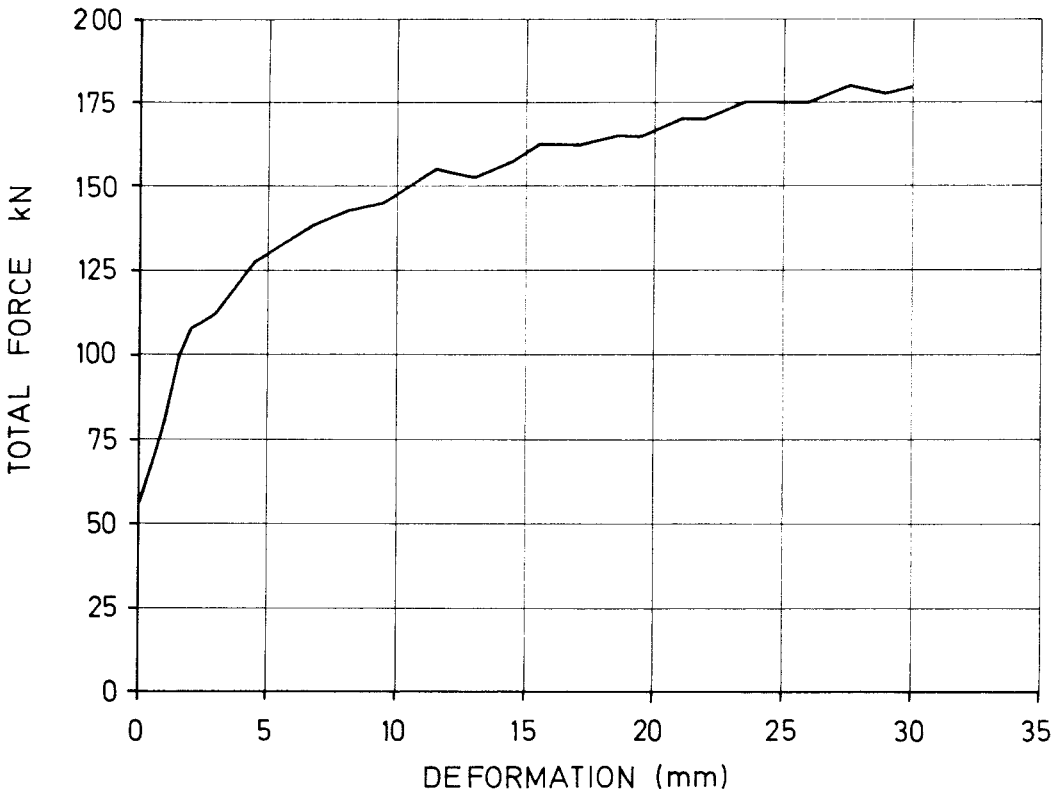

Fig 4:15. Total force plotted as function of the shear deformation (Test 2)

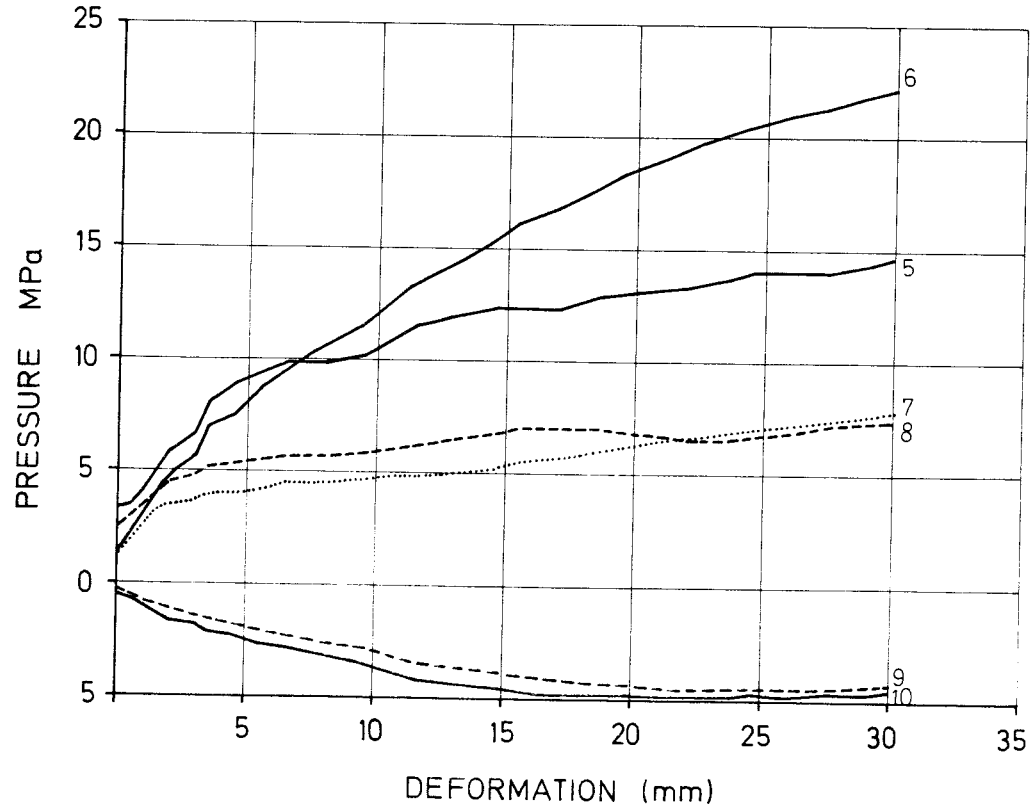

Fig 4:16. Change in pressure from the bentonite on the canister and filter during Test 2 (see Fig 3:3)

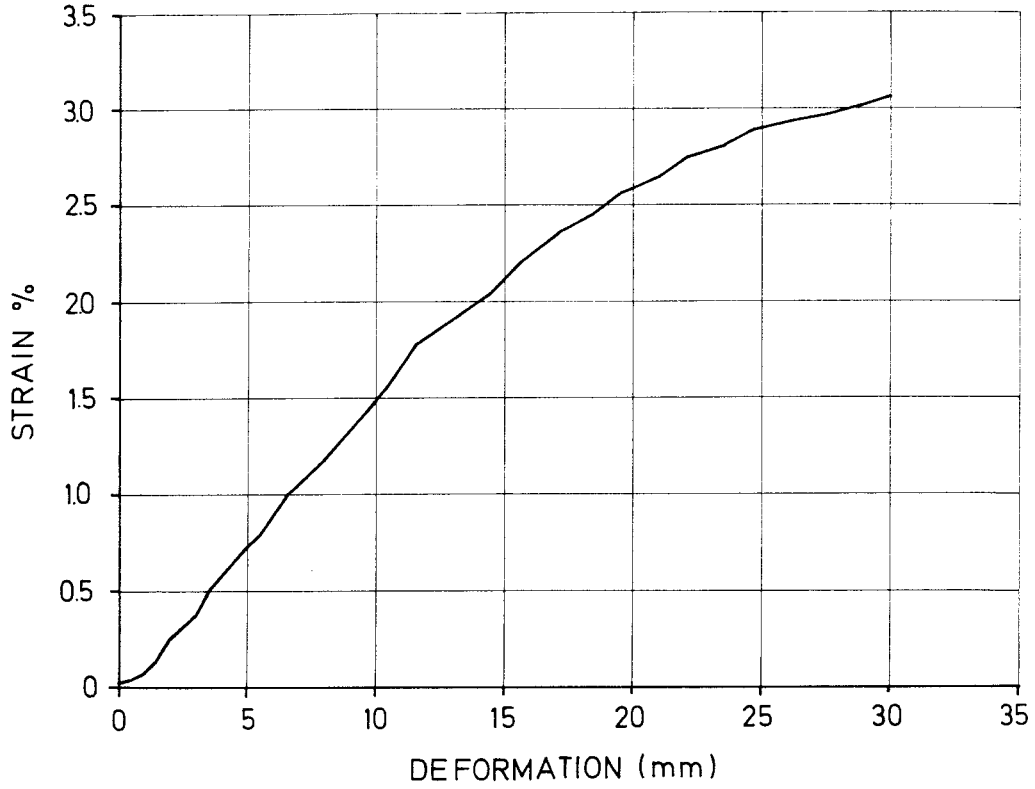

Fig 4:17. Strain measured by Gauge 17 in Test 2 (see Fig 3:3)

The measurement of the canister strain by the strain gauges was not very successful. Only one of the 5 gauges was working at the start of the shear test. The other 4 failed during the saturation phase. The maximum strain measured by the functioning gauge 17 (Fig 4:17) was a compression of 3 % at the end of the test.

The total maximum force was 180 kN which is 20 kN or 13 % higher than in Test 1. A small rate effect therefore seems to exist.

The day after the shear test the apparatus was taken apart and excavation started from both ends at the same time in order to finish the sampling as soon as possible after exposure of the bentonite. The whole excavation was finished within 8 hours. Results from the water ratio and density measurements are shown in Table IV. The location of the different samples are shown in Fig 4:10. The densities shown in Table IV refer to the water content determinations indexed 1 or 2.

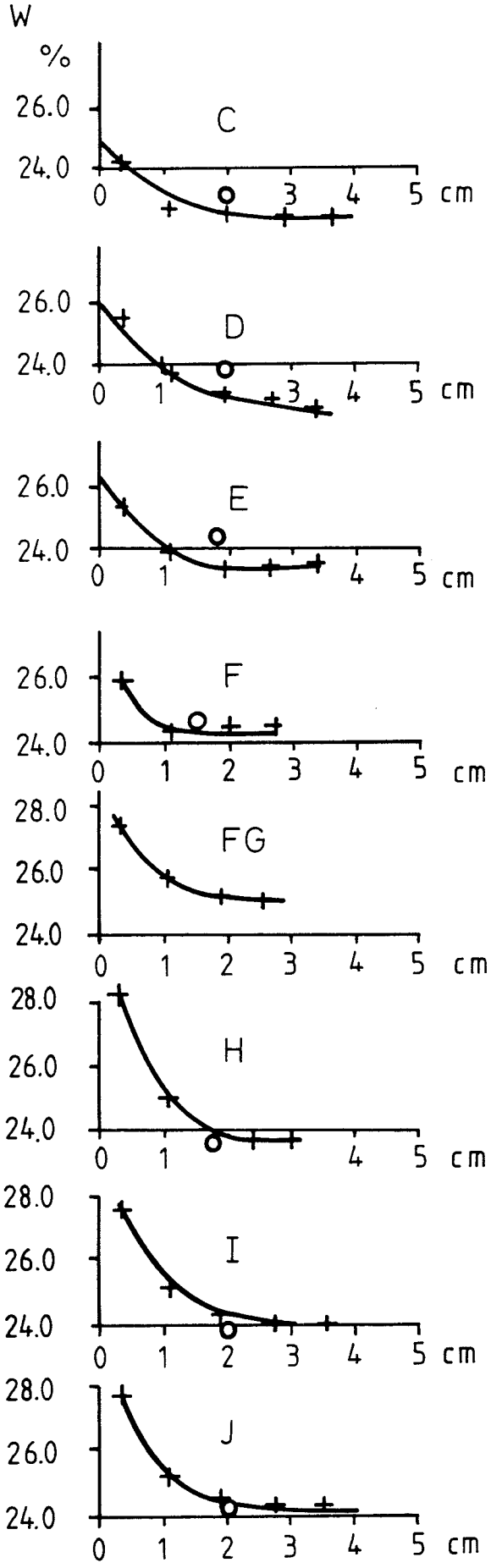

Fig 4:18. Radial water content distribution as function of the distance from the filter (Test 2)

Fig 4:18 shows the radial distribution of the water contents measured at the different levels. It is clearly seen that there is a remaining difference in water content meaning that the clay had not been homogenized in the four months period. The dot marked with a small circle represent the average water content at the corresponding level in Table IV. The weighted average water ratio was w=24.7 % while the weighted average density was ρ=2.02 t/m^3. These values were calculated taking into account the inhomogeneity of the bentonite and the variation in sampling frequency.

Table IV. Water content and density (t/m^3) determined in Test 2 (see Fig 4:10)

Lev/ pos	1	2	3	4	5	6	7	8	10	ρ_1	ρ_2	Dist from shear plane (cm)
A	24.4		24.3		24.3[1]		24.4		28.7[2]	1.90	1.94	30
B	23.0		23.1		23.3		22.9[1]		25.3[2]	2.03	1.96	25
C	23.1	23.6	23.6	24.2[1]	23.3	23.0	22.7	22.6[2]		2.05	2.08	20
D	22.6	23.8	24.5	25.0	24.5	24.0	23.4	22.0		2.04	2.10	15
E	23.5	24.4	24.9[1]	25.3		24.1	24.0	23.6		2.08	2.04	10
F	24.1	24.8	24.6[1]	25.4	24.6	24.2	24.2	24.2[2]		2.02	2.07	5
G	24.3[1]	25.3[2]			(ρ=2.05)-	24.5		24.8-(ρ=2.04)		2.03	2.03	0
H	25.0	24.9	24.6[1]	24.3	24.4	24.2[2]	24.4	24.3		2.04	2.06	-5
I		23.8	23.5	23.6[1]	23.5	24.0	23.5	23.6		2.05	2.08	-10
J		23.8	23.6	23.8[1]	24.2	24.1	23.5	23.6		2.03	2.04	-15
K	25.2	24.3	24.0[1]	24.1	24.6	24.1	23.8[2]	24.0		2.03	2.02	-20
L	24.3		24.2		24.3		24.0[1]		26.8[2]	2.01	1.96	-25
M	26.3		25.8[1]		25.3	(ρ=1.99)-	26.0		30.8[2]	2.01	1.94	-30

Using ρ_s=2.70 t/m^3 and ρ_w=1.00 t/m^3 the degree of saturation will be S_r=100 %. As in test 1 there is some disagreement between the expected and measured density after the test. This is further dealt with in Chapter 6.

The position of the canister after the shear test is shown in Fig 4:19. The deformed shape of the canister, with a 10 times increased scale of deformation, is shown in Fig 4:20. The shape is very similar to the shape of the canister after test 1. However, the canister has deformed by 18.5 mm which is 62 % of the total shear deformation and thus more than in Test 1, where the percentage was only 50 %.

4.5 Super quick test (Test 3)

The third test was made at a rate of shear of 160 mm/sec. The instrumentation was identical to that of the prior tests. Data collection in this test was made by a computer and the results recorded on tape.

4.5.1 Saturation phase

The apparatus was loaded by 18.2 kg highly compacted bentonite with a water ratio of 8.5 % as in the two prior tests. The expected final density was ρ_m=2.05 t/m^3 for this test as well.

The saturation was continued for only 2 months for the following reasons:

1 Two months is sufficient theoretically as well as according to the experience from the other two tests

2 The influence of the time between water connection and sampling on the degree of homogenization can be studied (2, 3 and 4 months in the three tests)

Fig 4:21 shows the development of the measured swelling pressures. The scatter is very small for all the transducers except for No 9. The average final pressure was σ_s=9.3 MPa (9.4 MPa and 8.9 MPa at the preceding tests) which confirms the earlier measurements and shows that the bentonite is very close to complete saturation.

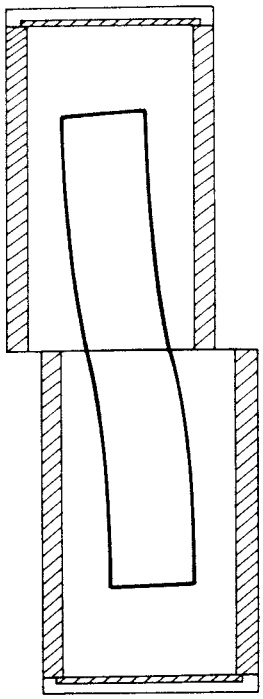

Fig 4:19. Position of the canister after shear in Test 2

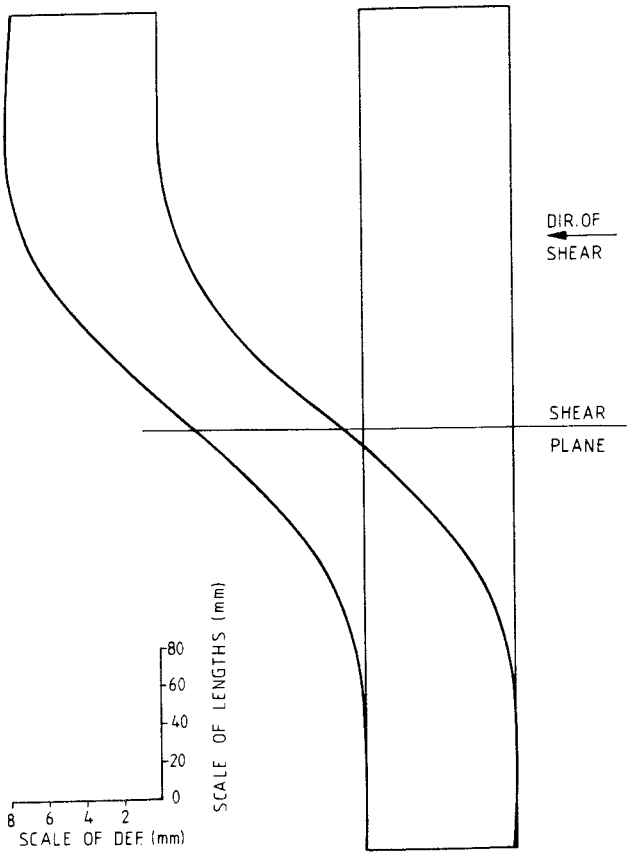

Fig 4:20. Deformed shape of the canister after shear in Test 2

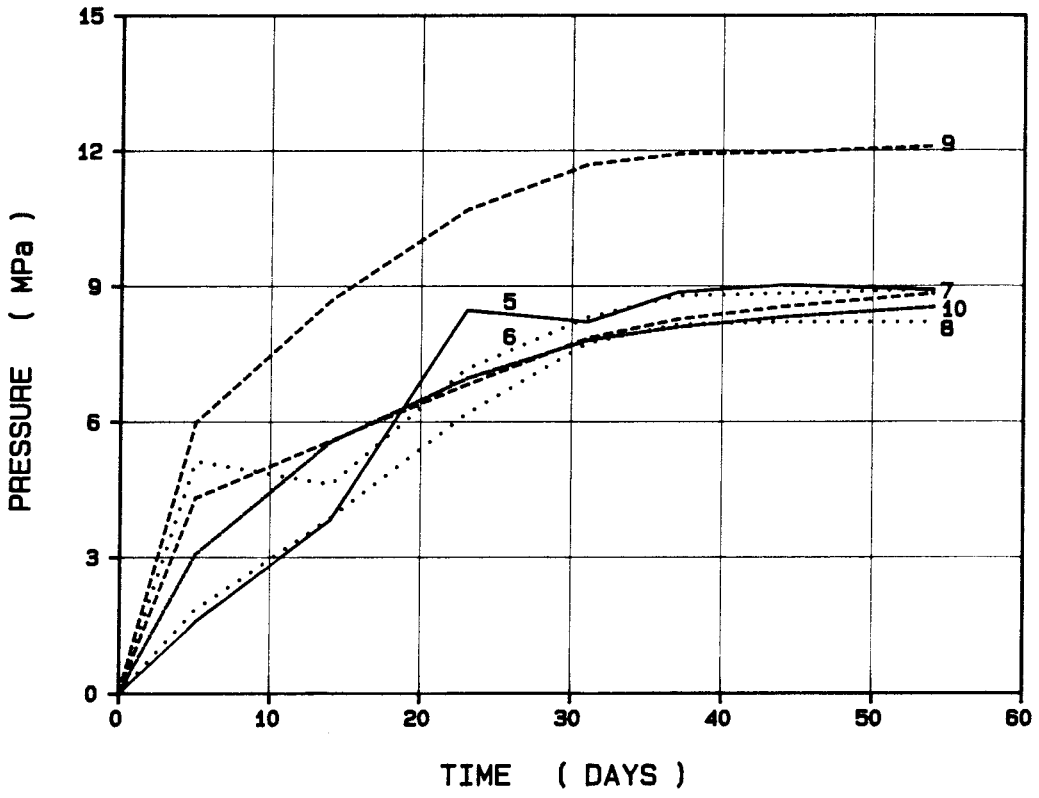

Fig 4:21. Swelling pressure measured during the water uptake process in Test 3 (see Fig 3:3)

4.5.2 Shearing phase

The shearing in test 3 could not be made at the Technical University because the compression machines were too slow. Instead the test was made in a huge machine at the private company Alfa Laval in Lund. This machine is usually occupied in the production of units for heat exchangers and designed for a compression speed of 160 mm/sec which is 85 times faster than the rate of shear at test 2. The rate is higher than originally intended for this test, but was still applied since it was expected to high-light the rate dependence.

Unfortunately, the total shear deformation was only 19 mm at the shear plane (transducer 12) and 23 mm at the upper end (transducer 11), which was 8-10 mm less than in tests 2 and 3. The first 15 mm were sheared at the rate 160 mm/sec while the last 4 mm were sheared at a slower rate. These deviations from the intentions were caused by difficulties in operating the compression machine.

With the above-mentioned small exceptions the super quick test was very successful. The data collection and all transducers, except for two, worked and gave reliable results although the first 15 mm were sheared in less than 0.1 sec. The results are shown in Figs 4:22-4:24. Fig 4:22 shows the total force as a function of the deformation. In this test no force was recorded by the outer transducer. The typical non-linear force-deformation curve, with a beginning of the plastic behaviour after about 3 mm, was registered in this test as in the other two tests. The force was 197 kN at the end of the test after 19 mm and this is 19 % higher than at the same deformation in Test 2, and 37 % higher than in Test 1.

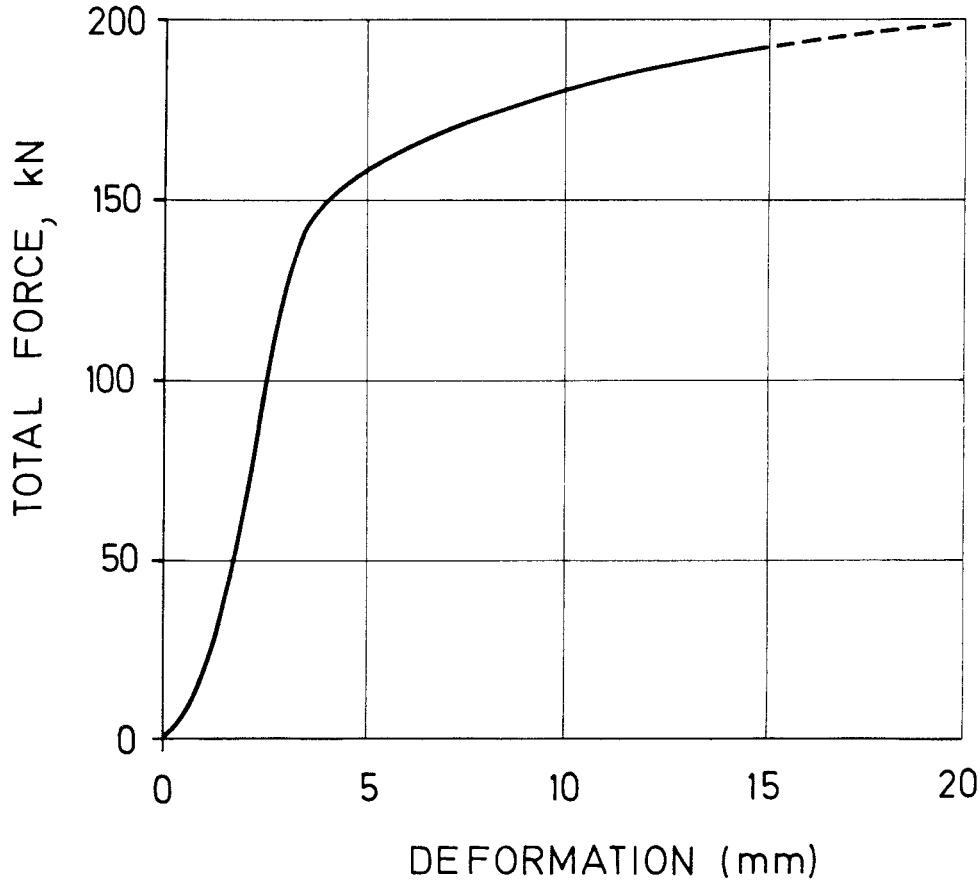

Fig 4:22. Total force as a function of the shear deformation in Test 3

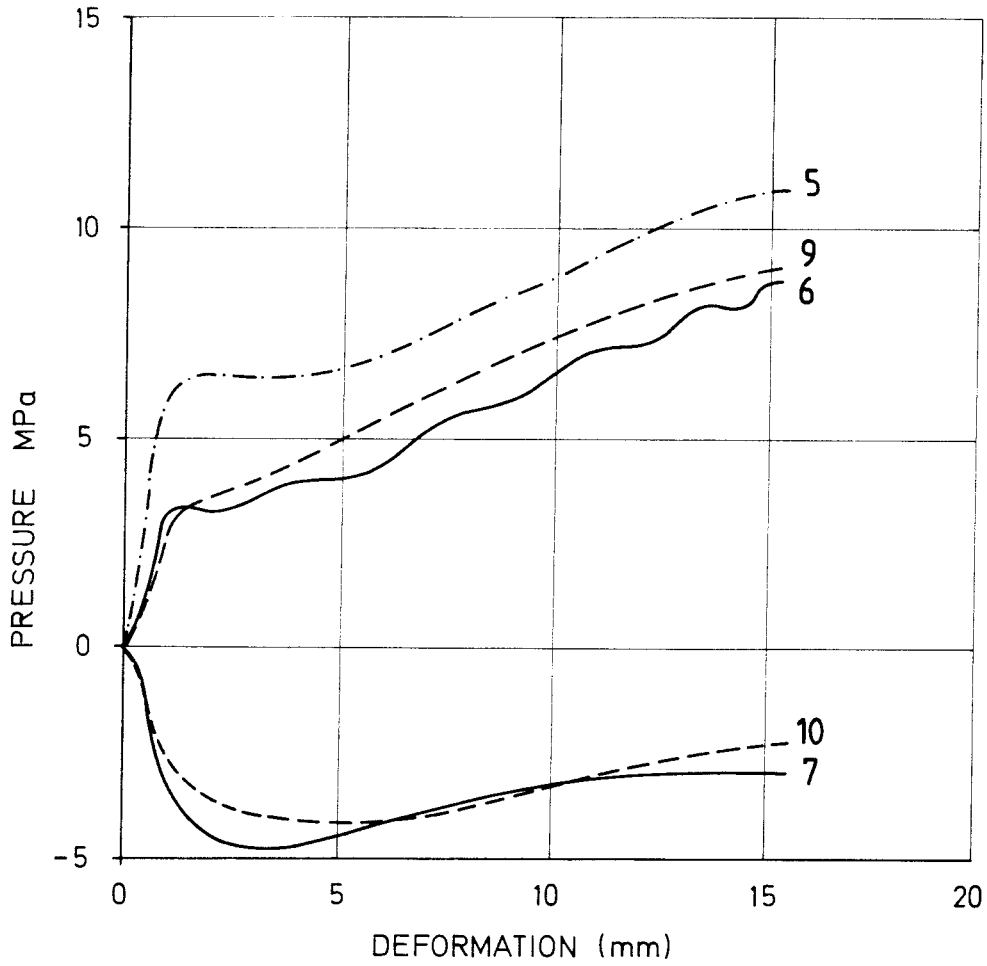

Fig 4:23. Change in pressure from the bentonite on the canister and filter as function of the shear deformation in Test 3 (see Fig 3:3)

Fig 4:23 shows the change in pressure from the bentonite during the shear. The pressures are similar to those measured in the prior tests with negative pressure at the outer transducers (7 and 10), medium high at the two middle (6 and 9) and high at the inner (5). Transducer 8 did not work.

The deformation of the canister as measured by the strain gauges is shown in Fig 4:24. The results agree very well with the results from the other tests with large compressive strains for Gauges 16 and 17 and small strains for the other ones. As in test 1, Gauge 14 was torn off after about 10 mm deformation, probably due to an axial displacement of the bentonite in relation to the canister. Gauge 18 did not work.

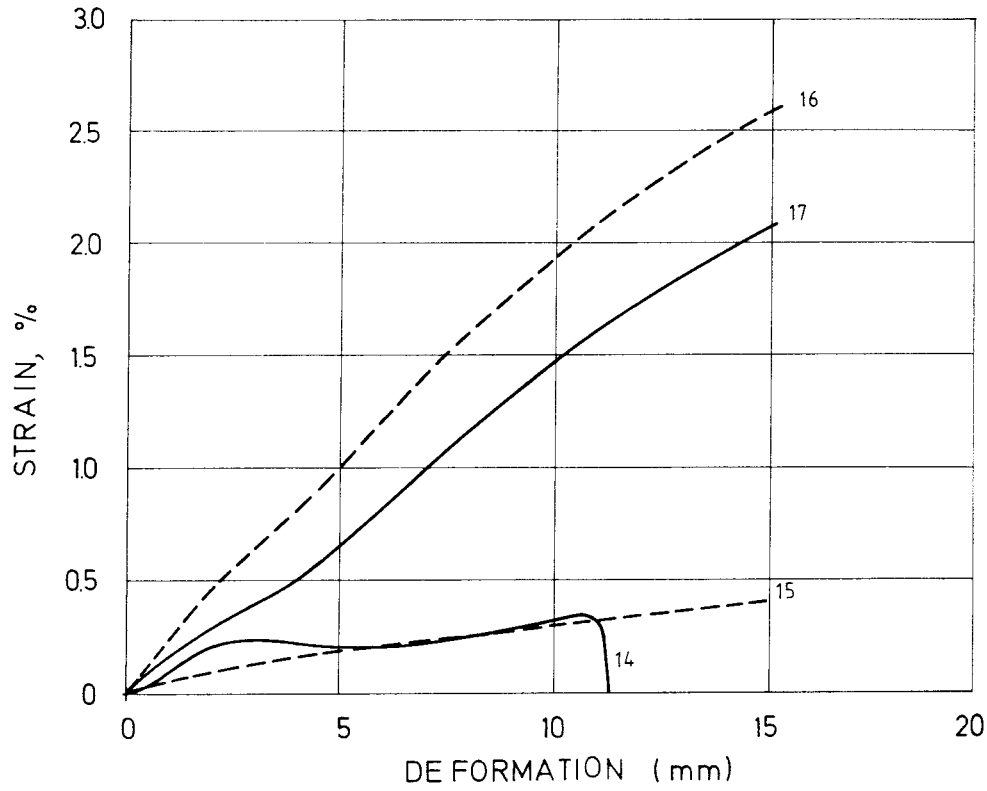

Fig 4:24. Strains in the canister as a function of the shear deformation in Test 3 (see Fig 3:4)

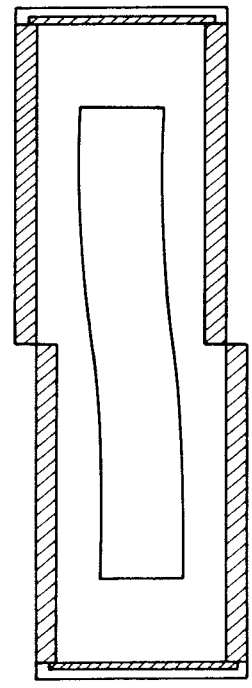

Fig 4:25. Position of the canister after shear (Test 3)

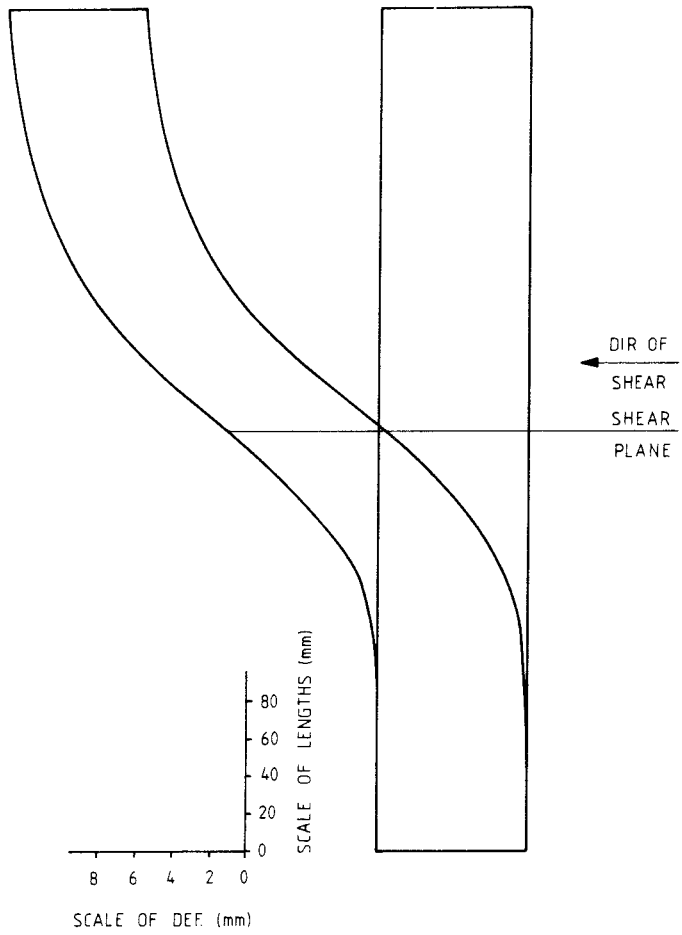

Fig 4:26. The deformed canister after shear in Test 3

The deformation of the canister and its position after shear are shown in Fig 4:25 and 4:26. The general appearance of the canister is identical to the shape of the canisters in Tests 1 and 2 but the canister is more deformed than in the other tests despite the small shear deformation. The strain was not symmetrical, however, the total shear deformation being 20 mm at one end, but only 14 mm at the other end. If the end faces of the canister are taken as points of reference the shear deformation was 18-20 mm. It seems that 70-100 % of the "rock" shear was transferred to the canister.

The excavation was made exactly as in Test 2. The results are shown in Table V. The scatter is similar to that of Test 2 with lower densities and higher water contents below and above the canister.

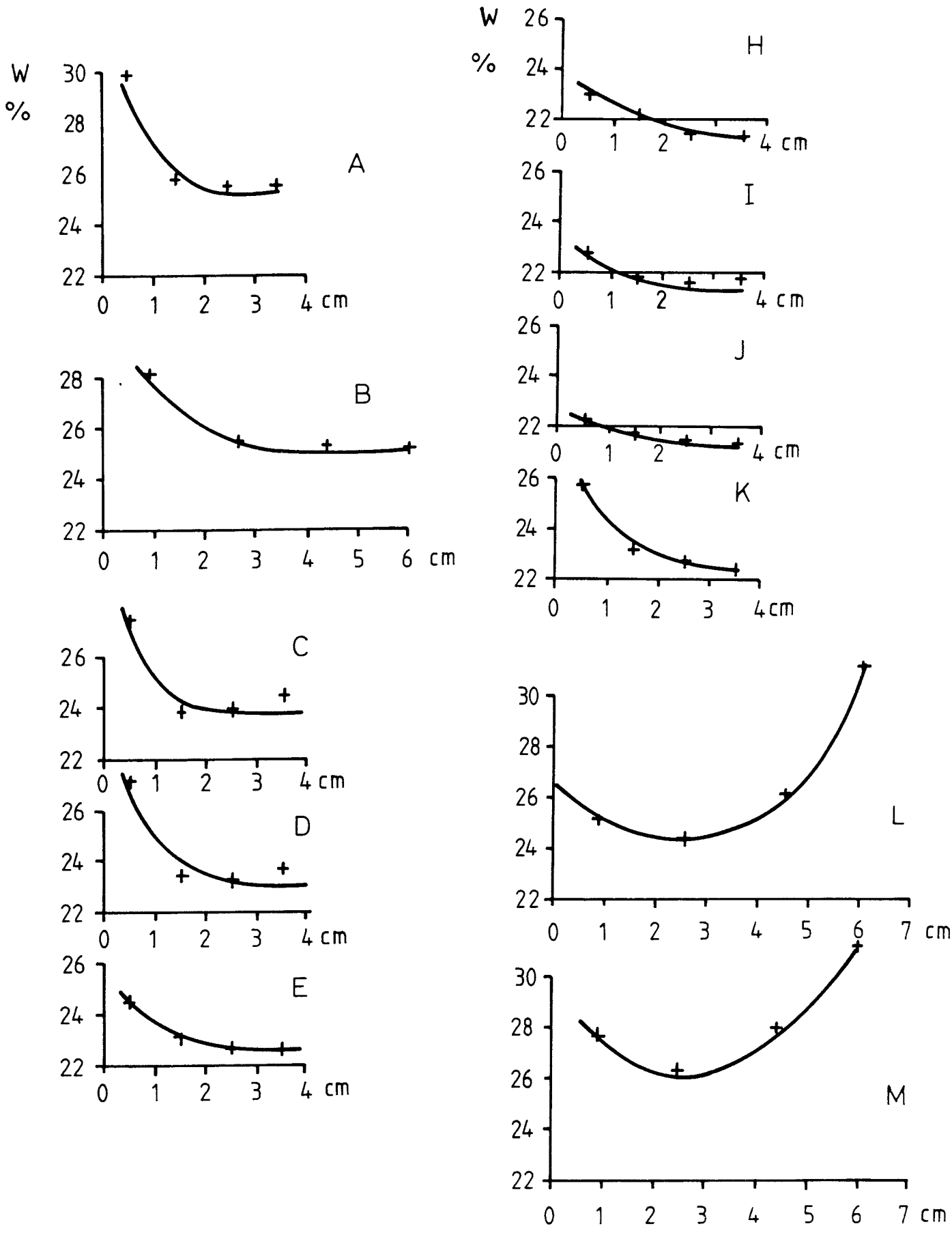

Fig 4:27. Radial water content distribution in Test 3. The distribution is plotted as a function of the distance from the filter

Fig 4:27 shows the radial water content distribution at all levels. The homogenization is about the same as in Test 2 despite the fact that the clay had matured for only half the time in Test 3. The increase in water content at larger distance from the filter at levels L and M was caused by the central hole in the original bentonite block.

If the inhomogeneity is taken into account the weighted average density is ρ=2.04 t/m^3 (2.037) and the weighted average water content w=23.9 %. This makes the degree of saturation S_r=100 % for this test as well as for test 2 (using the density values ρ_s=2.70 t/m^3 and ρ_w=1.00 t/m^3). The density is in better agreement with the expected value than in the other two tests, but it leaves about 1 % difference which probably can be explained by elastic swelling.

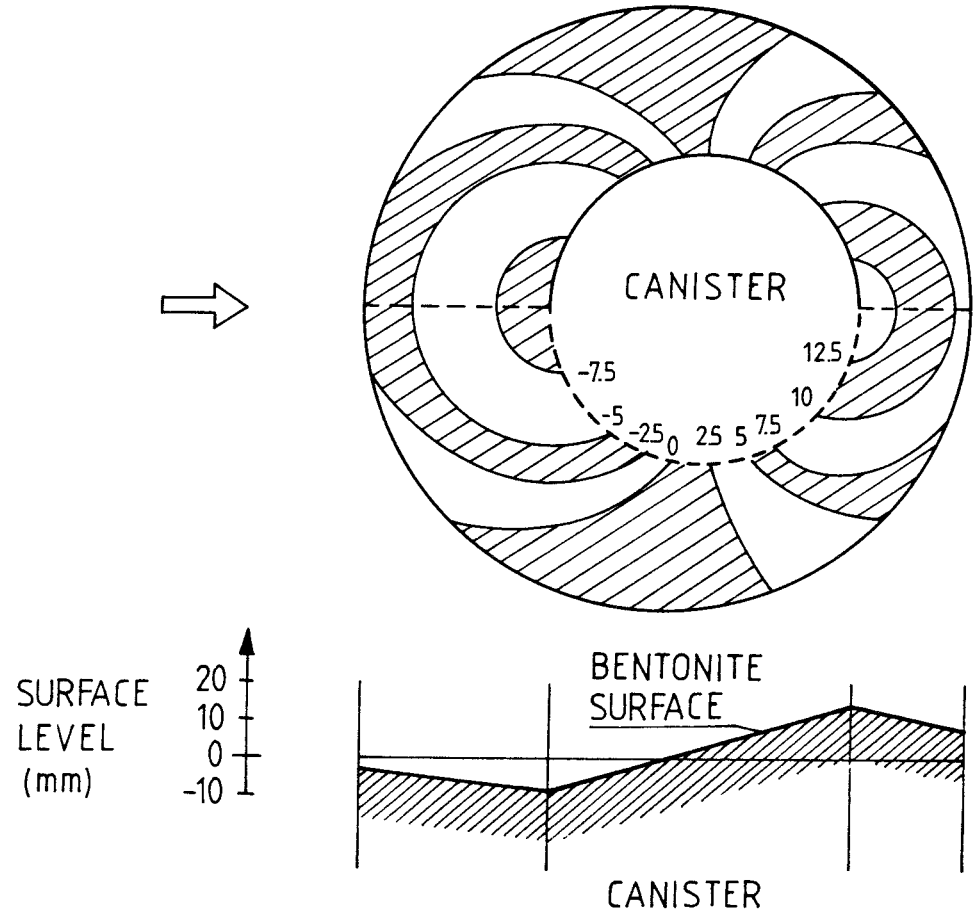

Fig 4:28. Plane and section after shear of the originally horizontal surface between the bentonite blocks in the shear plane. The upper drawing shows the isolines with the divergence from the horizontal in mm

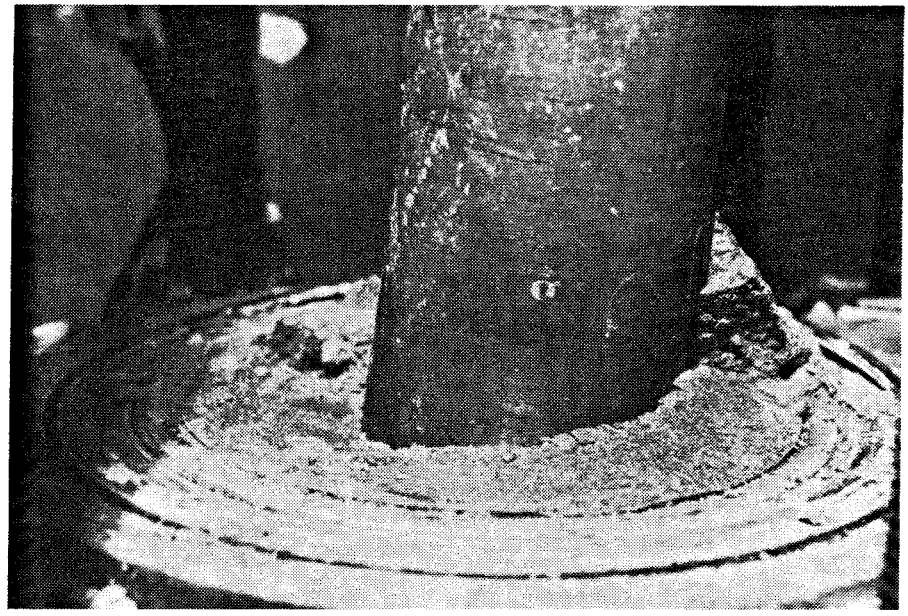

Fig 4:29. Photo of the deformed surface in the shear plane. The surface of the bentonite piece left on the right side of the canister is a shear surface

The displacement of the bentonite during shear has been detected by measuring the interface between the bentonite blocks. Fig 4:28 shows how the surface of the bentonite blocks in the shear plane was displaced axially. The isolines and the section show that the bentonite has moved from the compressed part to the expanded part. Fig 4:29 shows a picture of this surface with the deformed canister passing through it. On the right side of the canister there is a piece of bentonite left. The surface of this piece is a shear plane forming an angle of 35°-40° to the canister surface. The original angle of this surface was obviously 45° since the height is 4 cm or equal to the original bentonite thickness. This confirms the assumption made in the calculation in Chapter 2.2 that the length involved l_s in the shear is equal to the diameter of the deposition hole.

Table V. Water contents (%) and densities (t/m^3) determined at the excavation of Test 3 (see Fig 4:10)

Lev/pos	1	2	3	4	5	6	7	8	10	ρ_1	ρ_2	Dist from shear plane (cm)
A	26.2	25.8	25.7	25.6	25.2[1]	25.9	26.5	26.0[2]	29.5	2.02	2.02	30
B	25.2	25.0[1]	24.9	25.2[2]		25.1	25.4	25.4	25.8	2.02	2.03	25
C	23.6	23.2[1]	23.3	23.8		23.7	23.7	23.6[2]		2.02	2.04	20
D	23.3	22.6	22.7	23.3		24.0[1]	22.9[2]	23.0		2.01	2.07	15
E	23.6	22.3	22.2[1]	22.7		21.9	22.0[2]	21.9		2.02	2.07	10
F	23.9[1]	23.0	22.9	22.1[2]		22.3	23.8	22.0		2.06	2.06	5
G	22.9		23.5		22.5		22.7					0
H		21.5	21.1	20.7	20.0	20.2[1]	20.9	20.8[2]		2.10	2.05	5
I		20.5	20.7	20.9[1]	20.8[2]	20.1	20.6	20.9		2.06	2.08	10
J		21.2	21.3[1]	21.6	21.3[5]	21.4	21.6	21.6		2.08	2.05	15
K	23.5	22.3[1]	22.6	22.4	22.1	22.3[2]	22.4	22.6		2.03	2.05	20
L	24.8	24.4[1]	24.0	23.9	24.3	24.3	24.5	24.5[2]	38.3	2.05	2.05	25
M	26.0	26.1	25.8[1]	25.8	25.9	26.0	26.0	26.2	37.1[2]	2.00	1.87	30

5 CRYSTAL ANALYSIS OF THE CANISTER AFTER SHEAR

The deformation of the canister was quite small with a maximum measured axial strain of the canister, measured at the surface, of 3 %. Large crystal deficiencies, such as compound crystal formation or microcracks, were therefore not expected, but a crystal analysis was still conducted. Only the copper canister from the first test was investigated.

Three 2 centimeter wide samples were bored from the canister on the side subjected to tensile stresses. The samples were taken 4, 7 and 10 cm from the shear plane (Fig 5:1). They were sent to the Swedish National Testing Institute (SNTI) in Borås for examination.

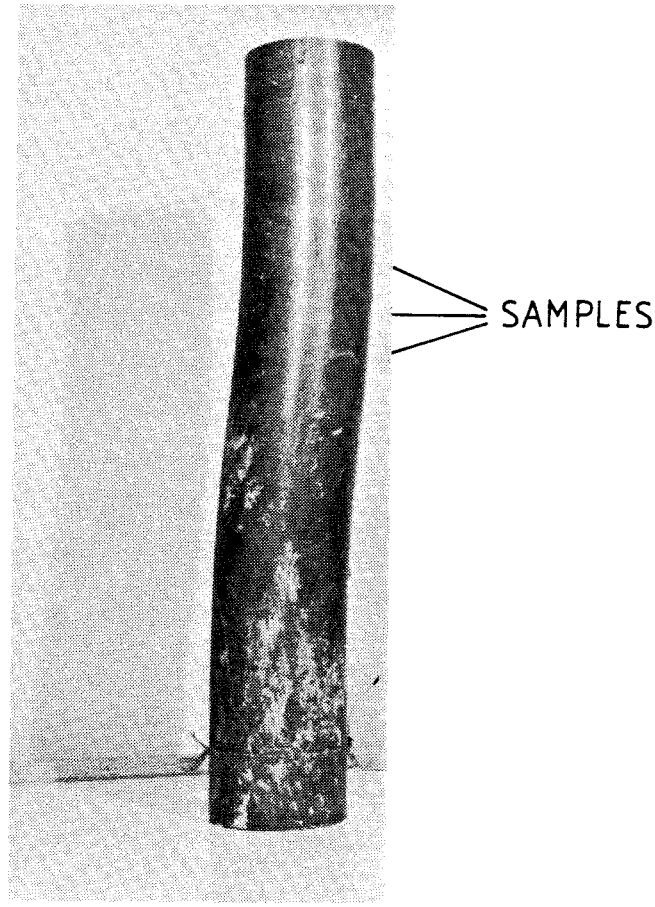

Fig 5:1. Sampling in the canister for the crystal analysis

For this purpose the samples were split by sawing ground, polished and treated with acid and the investigated by light microscopy. Fig 5:2 shows the surface at a magnification of 50 and a part of all three samples at a magnification of 10 with the canister surface facing downwards. According to Lars Andersson of SNTI there were no signs of crystal deficiencies or microcracks in the copper except for the damage surfaces produced by the cutting edge at the boring.

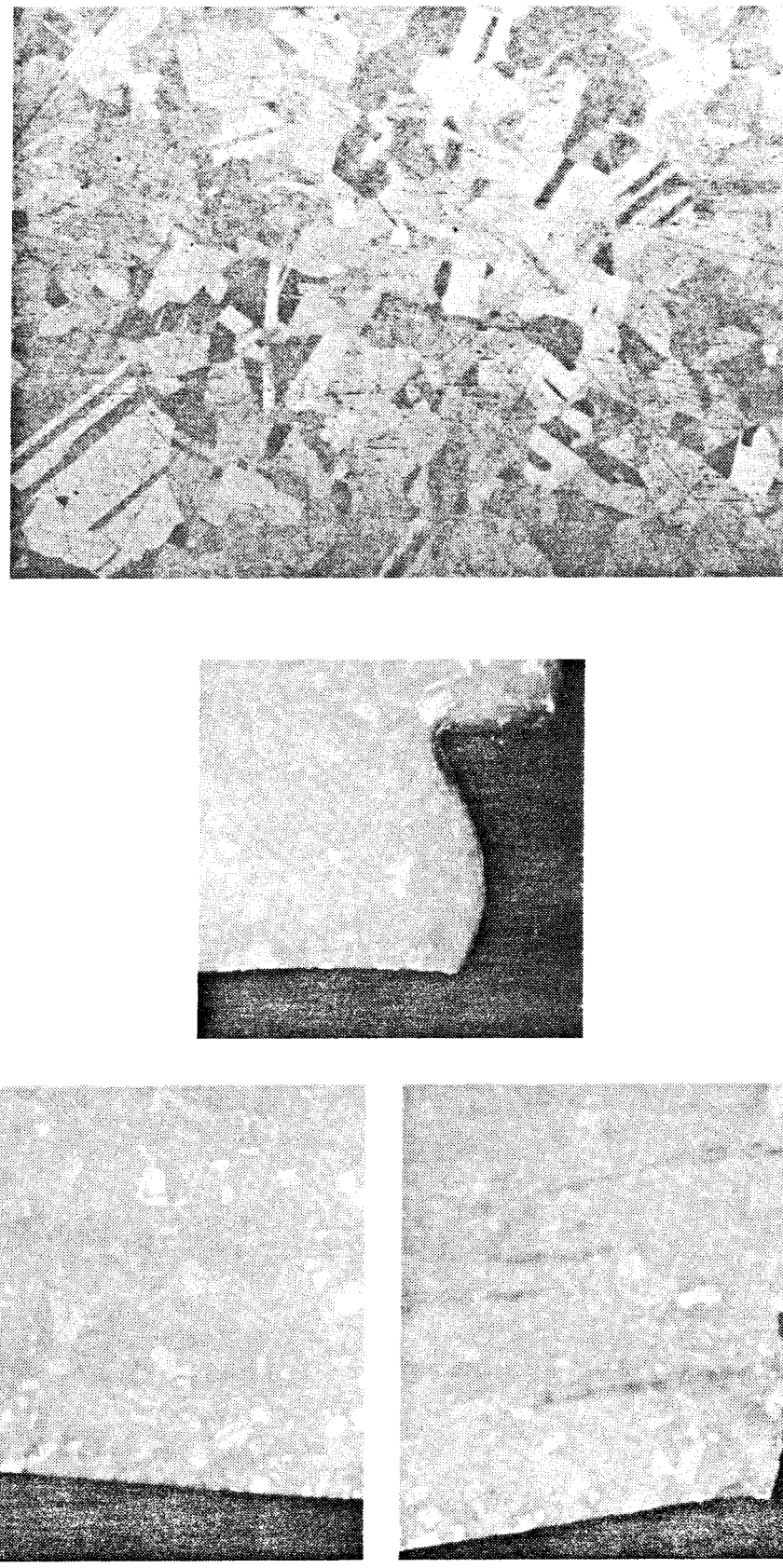

Fig 5:2. Photos of the polished cuts of the canister samples. Magnification 50:1 at the upper photo and 10:1 at the three lower photos

6 DISCUSSIONS AND CONCLUSIONS

6.1 General

Although the primary aim of this project has been to study the effect of shearing of the clay/canister system, a lot of other informations of importance for the concept has been received. The water uptake process, swelling pressure development, degree of saturation, homogenization, and density at excavation, serve as examples. These results together with the evaluated effect of the shearing on the clay and the canister will be discussed in this chapter.

6.2 Water uptake process

The calculation of the water uptake using a coefficient of water diffusion $D_w = 0.3 \cdot 10^{-9}$ m/s^2 showed that the average degree of saturation would be $S_r = 83$ % after 20 days and $S_r \sim 100$ % after less than 60 days. This seems to be in very good agreement with the observed degree of saturation at excavation as well as with the development of the swelling pressure during the water uptake.

When the last test was excavated after 60 days it was completely saturated. The development of the swelling pressure shows that the water uptake probably was completed after about 40 days. After 20 days about 75 % of the swelling pressure had been developed.

6.3 Swelling pressure development

The average swelling pressures measured after saturation are 8.9, 9.4 and 9.3 MPa at the three tests. These values agree very well with the proposed relation between density and swelling pressure for sodium bentonite (Börgesson & Pusch, 1986):

$$p_s = 2.86 \, (B_c + 0.2)^{10/3} \cdot e^{\frac{\rho_m - 2.0}{0.095}} \qquad (6:1)$$

where

p_s = swelling pressure (MPa)
ρ_m = density at saturation (t/m^3)
B_c = bentonite content (dry bentonite mass/total dry mass)

According to this equation the swelling pressure at ρ_m = 2.05 t/m^3 would be σ_s = 8.9 MPa.

The span of the individual values was quite high (5.2 MPa - 12.0 MPa) which may have the following explanations:

1 The reference value of the transducers are uncertain due to the complex mounting. The variation could thus depend on false reference values

2 The swelling pressure is extremely density-dependent as illustrated by Eq. (6:1). The measured densities in the vicinity of the transducers vary between 2.01 and 2.10 t/m^3 which corresponds to a variation in swelling pressure from 5.8 to 15.0 MPa

Thus the inhomogeneity can explain the variation in swelling pressure. It is probable that part of the pressure variation is due to a variation in density, while part of it might be due to the uncertain reference values. However, the measured change in pressure during rock deformation is not effected by these phenomena.

The calculated degree of saturation after 20 days was S_r ~83 %. Since the swelling pressure is known to be proportional to the degree of saturation (Börgesson, 1984) the swelling pressure should be ~80% of the final values after 20 days. This is confirmed by the measured values from tests 1 and 3, which vary between 60 and 85 % of the final values despite the delay caused by the initial swelling.

6.4 Density and degree of saturation after the test

In the first test, the time of sampling was too long to preserve the state of the bentonite, and it swelled before the excavation was finished. This effect could clearly be seen from the density and water content determinations. The second and third tests were exca-

vated within 6-8 hours and no effect of swelling due to water uptake could be seen.

The following discussion about the density and degree of saturation is based on the results from the second and third tests. The weighted average data from these two tests are shown in Table VI.

Table VI. Measured average data from tests 2 and 3

Test	ρ t/m³	w %	S_r^1 %	S_r^2 %	S_r^3 %
2	2.02	24.7	100.0	99.1	95.6
3	2.04	23.9	100.6	99.8	96.3

1) $\rho_s = 2.70$ t/m³
   $\rho_w = 1.00$ t/m³

2) $\rho_s = 2.785$ t/m³
   $\rho_w = 0.965$ t/m³

3) $\rho_s = 2.785$ t/m³
   $\rho_w = 1.00$ t/m³

Since the density at saturation before excavation should be $\rho_m = 2.05$ t/m³ there is a discrepancy which can be explained in the following ways:

1) Systematic error in the density measurements

2) Erroneous values of ρ_s and ρ_w

3) Elastic swelling due to the stress release

The first alternative is not probable since it would mean $S_r > 100$ % if the actual density was higher than the measured one.

The use of different values of ρ_s and ρ_w require some consideration. If $\rho_s = 2.87$ t/m³, as suggested by NAGRA, (Muller-Vonmoos & Kahr,

1983) and ρ_w = 0.965 t/m³, which can be extrapolated from Duwayne Anderson's test results (Anderson & Low, 1958), the degrees of saturation will be <100 % for the two tests. The influence of ρ_s and ρ_w can be seen in Fig 6:1 where ρ_s is plotted as a function of ρ_w at different degrees of saturation calculated for test 2. The relations will be about the same for test 3. It can be seen from the diagram that a low value of ρ_w (<1.00) can only fit a high value of ρ_s (>2.70) to get S_r <100 %. The two combinations used in Table VI give similar values of S_r. The values ρ_s = 2.70 t/m³ and ρ_w = 1.00 t/m³, which are usually referred to, thus seem to give reliable results. This is actually confirmed by various earlier investigations in which S_r=100 % was usually reached after saturation using these values.

A third possibility is that the bentonite is nonsaturated. Using ρ_s = 2.785 t/m³ and ρ_w = 1.00 t/m³ give a degree of saturation S_r = 96 % for the two tests and a final density of 2.06 t/m³ and 2.07 t/m³ respectively. However, this is not very likely since several investigations have shown that ρ_w <1.00 t/m³ (Pusch & Karnland, 1986).

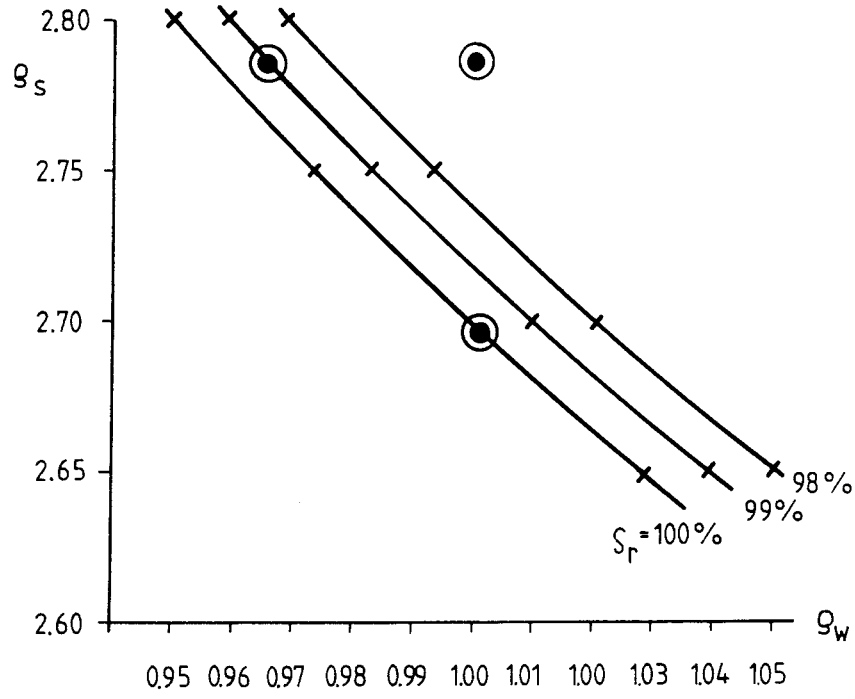

Fig 6:1. Relation between ρ_s and ρ_w as function of the degree of saturation S_r in Test 2. The three dots correspond to the values discussed in the text

Since the explanations termed 1 and 2 on the preceding page are thus not probable, it leaves elastic swelling of the water as the most likely explanation. If ρ_s = 2.785 t/m³ and ρ_w = 0.965 t/m³ are used the density at saturation was 2.020 t/m³ and 2.042 t/m³ in Tests 2 and 3, giving an average of 2.035 t/m³. Swelling to ρ=2.05 t/m³ would correspond to ~0.75 % and the question is therefore whether this expansion can be explained by elastic rebound of the pore water. If bulk modulus of the pore water is taken to be the same as for free water $E_v = 2.1 \cdot 10^6$ kPa we find that the porosity n=0.38 and the stress release $\Delta\sigma$ = 9 MPa give a swelling of

$$\varepsilon_v = n \cdot \frac{\Delta\sigma}{E_v} = 0.16\ \%$$

which is only 1/4 - 1/5 of the total swelling. As indicated by various investigations of the physical state of interlamellar water in montmorillonite it is probable, however, that this water is much more deformable than ordinary water and since it forms at least 50 % of the total porewater it may well be responsible for the elastic rebound (Pusch & Karnland, 1986).

The small deviations from the measured and expected results (<1%) and the moderately high accuracy of the measured values make it difficult to draw any far-reaching conclutions but it seems as if the degree of saturation of the bentonite in the tests is close to 100 %. It is also reasonable to believe that the swelling of the bentonite after release of the confinements is caused by a swelling of the interlamellar water in the clay. The results also show that a low density of the absorbed water (<1.00) fits a high particle density (>2.70). The final conclusion as to whether elastic rebound or non-complete saturation was the main or sole cause of the expansion, cannot be solved until the density of the porewater is finally settled.

6.5 Homogenization of the bentonite

The difference in average water content of the bentonite at the top/bottom and at the centre of the simulated deposition hole as well as the variation in water content in the radial direction suggest that the homogenization of bentonite was not complete, and that perfectly homogeneous conditions would probably never have been achieved. The

different time that passed until excavation took place in Tests 2 and 3 did not result in any different degree of homogenization which also show that the homogenization is a very slow process.

6.6 Influence of shear on the bentonite and the canister

Three tests under almost identical conditions have been conducted. The only difference between the tests was the rate of shear. The relation between the rate of the slow and the super quick test was ~1:5000. As expected, the required force increased with increased rate of shear but the rate influence was not very large.

Fig 6:2 shows the measured force after 15 mm shear deformation in the three tests as a function of the rate of shear. The rate dependence is that the force increases by 10 % per decade of increased rate of shear. This is in good agreement with the rate dependence measured for other clays although most of the shear resistance originates from the copper canister.

The obvious rate dependence means that there is a great difference in stress impact on the canister at instantaneous shear deformations originating from earthquakes, and at very slow strain during hundreds or thousands of years caused by rock creep. It also means that the stress-strain properties of the bentonite and canister must be related to the strain rate used in the calculation otherwise the results will be erroneous.

The influence of the shear rate is also demonstrated by the appearance of the deformed canisters. If the ratio of the canister shear deformation to the total shear deformation is plotted as a function of the rate of shear, the relation shown in Fig 6:3 is obtained. The canister deformation is obviously more rate dependent than the force but there is a clear relation between the two functions which can be seen by comparing Fig 6:3 with Fig 6:2.

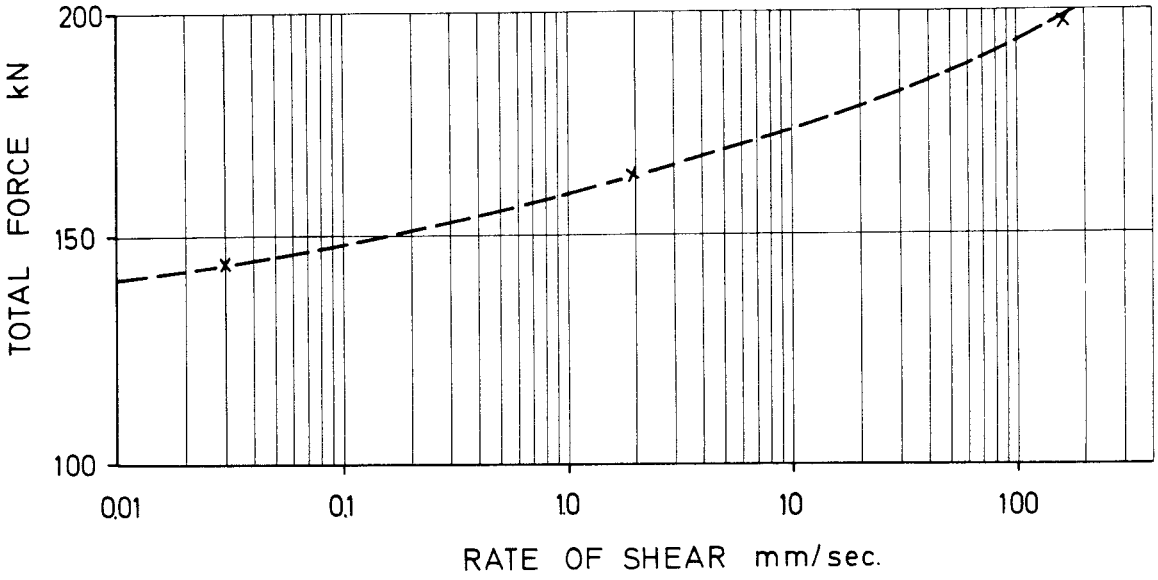

Fig 6:2. The total force after 15 mm shear deformation in the three tests as a function of the rate of shear

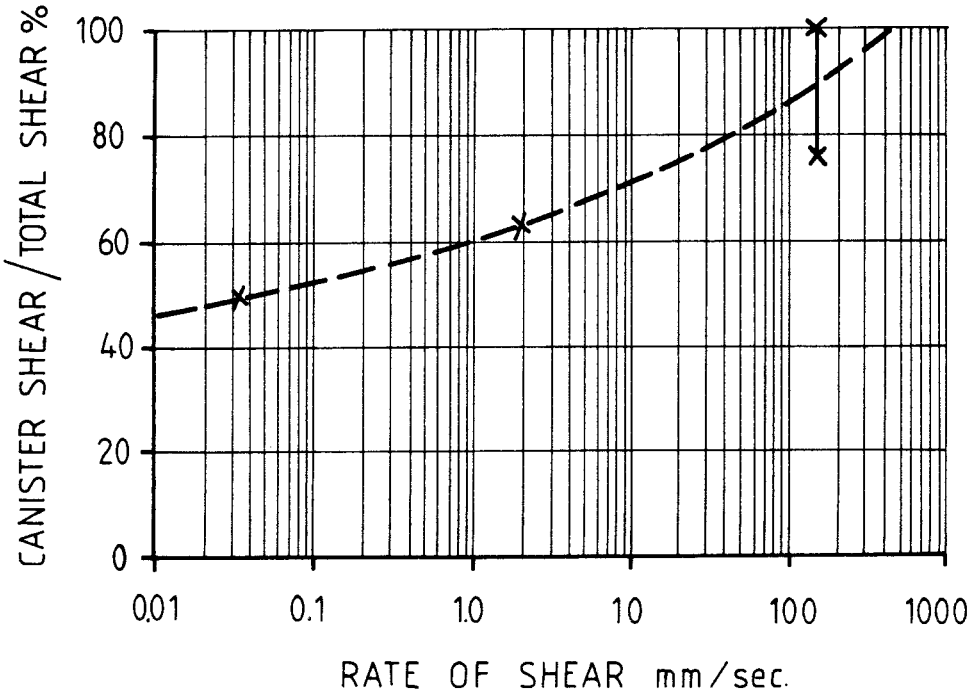

Fig 6:3. The ratio of the canister shear deformation to the total shear deformation as a function of the rate of shear

The deformed shape of the canister is that of shape e in Fig 2:1. This shape is generalized in figures c and d, were c nearly corresponds to the super-quick test with about the same canister shear as total shear, while figure d corresponds to the other tests with simultaneous shear and rotation of the canister.

The measured force is, however, only half of the force expected from the simple calculations in Chapter 2:2 (F~200 kN in test 3 compared to F~400 kN calculated for case c and F~150 kN in test 1 compared to F ~300 kN calculated for case d). The overestimation may be due to bending as a contributing mechanism to the deformation caused by shearing. However there is an obvious relation between the required force, the final shape of the canister and the rate of shear.

The shapes of the canisters after shear in the different tests were very similar and no shortening of the length l_s of the sheared zone (Fig 2:1c) with increased rate could be observed. This means that there is no sign of getting close to shape a in Fig 2:1 even at very high rates of shear. However, this analysis does not take any dynamic effects into account in a potential shear which will last for only a few milliseconds.

No rate effects could be seen on the measurements from the strain gauges or the pressure transducers. The accuracy of measurements was not good enough to detect such small differences.

The axial stresses in the canister surface can be estimated from the measured strains, which varied from very small values up to 3 %. The highest values were signalled by strain gauges 16 and 17, which means that the zone close to the shear plane was not the most stressed one, the major strain taking place in the zone 6-12 cm from the shear plane. This agrees well with the shape of the canister after shear since this is the zone where the canister is most deformed. It also agrees with the 3D calculations.

Three percent strain of the copper shear corresponds to a stress of about 100 MPa, which is reached after very large shear deformation (2-3 cm corresponding to 50-75 % of the bentonite thickness). It is difficult to compare the measured stresses to the calculated ones

because of the difference in geometry and properties. The calculations made of the large scale model, simulating the real deposition holes (the three- dimensional elastic and the two-dimensional elasto-plastic calculations) used a very small shear deformation corresponding to only 1.1-2.9 % of the bentonite thickness. These small deformations are equivalent to 0.44-1.16 mm in the model shear tests. The strain at these deformations cannot be evaluated with any certainty but the maximum measured one is (gauge 16, test 3) 0.1-0.25 % corresponding to 30-50 MPa. These values are in fair agreement with the stresses calculated from the two-dimensional elasto-plastic calculation. In the three-dimensional elastic calculation, however, the maximum stress was as high as 390 MPa because the stiffness and modulus of elasticity of the bentonite were over-estimated.

According to the viscous, three-dimensional calculation with μ=20 MPas after an intended deformation of 2 mm, the maximum shear stress at the canister surface 7.5 cm from the shear plane is 120 MPa. The measured strain in the canister after 2 mm deformation 7.0 cm from the shear plane was 0.5 % which corresponds to a shear stress of 65 MPa. Fig 6:4 shows a comparison between the measured stresses and the calculated stresses after 2 mm deformation. The shape of the measured curve and the magnitude of the measured values verify the calculation. An almost perfect agreement is reached if either the viscosity μ=10 MPas is used in the calculations or if the comparison is made at 5 mm deformation in the test.

A general trend of the strain measurements is that the strain was large and that high axial stresses were generated 6-12 cm from the imposed shear plane. This tendency is confirmed both by appearance of the deformed canisters and by the calculations. The very small strain in the copper makes Fig 1:5 unsuitable for evaluation of stresses. A careful measurement of the stress-strain properties between 0 and 5 % strain has been used instead.

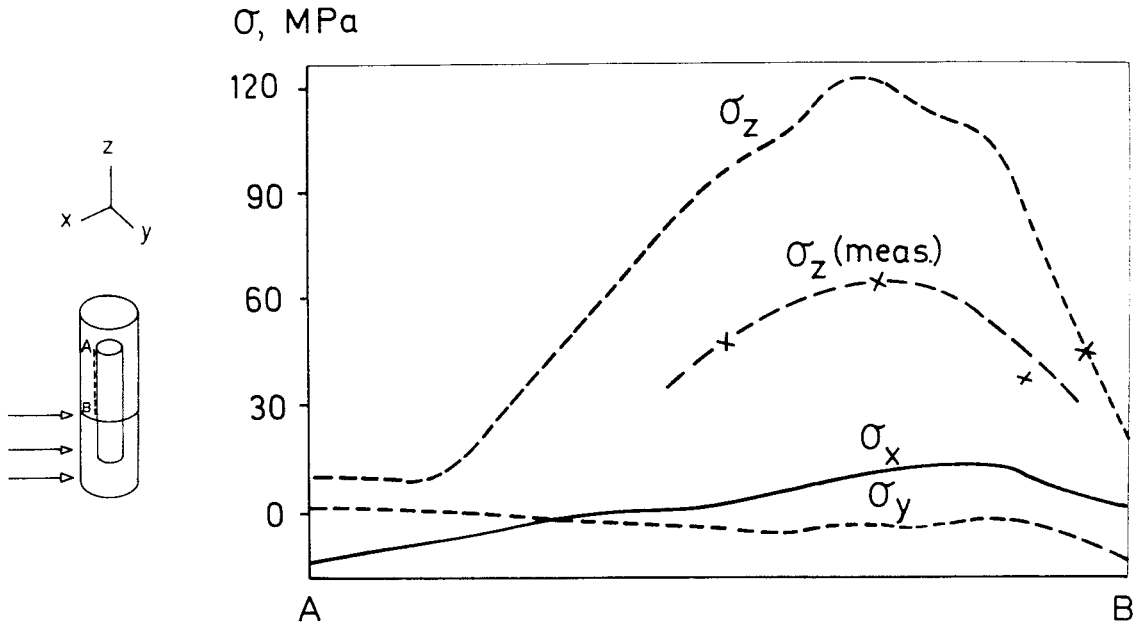

Fig 6:4. Comparison between calculated and measured stresses in the canister. σ_z, σ_x, σ_y were calculated using the viscous model with ν = 20 MPas while the measured values are derived from Test 3. Compression is termed positive

There are some trends in the pressure measurements as well. In the region 0-15 cm from the shear plane there is an increase in pressure between the bentonite and the canister on the compressed side of the canister, while the outer 7.5 cm are exposed to a decrease in pressure. There is a similar trend in the pressure between the bentonite and the rock. Fig 6:5 shows a comparison between the calculated and the measured change in normal stress on the canister after a simulated shear deformation of 5 mm using μ = 60 MPas. As can be seen in the figure the stresses are overestimated in the calculation but agree quite well if the measured stresses are multiplied by 6 (or if the calculated ones are divided by 6) which means that the viscosity μ=10 MPas would be correct (if the rates of deformation were the same). Since the viscous calculation agree with an elastic if E = 3μ this means that using an E-modulus of E = 30 MPa for the bentonite in the calculation should lead to an acceptable correspondence between the experimental and calculated data.

A 5 mm shear deformation of the 40 mm bentonite cover corresponds to a strain of ~5/40 = 12.5 %, which means $\varepsilon \sim 8$ %. Since the stress-strain curve of bentonite is nonlinear a correct value of E must be determined at the same strain. Fig 6:6 shows the probable stress-strain relation for the bentonite (Fig 1:4) with some different values of E plotted in the diagram. The E-modulus corresponding to $\varepsilon \sim 8$ % is E=23 MPa which is quite close to the "correct" value E~30 MPa according to the comparison between the calculation and the test. However, a calculation using E~23 MPa would differ from the test results at shear deformations deviating from 5 mm due to the non-linearity of the clay. This shows that a non-linear three-dimensional elasto-plastic calculation is necessary and probably will give accurate results.

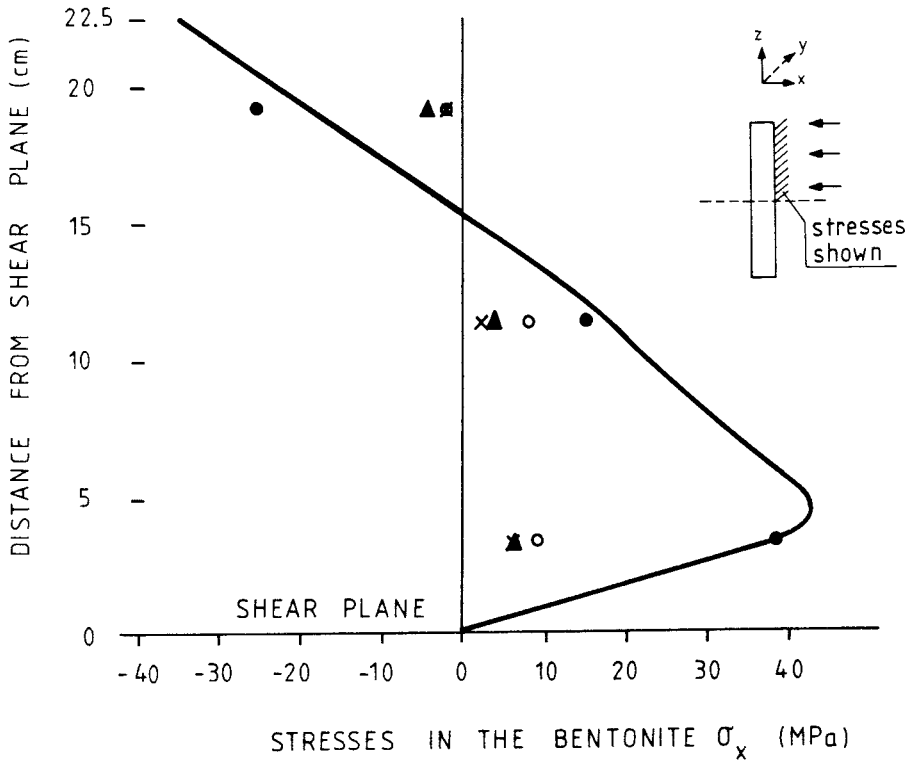

Fig 6:5. Comparison between calculated stresses in the bentonite on the canister using ν = 60 MPas (line) and measured after 5 mm shear from the three tests.

▲ results from Test 1

x results from Test 2

○ results from Test 3

● results from Test 2 multiplied by 6

The deformed shape of the canister derived from the three-dimensional viscous calculation agree quite well with the deformed canisters from the tests. The calculated shape of half the cylinder is shown in Fig 6:7.

It is interesting to see that if the author's model can be applied to the full-scaled KBS 3 case, an "instantaneous" (super-quick) shear of 5 cm would be acceptable without critical stresses being generated in the canisters. This would correspond to a very severe earthquake. It remains to be verified, however, that this holds also in a proper stress/strain analysis based on non-linearity of the clay stress/strain properties.

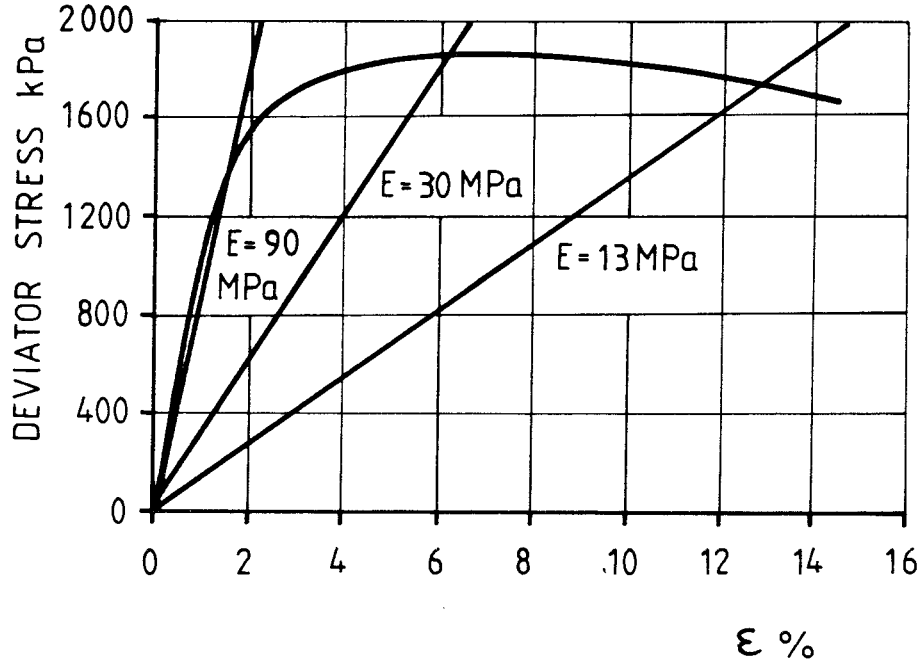

Fig 6:6. The stress-strain properties of bentonite. The figure shows that the "E-modulus" used in a linear calculation must be related to the strain

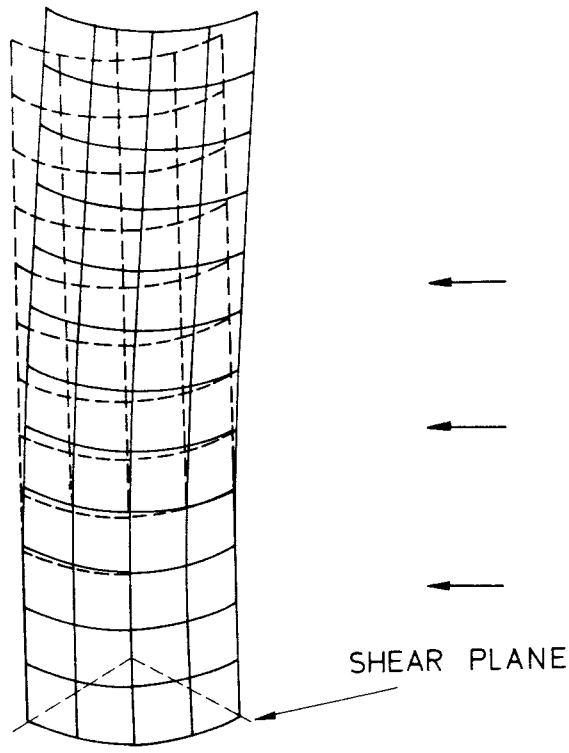

Fig 6:7. The shape of the canister according to the viscous calculation. The similarity with the canisters in the tests can be seen if a small counter-clockwise turning of the canister around the shear plane is imagined

7 RECOMMENDATIONS FOR FURTHER WORK

The model shear tests reported here give a considerable amount of information about the processes involved in rock shearing of a deposition hole. The data received from the tests are valuable for comparing not only with the calculations made so far but also with the planned ones. The basic relationships between the development of stress and strain cannot be sufficiently well modelled by using the calculation models applied so far.

A final goal must be to combine a mathematical model with a physical understanding of the behaviour. From the tests performed in this project it can be concluded that there is an elastic response to isotropic as well as deviatoric stress-changes which is followed by a plastic behaviour at a certain stress level at a certain strain.

The material is also viscous in the sense that it increases the upper stress -limit for elastic response with increasing strain-rate. This is reflected by the increased canister deformation with increased strain-rate.

A material model which takes both the non-linear stress-strain relation and the viscous rate-dependent behaviour into account is desirable. However, such a model is very complicated for use in a 3 D FEM calculation and at first a non-viscous model is planned using the FEM program ABAQUS. This would be a basic instrument in the parameter analyses that is intended for optimization of the geometry of the deposition hole and the density and composition of the clay material surrounding the canister.

The calculations must of course be accompanied by careful laboratory measurements of the clay and canister material. This comprises determination of the rate and temperature dependence of the stress-strain properties to cover the entire thermo-mechanical scenario which the clay/canister/rock system undergoes in a real repository.

The calculations simulating clays with different densities or compositions should be checked with one or two additional model shear tests. Of great interest would also be the very slow creep case to

see if the resistance and deformation of the canister continue to decrease according to an extrapolation of the curves in Figs 6:2 and 6:3.

8 REFERENCES

1 Anderson, D. and Low, Ph. (1958). The density of water absorbed by lithium-, sodium-, and potassium-bentonite. Soil Science Society of America Proceedings, Vol. 22, No 2

2 Axelsson, K. (1982) Elasto-plastisk analys av kopparkapsel utsatt för bergförskjutning. University of Luleå. Internal report

3 Bjerrum, L. (1973). Shear strength of normally consolidated clays. Proc. 8th Int. Conf. on Soil Mech. a. Found. Engng. Moscow

4 Börgesson, L. (1982). Buffer Mass Test - Predictions of the behaviour of the bentonite based buffer materials. Stripa Project, Internal Report (SKBF/KBS) 82-08

5 Börgesson, L. (1984). Water flow and swelling pressure in non-saturated bentonite-based clay barriers. Engineering Geology, 21 (1985) pp. 229-237

6 Börgesson, L. and Stenman, U. (1985). Laboratory determined properties of sand/bentonite mixtures for WP-Cave. SGAB Internal Report 85511

7 Börgesson, L. and Pusch, R. (1986). Basic properties of bentonite-based buffer materials and their function in WP-cave repositories. SGAB Internal Report 86501

8 CMC (1984). Report on stress analysis of clay/canister system. Computational Mechanics Consultants. Southampton. Internal Report

9 Hansbo, S. (1975) Jordmateriallära. Almqvist & Wiksell Förlag AB, Stockholm.

10 SKBF/KBS Final Storage of Spent Nuclear Fuel - KBS 3. Stockholm (1983)

11 Müller-Vonmoos, M. and Kahr, G. (1983) Mineralogische untersuchungen von Wyoming bentonit MX-80 und Montigel. NAGRA, Technischer Bericht 83-12

12 Nilsson, F. (1982). Linjär analys av kopparkapsel utsatt för bergförskjutning. Tekniskt Meddelande. IFM Akustikbyrån

13 Pusch, R. (1983). Stress/strain/time properties of highly compacted bentonite. SKBF/KBS Teknisk Rapport 83-47

14 Pusch, R. (1983). Use of clays as buffers in radioactive repositories. SKBF/KBS Teknisk Rapport 83-46

15 Pusch, R. and Karnland, O. (1986). Aspects of the physical state of adsorbed water. SKB Technical Report

16 Torstensson, B.A. (1977). Time-dependents effects in the field vane test. International symposium on soft clay, Bangkok

List of SKB reports

Annual Reports

1977–78
TR 121
KBS Technical Reports 1 – 120.
Summaries. Stockholm, May 1979.

1979
TR 79–28
The KBS Annual Report 1979.
KBS Technical Reports 79-01 – 79-27.
Summaries. Stockholm, March 1980.

1980
TR 80–26
The KBS Annual Report 1980.
KBS Technical Reports 80-01 – 80-25.
Summaries. Stockholm, March 1981.

1981
TR 81–17
The KBS Annual Report 1981.
KBS Technical Reports 81-01 – 81-16.
Summaries. Stockholm, April 1982.

1982
TR 82–28
The KBS Annual Report 1982.
KBS Technical Reports 82-01 – 82-27.
Summaries. Stockholm, July 1983.

1983
TR 83–77
The KBS Annual Report 1983.
KBS Technical Reports 83-01 – 83-76
Summaries. Stockholm, June 1984.

1984
TR 85–01
Annual Research and Development Report 1984
Including Summaries of Technical Reports Issued during 1984. (Technical Reports 84-01– 84-19)
Stockholm June 1985.

1985
TR 85-20
Annual Research and Development Report 1985
Including Summaries of Technical Reports Issued during 1985. (Technical Reports 85-01-85-19)
Stockholm May 1986.

Technical Reports

1986

TR 86-01
I: An analogue validation study of natural radionuclide migration in crystalline rock using uranium-series disequilibrium studies
II: A comparison of neutron activation and alpha spectroscopy analyses of thorium in crystalline rocks
J A T Smellie, Swedish Geological Co, A B MacKenzie and R D Scott, Scottish Universities Research Reactor Centre
February 1986

TR 86-02
Formation and transport of americium pseudocolloids in aqueous systems
U Olofsson
Chalmers University of Technology, Gothenburg, Sweden
B Allard
University of Linköping, Sweden
March 26, 1986

TR 86-03
Redox chemistry of deep groundwaters in Sweden
D Kirk Nordstrom
US Geological Survey, Menlo Park, USA
Ignasi Puigdomenech
Royal Institute of Technology, Stockholm, Sweden
April 1, 1986

TR 86-04
Hydrogen production in alpha-irradiated bentonite
Trygve Eriksen
Royal Institute of Technology, Stockholm, Sweden
Hilbert Christensen
Studsvik Energiteknik AB, Nyköping, Sweden
Erling Bjergbakke
Risö National Laboratory, Roskilde, Denmark
March 1986

TR 86-05
Preliminary investigations of fracture zones in the Brändan area, Finnsjön study site
Kaj Ahlbom, Peter Andersson, Lennart Ekman, Erik Gustafsson, John Smellie,
Swedish Geological Co, Uppsala
Eva-Lena Tullborg, Swedish Geological Co, Göteborg
February 1986

TR 86-06
Geological and tectonic description of the Klipperås study site
Andrzej Olkiewicz
Vladislav Stejskal
Swedish Geological Company
Uppsala, October, 1986

TR 86-07
Geophysical investigations at the Klipperås study site
Stefan Sehlstedt
Leif Stenberg
Swedish Geological Company
Luleå, July 1986

TR 86-08
Hydrogeological investigations at the Klipperås study site
Bengt Gentzschein
Swedish Geological Company
Uppsala, June 1986

TR 86-09
Geophysical laboratory investigations on core samples from the Klipperås study site
Leif Stenberg
Swedish Geological Company
Luleå, July 1986

TR 86-10
Fissure fillings from the Klipperås study site
Eva-Lena Tullborg
Swedish Geological Company
Göteborg, June 1986

TR 86-11
Hydraulic fracturing rock stress measurements in borehole Gi-1, Gideå Study Site, Sweden
Bjarni Bjarnason and Ove Stephansson
Division of Rock Mechanics,
Luleå University of Technology, Sweden
April 1986

TR 86-12
PLAN 86— Costs for management of the radioactive waste from nuclear power production
Swedish Nuclear Fuel and Waste Management Co
June 1986

TR 86-13
Radionuclide transport in fast channels in crystalline rock
Anders Rasmuson, Ivars Neretnieks
Department of Chemical Engineering
Royal Institute of Technology, Stockholm
March 1985

TR 86-14
Migration of fission products and actinides in compacted bentonite
Börje Torstenfelt
Department of Neclear Chemistry, Chalmers University of Technology, Göteborg
Bert Allard
Department of water in environment and society, Linköping university, Linköping
April 24, 1986

TR 86-15
Biosphere data base revision
Ulla Bergström, Karin Andersson, Björn Sundblad, Studsvik Energiteknik AB, Nyköping
December 1985

TR 86-16
Site investigation
Equipment for geological, geophysical, hydrogeological and hydrochemical characterization
Karl-Erik Almén, SKB, Stockholm
Olle Andersson, IPA-Konsult AB, Oskarshamn
Bengt Fridh, Bengt-Erik Johansson,
Mikael Sehlstedt, Swedish Geological Co, Malå
Erik Gustafsson, Kenth Hansson, Olle Olsson,
Swedish Geological Co, Uppsala
Göran Nilsson, Swedish Geological Co, Luleå
Karin Axelsen, Peter Wikberg, Royal Institute of Technology, Stocholm
November 1986

TR 86-17
Analysis of groundwater from deep boreholes in Klipperås
Sif Laurent
IVL, Swedish Environmental Research Institute
Stockholm, 1986-09-22

TR 86-18
Technology and costs for decommissioning the Swedish nuclear power plants.
Swedish Nuclear Fuel and Waste Management Co
May 1986

TR 86-19
Correlation between tectonic lineaments and permeability values of crystalline bedrock in the Gideå area
Lars O Ericsson, Bo Ronge
VIAK AB, Vällingby
November 1986

TR 86-20
A Preliminary Structural Analysis of the Pattern of Post-Glacial Faults in Northern Sweden
Christopher Talbot, Uppsala University
October 1986

TR 86-21
Steady-State Flow in a Rock Mass Intersected by Permeable Fracture Zones. Calculations on Case 2 with the GWHRT-code within Level 1 of the HYDROCOIN Project.
Björn Lindbom, KEMAKTA Consultants Co, Stockholm
December 1986

TR 86-22
Description of Hydrogeological Data in SKBs Database Geotab
Bengt Gentzschein, Swedish Geological Co, Uppsala
December 1986

TR 86-23
Settlement of Canisters with Smectite Clay Envelopes in Deposition Holes
Roland Pusch
Swedish Geological Co
December 1986

TR 86-24
Migration of Thorium, Uranium, Radium and Cs—137 in till Soils and their Uptake in Organic Matter and Peat
Ove Landström, Björn Sundblad
Studsvik Energiteknik AB
October 1986

TR 86-25
Aspects of the Physical State of Smectite-adsorbed Water
Roland Pusch, Ola Karnland
Swedish Geological Co, Lund
Engineering Geology
December 1986